UNIVERSITÀ DEGLI STUDI DI TRIESTE

XXXIII CICLO DEL DOTTORATO DI RICERCA IN

BIOMEDICINA MOLECOLARE

The mechanisms of bilirubin protection against cellular metabolic damage

Settore scientifico-disciplinare: BIO/11

DOTTORANDA
ANNALISA BIANCO

COORDINATORE
PROF.GERMANA MERONI

SUPERVISORE DI TESI
PROF. CLAUDIO TIRIBELLI

ANNO ACCADEMICO 2019/2020

To my mom
My lighthouse
Shining in the darkness

Contents

List of figures

List of tables

List of Abbrevations

ABC ATP Binding Cassette
ABCB1 ATP Binding Cassette Subfamily BMember 1
ABCC1 ATP Binding Cassette Subfamily C Member 1
ABCC2 ATP Binding Cassette Subfamily C Member 2
ABCC3 ATP Binding Cassette Subfamily C Member 3
AGEs Advanced Glycation End Products
AOP index Antioxidant power index
AOP1 Antioxidant power 1 assay
ATF6 Activating transcription factor 6
BBB Blood–brain barrier
Bf Free bilirubin
BIND Bilirubin-Induced Neurologic Dysfunction
BiP Immunoglobulin heavy-chain-binding protein
BLVR Biliverdin reductase
BLVRA Biliverdin reductase alpha gene
BMI body mass index
BSA Bovine serum albumin
CAT Catalase enzyme
CBP/p300 coactivator family cAMP-response-element-binding protein EP300 and E1A binding protein p300
CHOP C/EBP homologous protein
CKD Chronic kidney disease
CRP C-reactive protein
CTGF Connective tissue growth factor
CuZnSOD Superoxide dismutase [Cu-Zn]
CVD Cardiovascular deseases
CYPs Cytochrome P-450-oxygenases
DCF 2′,7-dichlorofluorescein
DMCK kidney disease in patients with diabetes mellitus
DMSO Dimethyl sulfoxide
DN Diabetic Nephropathy
EC_{50} Half maximal effective concentration
eGFR Estimated Glomerular Filtration Rate
EMT Epithelial–mesenchymal transition
eNOS Endothelial Nitric Oxide Synthase
ER-Stress Endoplasmic reticulum stress
FABP 1 Fatty Acid-Binding Protein 1
FL Fatty liver
GLUT1 Glucose transporter 1
$gp91^{phox}$ glycosylated 91-kDa glycoprotein
GPx Glutathione peroxidase
GRP78/BiP 78-kDa glucose-regulated protein also referred Bip
GS Gilbert syndrome
GSH Reduced glutathione
GSTs Glutathione S-transferases

GTPase nucleotide guanosine triphosphate hydrolase enzyme
H2DCFDA 2′7′-dichlorodihydrofluorescein diacetate
H_2O_2 Hydrogen peroxide
HBV hepatitis B
HCC Hepatocellular carcinoma
HCV hepatitis C
HDL high-density lipoprotein
HIF-1α Hypoxia-inducible factor 1-alpha
HMOX Heme oxygenase
HNO_2 Nitrous acid
HOMA Homeostatic Model Assessment for Insulin Resistance
HO-1 Heme oxygenase-1
HPLC High Performance Liquid Chromatography
HREs hypoxia-response elements
ICAM Intercellular adhesion molecule-1
IDNT Irbesartan Diabetic Nephropathy Trial
IgA Immunoglobuline A
IkB inhibitor of nuclear factor kappa B
IL-6 Interleukin 6
iNOS Nitric oxide synthase
IRE1 Inositol-requiring enzyme 1
iUCB Intracellular unconjugated bilirubin
kB nuclear factor kappa B
LC3 Microtubule-associated protein 1A/1B-light chain 3
LC3 I cytosolic form of Microtubule-associated protein 1A/1B-light chain 3
LC3 II LC3-phosphatidylethanolamine conjugate
LDL low-density lipoprotein
LOX Lysyl oxidase
LOXL2 lysyl oxidase-like protein 2
LUCs Light-Up Cell System
MDR1 Multidrug resistance protein 1
MDRD Diet in Renal Disease
MetS Metabolic Syndrome
MMP-2 Matrix metalloproteinase-2
MnSOD manganese superoxide dismutase (SOD2)
MRP3 Multidrug resistance-associated Protein 3
MTT 3(4,5-dimethylthiazolyl-2)-2,5 diphenyl tetrazolium
NADH β-Nicotinamide adenine dinucleotide reduced
NADP Nicotinamide adenine dinucleotide phosphate reduced form
NADPH Nicotinamide adenine dinucleotide phosphate
NAFL Non-Alcoholic Fatty Liver
NAFLD Nonalcoholic fatty liver disease
NASH Nonalcoholic steatohepatitis
NBT Nitro blue tetrazolium
NHANES The National Health and Nutrition Examination Survey
NO Nitric oxide
Nox-4 NADPH oxidase 4

O_2^- negative oxygen ions
OGLM ordinal generalized linear model
OGTT glucose tolerance test
$ONOO^-$ Peroxynitrite
$p22^{phox}$ 22-kDa protein of phagocytic oxidase
$p40^{phox}$ 40-kDa protein of phagocytic oxidase
$p47^{phox}$ 47-kDa protein of phagocytic oxidase
$p67^{phox}$ 67-kDa protein of phagocytic oxidase
PAI-1 Plasminogen activator inhibitor-1
PARP poly(ADP-ribose) polymerase
PERK protein kinase R (PKR)-like endoplasmic reticulum kinase
PGK Phosphoglycerate kinase
PGP1 phagocyte glycoprotein- 1
PHD prolyl hydroxylase domain
PI Propidium Iodide
PKC Protein kinase C,
PMS Phenazine methosulfate
PPARα Peroxisome proliferator-activated receptor alpha
pVHL VHL protein
RAA renin-angiotensin (RAA) system
Rac2 Ras-related C3 botulinum toxin substrate 2
RAGEs Receptor for Advanced Glycation End Products
RENAAL Angiotensin II Antagonist Losartan (RENAAL) trial
RFU Relative fluorescence units
ROS Reactive oxygen species
ROS/RNS reactive oxygen and nitrogen species
SOD1 Superoxide dismutase [Cu-Zn]
SOD2 mitochondrial manganese superoxide dismutase
SOD3 extracellular, superoxide dismutase 3
TAG Triglycerides
T2DM Type 2 Diabetes Mellitus
TBili Total Bilirubin
TGF-β Transforming growth factor-β
TIF Tubulointerstitial fibrosis
TIMP-1 tissue inhibitor of metalloproteinases
TNF-α tumor necrosis factor alpha
UCB unconjugated bilirubin
UGT1A1 UDP Glucuronosyltransferase family 1 member A1
UGTs UDP-glucuronosyltransferase
UPR unfolded protein response
VCAM vascular cell adhesion molecule 1
VEGF Vascular endothelial growth factor
WHO World Health Organization
XBP X-box binding protein 1
α-SMA Smooth muscle alpha-actin

Abstract

Unconjugated bilirubin (UCB) is a metabolic end-product of heme catabolism. Bilirubin's behavior in a human body has two faces similar to Janus Bifrons. Elevated serum/plasma UCB concentration exposes babies to the risk of neurotoxicity. Conversely, mildly elevated systemic bilirubin concentrations such as in Gilbert syndrome (GS) protect against various oxidative stress-mediated and metabolic diseases including cardiovascular diseases (CVD) and diabetic nephropathy (DN). Gilbert syndrome was considered as a selective genetic advantage. Indeed, some scientists suggested that a mildly increase of bilirubin levels could have a therapeutical potential to suppress pathway leading to the development of metabolic diseases. The main aim of the present thesis work is to contribute to ameliorate the understanding of the molecular mechanism involved in the protective impact of bilirubin. Our study is divided into three parts entitled task 1, 2 and 3 and it is focused to define intracellular bilirubin thresholds for anti- and pro-oxidant effects; to investigate the pathways involved in mild hyperbilirunemia protective effect in *in vitro* models of atherosclerosis and diabetic nephropathy and to study the correlation between serum UCB level and Metabolic syndrome (MetS) and Non-alcoholic fatty liver disease (NAFLD) in a cohort of extremely obese children and adolescents.

Task 1 is an *in vitro* comparative study, performed on four different cell lines coming from different organs. It is focused on the evaluation of the effects of increasing concentration of bilirubin on redox balance. The aim is to determine the UCB threshold for its anti- and prooxidant activity. Hepatic (HepG2), hearth endothelial (H5V), kidney tubular (HK2) and neuronal (SH-SY5Y) cell lines were exposed to the same UCB treatments and intracellular bilirubin concentration (iUCB), cytotoxicity, intracellular ROS concentrations, and antioxidant capacity (EC_{50}) were determined. Exposure of SH-SY5Y to UCB concentration > 3.6 μM (iUCB of 25 ng/mg) and >15 μM in H5V and HK2 cells (iUCB of 40 ng/mg) increased intracellular ROS production ($p<0.05$). EC_{50} of the antioxidant activity was 21 μM (iUCB between 5.4 and 21 ng/mg) in HepG2 cells, 0.68 μM (iUCB between 3.3 and7.5 ng/mg) in SH-SY5Y cells, 2.4 μM (iUCB between 3 and 6.7 ng/mg) in HK2 cells, and4 μM (iUCB between 4.7 and 7.5 ng/mg) in H5V cells. UCB metabolism was found to be cell-specific resulting in different iUCB. iUCB and not the external UCB treatment, determine and define a threshold for antioxidant or cytotoxic effect. Considering the iUCB, regardless of the UCB concentration treatment and cell line origin, we observed that iUCB around 7 ng/mg acts as an antioxidant, while at iUCB higher than 25 ng/mg is associated with a pro-oxidant and cytotoxic effects.

Task 2 investigates the effect of mild elevated bilirubin concentration in *in vitro* models of atherosclerosis and diabetic nephropathy. Fibrosis of tubular epithelial cells, apoptosis of podocytes, endoplasmic reticulum stress (ER-stress) and inflammation are the main pathways activated in DN and atherosclerosis, respectively. The principal aim is to detect the effect of life-long hyperbilirubinemia and bilirubin-priming on the main pathways activated, at the cellular level, upon damage induction. Primary aortic endothelial cells and podocytes obtained from hyperbilirubinemic homozygous jj and normobilirubinemic heterozygous Nj Gunn rats were exposed to Palmitic acid (PA) and Angiotensin II (Ang II), respectively. Results were validated on immortalized H5V and HK2 cells exposed to damage after UCB pre-treatment.
In both primary cell models, we observed that the viability of cells harvested from hyperbilirubinemic jj Gunn rats was significantly higher than the viability of normobilirubinemic Nj Gunn rats at any dose of the toxic agent. Reduction in CHOP expression and IL-6 release was

detected in hyperbiliruninemic jj primary aortic endothelial cells exposed to PA compared to normobilirubinemic Nj cells. The same occurred on H5V pretreated with UCB. Upon Ang II treatment, primary podocytes from jj Gunn rats showed lower DNA fragmentation, cleaved caspase-3, and cleaved Poly-(ADP-ribose)-polymerase (PARP) induction than primary podocytes from normobilirubinemic Nj Gunn rats. By investigating the possible mechanism responsible for UCB anti-fibrotic and anti-apoptotic effect, we observed that jj podocytes showed a higher basal expression of Microtubule-associated protein 1A/1B-light chain 3 (LC3) II compared to Nj. In HK2 cells, the induction by Ang II of hypoxia-inducible factor 1, alpha subunit (HIF-1α) and lysyl oxidase-like 2 (LOXl2) was significantly reduced by UCB pre-treatment. Our data suggest that life –long hyperbilirubinemia exposure or bilirubin-priming significantly contribute to increase cell viability and enhance responses to damage in *in vitro* models of atherosclerosis and DN.

Task 3 is focused on the association between serum bilirubin levels and the prevalence of NAFLD and MetS. The association between total bilirubin levels, age, pubertal stage, anthropometric, clinical, and laboratory data were evaluated in a retrospective cross-sectional study performed on 1672 consecutive extremely obese children and adolescents. Total bilirubin level correlates positively with age in the total population and increased according to the pubertal stage. Among others, high triglycerides, waist /height ratio, insulin, homeostatic model assessment (HOMA), and C-reactive protein (CRP) showed a negative weak correlation with bilirubin. However, any significative relationship between serum total bilirubin, Mets and NAFLD was not detected. Although most association were statistically significant, they cannot be considered biologically relevant on the basis of the underlying effect size. Even if apparently in contrast with previously publications, our data strength the observation that serum bilirubin levels, even in their normal ranges, might have graded associations with the prevalence of MetS and NAFLD in young ages, when the metabolic dysregulation is in its early stage, but not in extremely obese population.

We believe that the present thesis work have contributed to a better understanding of the molecular mechanism involved in the protective impact of bilirubin through 3 statements:
1) The definition of the intracellular UCB thresholds that set the switch between anti- and prooxidant effects of bilirubin. An intracellular UCB concentration of around 7 ng/mg protein had antioxidant activities, while its intracellular concentrations >25 ng/mg protein resulted in prooxidant and cytotoxic effects;
2) the demonstration that life-long hyperbilirubinemia exposure or bilirubin-priming significantly contribute to the activation of protection against metabolic syndrome, by enhancing responses to damage and increasing cell viability in *in vitro* models of atherosclerosis and DN;
3) the observation that serum bilirubin levels, even in their normal ranges, might have graded associations with the prevalence of MetS and NAFLD in young ages, when the metabolic dysregulation is in its early stage, but not in extremely obese population.

Riassunto

La bilirubina è il prodotto endogeno finale del catabolismo dell'eme. A causa dei suoi duplici effetti nell'organismo, è considerata un come Giano Bifronte, l'antico dio romano. Infatti, è ben noto che livelli molto elevati di bilirubina sierica sono neurotossici in particolare nel neonato. Al contrario, concentrazioni leggermente più elevate del normale di bilirubina sierica, come quelle presenti nei soggetti Gilbert, proteggono da varie malattie metaboliche e patologie legate allo stress ossidativo, comprese quelle cardiovascolari (CVD) e la nefropatia diabetica (DN). GS è stata considerata un vantaggio genetico selettivo e, per questo, alcuni scienziati hanno suggerito che un aumento lieve rispetto al normale dei livelli di bilirubina potrebbe avere un potenziale terapeutico per sopprimere il percorso che porta allo sviluppo di malattie metaboliche.

Lo scopo principale di questo lavoro di tesi è stato quello di contribuire alla comprensione dei meccanismi molecolari coinvolti nell'effetto protettivo esercitato da determinati livelli di bilirubina in sistemi *in vitro*. Il nostro studio è stato diviso in tre parti distinte (task 1, 2 e 3) al fine di definire la soglia di bilirubina intracellulare che causa effetti anti- e pro-ossidanti a livello cellulare; di indagare le pathways coinvolte nell'effetto protettivo dato dall'iperbilirubinemia lieve in modelli *in vitro* di aterosclerosi e nefropatia diabetica; e di studiare la correlazione tra i livelli sierici di bilirubina non coniugata e lo sviluppo di sindrome metabolica e di steatosi epatica non alcolica (NAFLD) in una coorte di bambini e adolescenti con obesità severa.

Nella prima parte di questo lavoro è stato effettuato uno studio comparativo *in vitro*, utilizzando quattro linee cellulari provenienti da organi differenti. Sono stati valutati gli effetti di diverse concentrazioni di bilirubina sull'equilibrio redox delle cellule. Lo scopo è stato quello di determinare la soglia di concentrazione necessaria per l' attività antiossidante e pro ossidante della bilirubina non coniugata (UCB). Linee cellulari epatiche (HepG2), endoteliali cardiache murine (H5V), tubulari renali umane (HK2) e neuronali (SH-SY5Y) sono state esposte per 24 h agli stessi trattamenti di bilirubina (0.4, 0.9, 1.8, 3.6, 7.5, 15, 30 μM) in presenza di BSA 30 μM , e sono state determinate le corrispettive concentrazione di bilirubina intracellulare (iUCB), e valutata la citotossicità, la produzione intracellulare di specie reattive dell'ossigeno (ROS) ed anche la capacità antiossidante (EC_{50}) delle varie concentrazioni. I risultati mostrano che le concentrazioni di UCB> 3,6 μM (iUCB di 25 ng / mg) nelle SH-SY5Ye > 15 μM nelle cellule H5V e HK2 (iUCB di 40 ng / mg) sono in grado di aumentare in maniera significativa la produzione di ROS intracellulare ($p < 0,05$), cosa che invece non avviene nelle cellule epatiche. Misurando l'attività antiossidante attraverso un saggio definito Anti Oxidant Power 1 (AOP1) della nuova tecnologia Light-Up Cell System (LUCS), si sono ottenuti i seguenti EC_{50}: 21 μM (iUCB tra 5,4 e 21 ng / mg) per le cellule HepG2, 0,68 μM (iUCB tra 3,3 e 7,5 ng / mg) per le SH-SY5Y, 2,4 μM (iUCB tra 3 e 6,7 ng / mg) nelle cellule HK2 e 4 μM (iUCB tra 4,7 e 7,5 ng / mg) nelle cellule H5V. Questo ha confermato che il metabolismo della bilirubina è cellula-specifico, visto la diversa iUCB differente nelle varie linee cellulari a parità di trattamento. Dunque, è la bilirubina intracellulare e non il trattamento esterno, che determina e definisce la soglia per il suo effetto antiossidante o citotossico a livello cellulare. I risultati ottenuti sulle quattro linee usate, mostrano che iUCB intorno a 7 ng / mg di proteina agisce come antiossidante, mentre a iUCB superiore a 25 ng / mg è associata ad effetti pro-ossidanti e citotossici.

Nella seconda parte del lavoro ci siamo focalizzati sullo studio degli effetti dati da una lieve iperbilirubinemia (condizione pre-esistente e duratura nel tempo, che caratterizza la colonia di ratti Gunn così come i soggetti affetti dalla sindrome di Gilbert) e dal "priming" della bilirubina (priming inteso come trattamento con la bilirubina prima dell'esposizione delle linee cellulari al danno metabolico) in modelli *in vitro* di aterosclerosi e nefropatia diabetica. Diverse pathways sono modulate dalla bilirubina e possono spiegare molte delle sue azioni protettive contro la patogenesi delle malattie cardio-renali e metaboliche. La fibrosi delle cellule epiteliali tubulari, l'apoptosi dei podociti, lo stress del reticolo endoplasmatico (ER-stress) e l'infiammazione sono le principali vie attivate rispettivamente nella DN e nell'aterosclerosi e che sono state oggetto del nostro studio. Tutti gli esperimenti sono stati eseguiti sia su cellule primarie endoteliali da aorta e su podociti primari ottenuti da ratti Gunn sia omozigoti iperbilirubinemici jj che eterozigoti normobilirubinemici Nj. Le cellule endoteliali primarie sono state esposte ad acido palmitico (PA) mentre i podiciti primari ad angiotensina II (Ang II). I risultati sono stati poi validati sulle cellule immortalizzate H5V e HK-2 esposte agli stessi agenti di danno prima o dopo un trattamento con bilirubina. In entrambi i modelli di cellule primarie, abbiamo osservato che la vitalità delle cellule provenienti da ratti Gunn iperbilirubinemici jj era significativamente superiore alla vitalità di quelle provenienti da ratti Gunn normobilirubinemici Nj a qualsiasi dose dell'agente tossico usato. Si è dimostrato che la bilirubina attenua il rilascio della citochina IL-6 e l'induzione di CHOP sia nelle cellule endoteliali aortiche primarie endoteliali che nelle cellule endoteliali immortalizzate H5V. I podociti primari provenienti da ratti Gunn iperbiliruninemici jj, dopo il trattamento con Ang II per 24 h, hanno mostrato una minore frammentazione del DNA (TUNEL assay), minor induzione della forma attiva della caspasi-3 e della forma attiva di PARP rispetto ai podociti primari di ratti Gunn normobilirubinemici Nj. Studiando il possibile meccanismo responsabile dell'effetto anti-fibrotico e anti-apoptotico della bilirubina, abbiamo osservato che i podociti jj mostravano una maggiore espressione basale di LC3 II rispetto a quelli Nj. In più si è visto che nelle cellule HK2, l'induzione da Ang II di HIF-1α e LOXl2 è stata significativamente ridotta solo dal pretrattamento di bilirubina e non dal post-trattamento.

Infine, nella terza parte di questo lavoro, grazie alla collaborazione con il Prof. Sartorio dell'Istituto Auxologico, ci siamo focalizzati sull'associazione tra i livelli di bilirubina sierica, la prevalenza di NAFLD e MetS. L'associazione tra livelli di bilirubina totale, età, stadio puberale, dati antropometrici, clinici e di laboratorio è stata valutata in uno studio trasversale retrospettivo condotto su 1672 bambini e adolescenti estremamente obesi (BMI medio di 36). Si è visto che vi è una correlazione positiva tra il livello di bilirubina totale e l'età nella popolazione totale e questa aumenta in base alla fase puberale. Mentre si ha una debole correlazione negativa per quanto riguarda gli altri markers esaminati, tra cui trigliceridi alti, rapporto vita / altezza, insulina, HOMA e proteina C-reattiva (PCR). Tuttavia, non è stata rilevata alcuna relazione significativa tra la bilirubina totale sierica, Mets e NAFLD. Sebbene la maggior parte delle associazioni fossero statisticamente significative, non possono essere considerate biologicamente rilevanti sulla base della dimensione dell'effetto sottostante. Anche se apparentemente in contrasto con le precedenti pubblicazioni, i nostri dati rafforzano l'osservazione che i livelli di bilirubina sierica, anche nei loro range normali, potrebbero avere associazioni graduali con la prevalenza di MetS e NAFLD in giovane età, quando la disregolazione metabolica è nella sua fase iniziale, ma non nella popolazione estremamente obesa.

Collettivamente, i dati ottenuti in questo lavoro sottolineano i duplici effetti che la bilirubina può avere in diversi sistemi *in vitro* e il suo ruolo emergente e positivo nei confronti dello sviluppo di patologie che interessano diverse vie di segnalazione cellulare. Nello specifico, il nostro lavoro ha definito le soglie intracellulari di bilirubina non coniugata che determinano il passaggio tra gli effetti antiossidanti e pro-ossidanti della bilirubina stessa. La concentrazione intracellulare di UCB di circa 7 ng / mg di proteine si è vista avere attività antiossidanti, mentre le concentrazioni intracellulari> 25 ng / mg di proteine provoca effetti pro-ossidanti e citotossici. Inoltre i nostri dati hanno mostrato come la condizione persistente di una lieve iperbilirubinemia che si protrae per tutta la vita (come avviene nei soggetti Gilbert) e il priming della bilirubina contribuiscono in modo significativo alla protezione contro lo sviluppo di patologie legate alla sindrome metabolica, migliorando le risposte cellulari al danno. Da ultimo, lo studio retrospettivo sulla popolazione italiana di bambini e adolescenti estremamente obesi non ha evidenziato alcuna relazione significativa tra bilirubina totale sierica Mets e NAFLD. Questo permette di porre l'attenzione sul fatto che i livelli di bilirubina sierica, anche nei loro range normali, potrebbero avere associazioni graduali con la prevalenza di MetS e NAFLD in giovane età, quando la disregolazione metabolica è nella sua fase iniziale , ma non nella popolazione estremamente obesa.

Chapter 1
Introduction

1. INTRODUCTION

1.1 Bilirubin Metabolism

1.1.1 Bilirubin production, modifications and transport

Bilirubin belongs to the tetrapyrrolic compounds superfamily and it is the end product of heme catabolism occurring mainly in the splenic reticuloendothelial system and liver Kupffer cells (Vitek, 2012). The senescent erythrocytes are the principal sources of the heme group, but not the only ones: an adult healthy person produces around 4.4 ± 0.7 mg/ Kg by body weight daily (Vítek, 2020) and although approximately 80% of this quantity derives from hemoglobin of senescent red cells, the remaining part is shared between the turnover of myoglobin (another protein containing the heme group and specialized into O_2 transport), cytochromes, and other hemoproteins such as microsomal cytochrome CYP-450 (Fevery, 2008). All together, these proteins give the 15-20% of the available substrate; lastly, the destruction of immature red blood cells in the bone marrow donates 3% of the heme group (Vitek et al., 2019a). First, the heme group is converted by the heme oxygenase 1 enzyme (HMOX, OMIM1 No.*141250) into biliverdin releasing CO, Fe^{2+}, H_2O and contemporary oxydating NADPH into NADP. This enzyme induces the opening of heme ring, the freeing of iron ion, and the formation of a tetrapyrrolic chain. Biliverdin is subsequently reduced to bilirubin by cytosolic enzyme biliverdin reductase (BLVRA, OMIM No.*109750) in presence of NADPH (**Figure 1.1**) (Vitek et al., 2019a).

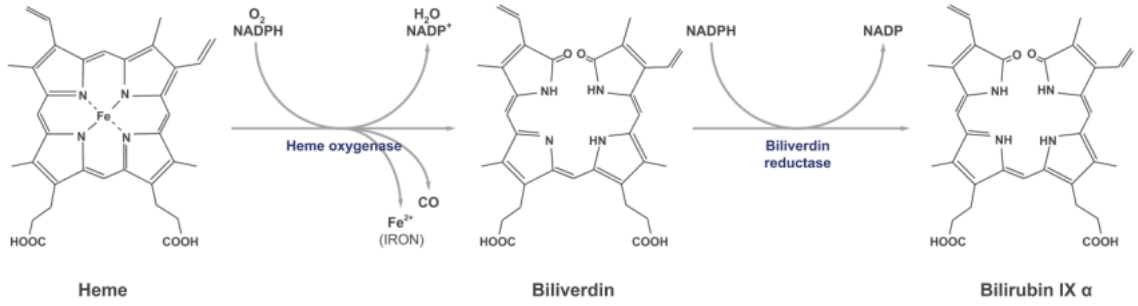

Figure 1.1 Bilirubin production. Heme oxygenase splits the cyclic tetrapyrrolic heme into biliverdin, carbon monoxide, and ferrus iron. Biliverdin is subsequently converted into bilirubin by the cytosolic enzyme biliverdin reductase. NADP, nicotinamide adenine dinucleotide phosphate; NADPH, reduced form of NADP; CO, carbon monoxide (picture from Kang et al, 2014)

Bilirubin, as non-polar molecule at physiologic pH, can be carried in the vascular bed by the binding to albumin, the most abundant protein in the blood. Due to the strong binding affinity (Ka= $7x10^7$/M) and the high concentration of albumin in human serum, most bilirubin is bound to albumin and just less than 0,1% of bilirubin remains unbound and therefore named free bilirubin (Bf). The pathophysiological properties of this pigment are related to free bilirubin fraction rather than total bilirubin (Ahlfors et al., 2009; Zelenka et al., 2016).Thanks to the albumin binding, bilirubin can reach various organs, including the liver where the pigment is actively transported inside the hepatocytes at the sinusoidal membrane via the OATP1B1, organic anion transporting polypeptide 1B1 (OMIM No.*604843)(Vítek, 2020). Once in hepatocytes cytoplasm, bilirubin is solubilized by specific binding proteins - of which the two most interesting are protein Y (ligandin, α isoform of glutathione S-transferase B) and protein Z (liver-specific fatty acid binding protein,

FABP 1) - and directed to the endoplasmic reticulum (Vitek et al., 2019a). Within the hepatocytes, unconjugated bilirubin (UCB) is further conjugated by the uridine diphosphate glucuronosyl transferase type 1 (UGT1A1) (OMIM No.*191740) located in the smooth endoplasmic reticulum, with either one or two molecules of glucuronic acid, and consequently converted into mono or bis-glucuronosyl bilirubin. UGT1A1 has a binding site for bilirubin and another one for glucuronic acid, and both these sites are located on the luminal face of the endoplasmic reticulum membrane (Erlinger et al., 2014). Conjugated bilirubin (CB), in turn, is efficiently secreted into bile, mostly by the ATP-dependent MRP2/ABCC2 transporter (OMIM No.*601107), spilled in the duodenum, and then converted by intestinal bacterial enzymes to urobilinoids, in particular urobilinogen and stercobilinogen (**Figure 1.2**) (Méndez-Sánchez et al., 2019).

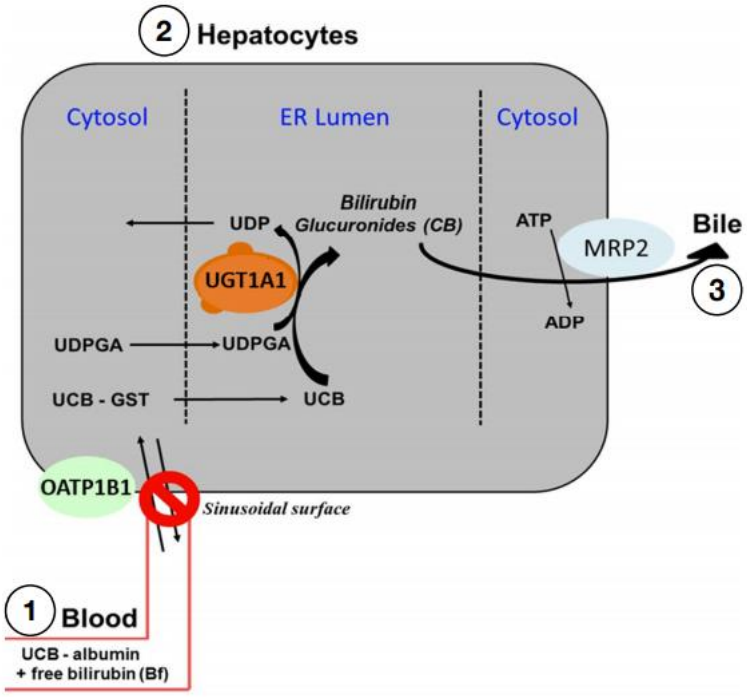

Figure 1.2 Schematic view of bilirubin transport and conjugation by hepatocytes. (1) Bilirubin binds to albumin in the blood and reach the liver (2). Within the lumen of the hepatocytes endoplasmic reticulum (ER), bilirubin is conjugated with glucuronic acid by the activity of the UDPglucuronosyltransferase (UGT)1A1 enzyme using UDP-glucuronic acid (UDPGA) as substrate (3). Conjugate bilirubin is actively secreted to bile via multi-drug resistance-associated protein 2 (MRP2) (picture modified from Vitek, Bellarosa et al. 2019)

In conjugated bilirubin, the hydrogen bonds are disrupted by esterification of propionic side chain carboxyl groups with highly hydrophilic glucuronic acid making bilirubin quite water soluble (Ostrow et al., 1994). Glucuronidation is essential for the biliary excretion of bilirubin, and deficiency in the UGT1A1 activity results in the increasing of unconjugated serum bilirubin levels (**Figure 1.3**) (Vitek et al., 2019).

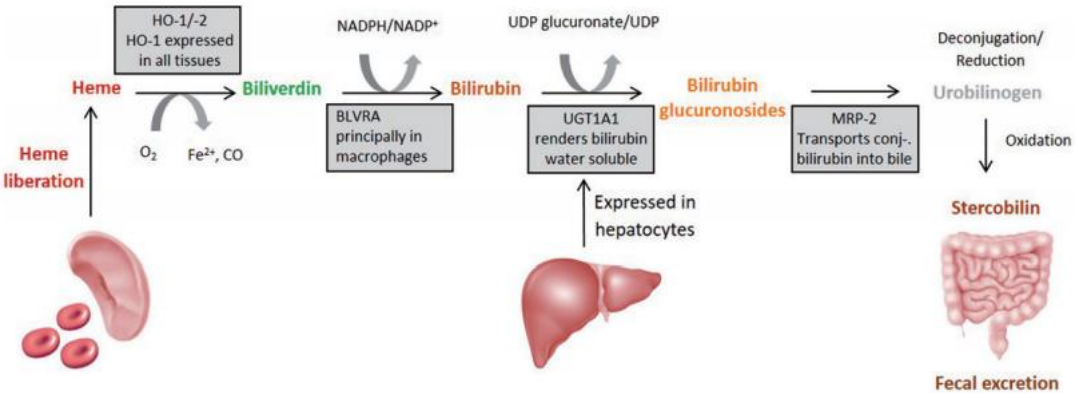

Figure 1.3 An overall of bilirubin metabolism. Bilirubin metabolism includes its production from heme group by the concerted action of HO-1 and BLVRA enzyme, its conjugation in the liver with glucuronic acid by UGT1A1 enzyme, and the subsequently biliary secretion. HMOX1/2, Heme oxygenase enzyme. BLVRA, biliverdin reductase enzyme. UGT1A1, UDPglucuronosyltransferase enzyme. UCB, unconjugated bilirubin (picture from Wagner, Shiels et al. 2018).

UCB can diffuse into any cell (Zucker et al., 1999; Zelenka et al., 2008) and although being a potent antioxidant at low concentrations, it is toxic at high concentrations. Hence, all cells must maintain the intracellular concentration of UCB below toxic thresholds. This is regulated by its intracellular metabolism (conjugation and oxidation) as well as by export out of the cells. UCB interacts mainly with three families of detoxifying enzymes: cytochromeP-450-oxygenase (CYPs)(Kapitulnik and Gonzalez, 1993; De Matteis et al., 2006), glutathione-S-transferases (GSTs)(Coles and Kadlubar, 2005), and UDP-glucuronosyl transferases (UGTs)(Nakamura et al., 2008). UCB export is another mechanism used by hepatic and non-hepatic cells to prevent its intracellular accumulation. The export proteins include ABCC2 involved in the hepatobiliary secretion of bilirubin conjugates, as well as other three ABC transporters that were demonstrated to transport of UCB: ABCB1 (also called MDR1/PGP1)(Schinkel, 1997), ABCC1 (alsocalled MRP1) (Rigato et al., 2004; Calligaris et al., 2006; Falcão et al., 2007; Corich et al., 2009) and ABCC3 (also called MRP3) (Scheffer et al., 2002). Under physiological conditions, these efflux pumps are expressed in organs involved in the elimination of endo- and xenobiotics,such as the liver and the kidney, and in epithelial tissues that protect the organs from the entry of xenobiotics, like the small intestine, testes, placenta, and blood-brain barrier (BBB) (Bellarosa et al., 2009).

1.1.2 Bilirubin as Janus bifrons

For long time, bilirubin has been considered as a useless waste product, at best, or a toxic compound, especially for central nervous system, at worst. Although its excessive accumulation is neurotoxic in neonates, more recent data assign potential protective role to bilirubin, when only mild elevated (Otero Regino et al., 2009; Vítek, 2020). The most vulnerable site to bilirubin toxicity is the central nervous system in which this pigment induces many neurological damages collectively named "Bilirubin induced neurological dysfunction (BIND)". The term "kernicterus" is referred to chronic and permanent clinical sequelae caused by severe serum hyperbilirubinemia. Free bilirubin is able to reach all brain regions and it affects much more certain type of nervous cells, e.g. Purkinje cells, rather than other types, e.g. astrocytes, by inhibiting DNA, RNA, and proteins synthesis, as well as by modifying carbohydrate metabolism (Sticova and Jirsa, 2013; Watchko and Tiribelli, 2014). However, studies published recently clearly recognized to this bile pigment numerous beneficial effects for the human body both in vivo and in vitro conditions (Vitek, 2012)(Kang et al., 2014). Since mammals spent energy and resources converting biliverdin (a non-toxic compound and relatively easy to secrete) into bilirubin (which needs to be further metabolized for its disposal via a biliary system), it is reasonable to believe that bilirubin is more than just a waste product of heme catabolism. In mammals, bilirubin is known to carry out important antioxidant properties even at physiological concentration, probably related to the redox system converting unconjugated bilirubin (UCB) into biliverdin and vice versa (Stocker et al., 1987).Notably, the biliverdin-bilirubin redox cycle, in which bilirubin is continuously formed by biliverdin reductase on one hand, and biliverdin is formed from bilirubin oxidation by reactive oxygen species (ROS) on the other hand (and heme catabolism as well), enables such low unconjugated bilirubin (UCB) concentrations to protect against vastly higher levels of hydrogen peroxide **(Figure 1.4**) (Vítek and Schwertner, 2007). One mole of albumin-unconjugated bilirubin complex can remove two moles of peroxyl radicals and contemporary bilirubin is self oxidized to its non toxic metabolic precursor, biliverdin (Stocker et al., 1987). Evidences for an *in vivo* antioxidant capacity of mild hyperbilirubinemia are provided by Gilbert subjects and Gunn rats models. Gilbert's syndrome (GS) is a benign condition, caused by a partial deficiency of hepatic bilirubin UDP glucuronosyl transferase (UGT1A1), without any signs of liver damage (Vítek and Ostrow, 2009; Wagner et al., 2015). Even if the mechanisms of *in vivo* protection in GS remain poorly described (Bulmer et al., 2008a), the reduced urinary excretion of bilirubin oxidation products (Vítek et al., 2007) and circulating advanced glycation end products (Kalousová et al., 2005) suggest that bilirubin protects from macromolecule modification *in vivo*. Furthermore, high concentrations of unconjugated bilirubin are associated with reduced markers of lipid and protein oxidation and this provides a unique opportunity to reveal the physiological importance of bilirubin, because the markers are related to future CVD mortality, which is reduced in GS (Vítek et al., 2002a). Gunn rats represent a well described animal model to study not only the toxic effects of hyperbilirubinemia in newborns (Vítek and Ostrow, 2009; Gazzin et al., 2012), but also the protective effects of hyperbilirubinemia in adults (Lanone et al., 2005; Ollinger et al., 2005; Pflueger et al., 2005; Vítek and Ostrow, 2009; Zelenka et al., 2012). Mildly elevated levels of bilirubin, in concentration comparable to those of Gilbert subjects and Gunn rats, decrease the mitochondrial and cytoplasmic reactive oxygen species (ROS) levels thus modulating the cellular ROS homeostasis in *in vitro* models of human and rodent cells (Zelenka et al., 2016) and protect against

various oxidative stress-mediated and metabolic diseases including cardiovascular diseases (CVD), type 2 diabetes, and/or metabolic syndrome (MetS) (Vítek, 2012).

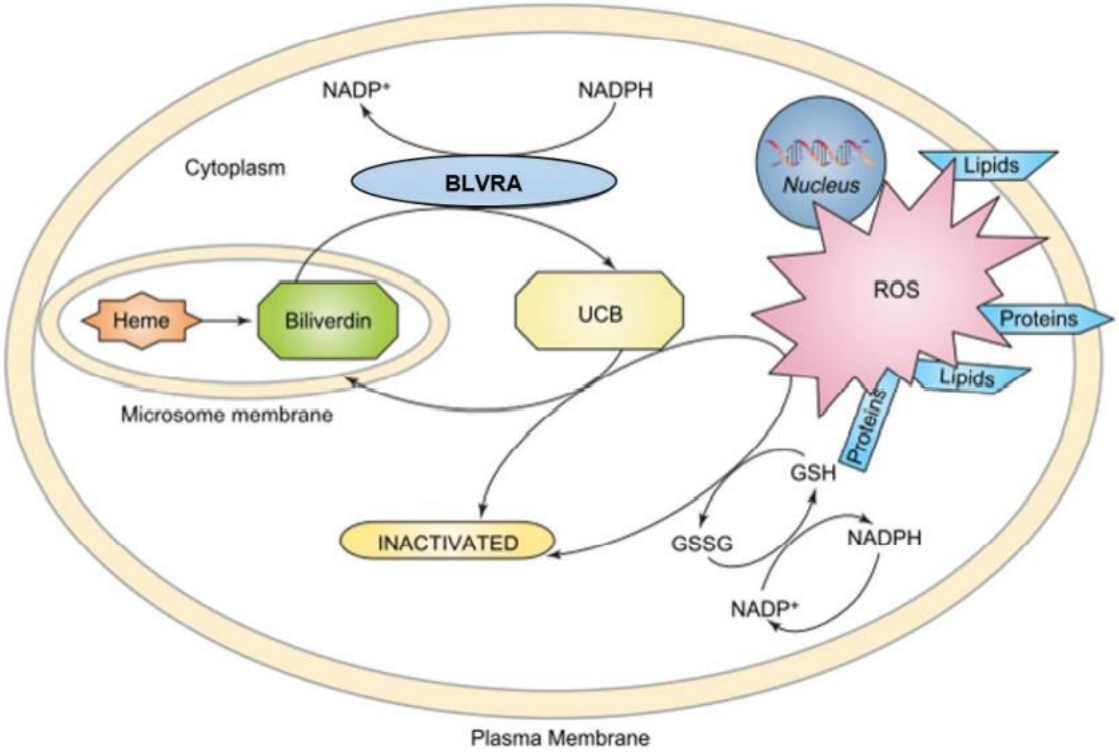

Figure 1.4 The antioxidant role of biliverdin-bilirubin redox cycle. Biliverdin is formed not only during the heme catabolism by heme oxygenase 1 enzyme but also by reactive oxygen species (ROS) which are able to oxydate UCB. After that, biliverdin is reduced to bilirubin by biliverdin reductase enzyme (BLVRA). This cycle is comparable to the glutathione one: these two cycles provide antioxidant compounds. NADPH, nicotinamide adenine dinucleotide phosphate; UCB, unconjugated bilirubin. (picture from Rigato et al., 2005).

Moreover, bilirubin is more effective than vitamin E in preventing the autoxidation of vitamin A, ultra-violet light induced autoxidation of linoleic acids, and other unsaturated fatty acids (Vítek and Schwertner, 2007). Among the beneficial properties of bilirubin is that of anti-inflammatory agent; indeed, mild hyperbilirubinemia is shown to have anti-complement action thus protecting tissues against inflammatory damage and inducing faster resolution of inflammation event (Stec et al., 2016; Hinds and Stec, 2019). It has been reported that albumin, in inflammatory exudates, carries bilirubin across the vascular wall into the sites of potential oxyradical damage by phagocytic cells (Vítek and Schwertner, 2007). Despite toxic concentrations of bilirubin induce endoplasmic reticulum (ER) stress (Qaisiya et al., 2017), mildly elevated levels are known to attenuate ER stress, as well as to be a ligand for peroxisome proliferator-activated receptor-α (Kang et al., 2014; Vitek et al., 2019). Such extensive and powerful effects of bilirubin do not seem probable without its affecting gene expression and cell signaling pathways. Bilirubin is known to activate various nuclear and cytoplasmic receptors, e.g hepatic nuclear receptors such as the aryl hydrocarbon receptor, the constitutive androstane receptor, and other signaling molecules, including fatty acid binding proteins 1 (FABP 1). All these bilirubin targets have broad metabolic effects, which in turn may offer protection against obesity, diabetes mellitus, diabetic nephropathy,

and other metabolic disorders. The mostly experimental data are supported by clinical evidences (Vítek, 2020).

1.1.3 Gilbert syndrome

Gilbert syndrome (GS) (OMIM No#143500) is a benign condition characterized by mild unconjugated hyperbilirubinemia occurring without any liver structural defects or overt hemolysis. The prevalence of Gilbert syndrome is about 8-10% worldwide and the prognosis is excellent (Wagner et al., 2018). While unconjugated bilirubin (UCB) levels are about 0,8 mg/dL in normal subjects, patients affected by Gilbert syndrome show mild unconjugated hyperbilirubinemia in the range of 1.2-6.0 mg/dL and discontinuous jaundice trigged by stress, alcohol, infections, prolongated fasting, fever, and strenuous exercise (Kang et al., 2014; Erlinger et al., 2014). In subjects with Gilbert syndrome, the activity of UGT1A1 enzyme (OMIM* 191740) is up to 30% that of normal healthy people (Danoff et al., 2004) and the most common molecular defect consists in an extra di-nucleotide sequence, TA, inside the promoter TATA box of its locus. The resulting genotype is designed A(TA)7TAA (instead of the wild type A(TA)6TAA) or UGT1A1*28 (**Figure 1.5).** Moreover, A(TA)5TAA, A(TA)8TAA, and some coding region mutations are much less common molecular defects to be found in the general population. A total of 130 UGT1A1 mutations have been identified to date. All these defects are inherited as an autosomal recessive disorder with the vastly differing prevalence in individuals of different ethnicities (Erlinger et al., 2014; Wagner et al., 2018). Since the molecular defect affects the conjugation step in the bilirubin metabolism, the mild hyperbilirubinemia in Gilbert syndrome regards the unconjugated bilirubin form.

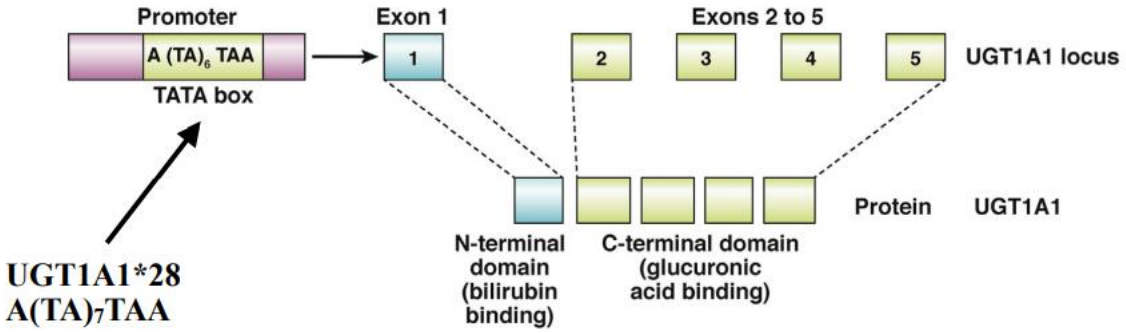

Figure 1.5 A schematic representation of the UGT1A1 locus and UGT1A1 protein. The most common polymorphism related to Gilbert syndrome is an addition of an extra nucleotide sequence, TA, within the promoter TATA box. This addition affects the UGT1A1 protein activity resulting in the accumulation of unconjugated serum bilirubin levels. (picture modified from Erlinger et al., 2014).

UGT1A1 variants resulting in mild hyperbilirubinemia may give a genetic advantage by reducing prevalence of metabolic syndrome, including obesity, overweight, diabetes type II, certain cancers, and cardiovascular diseases (CDV), whose prevalence is increasing worldwide (Wagner et al., 2018). For these reasons, it is conceivable that the high worldwide frequency of homozygous genetic variants of UGT1A1 gene might be due in part to an evolutionary advantages (Erlinger et al., 2014). Modulation of bilirubin levels may be an attractive issue to work on for metabolic

diseases treatment and/or prevention (Erlinger et al., 2014). Although Gilbert syndrome is known as benign condition, the metabolism of some drugs undergo to glucuronidation may be affected in these patients, being UGT1A1 an hepatic enzyme; e.g. non-steroidal inflammatory drugs, statins, and human immunodeficiency virus protease inhibitors. The reduced glucuronidation capacity of the hepatocytes can result in severe toxicity for the organism (Erlinger et al., 2014).

1.1.4 Gunn Rats

Gunn rat is a mutant strain of Wistar rat originally described by Gunn (1938) exhibiting a lifelong severe unconjugated hyperbilirubinemia, evident immediately after birth, as a result of the absence of hepatic UDP-glucuronosyltransferase 1A1 (UGT1A1) activity (Iyanagi, 1991). Experiments in Gunn rats have provided important insights into physiological, biochemical, and molecular mechanisms of bilirubin conjugation and disposition. The Gunn rat is a natural model for bilirubin encephalopathy (Gunn, 1944; Schutta and Johnson, 1967), and much of the knowledge of bilirubin toxicity and its treatment has come from studies performed in Gunn rats (Vítek and Ostrow, 2009; Gazzin et al., 2012). However, in recent years, Gunn rats was also utilized to study the protective effects of hyperbilirubinemia in adults (Lanone et al., 2005; Ollinger et al., 2005; Pflueger et al., 2005; Vítek and Ostrow, 2009; Zelenka et al., 2012). The lack of UGT1A1 is due to a deletion of one guanine base in exon IV which generates a frameshift resulting in a premature codon in mRNAs coding all UGT1 isoforms. This termination codon leads the production of truncated UGT1A1 proteins lacking 116 amino acids at the COOH terminus and rapidly degraded due to its high instability. For this reason, although the UGT1A1 mRNA is expressed in both Gunn rats and normal Wistar rats, the corresponding protein is completely absent from liver microsomes of Gunn rats (Emi et al., 2002). This molecular defect is inherited as an autosomal recessive trait and the hyperbilirubinemic homozygous Gunn rats (jj) maintain serum bilirubin concentrations close to the upper limit of Gilbert subjects showing also increased bilirubin levels in tissues and organs for their entire lives. UCB concentration in hyperbilirubinemic homozygous Gunn rats (jj) serum (approximately from 2,42 to 7.36 mg/dl) (Boon et al., 2012; Vianello et al., 2018) overlaps with elevated bilirubin concentrations seen in Gilbert subjects (Vítek et al., 2002b; Bulmer et al., 2008b; Boon et al., 2012).

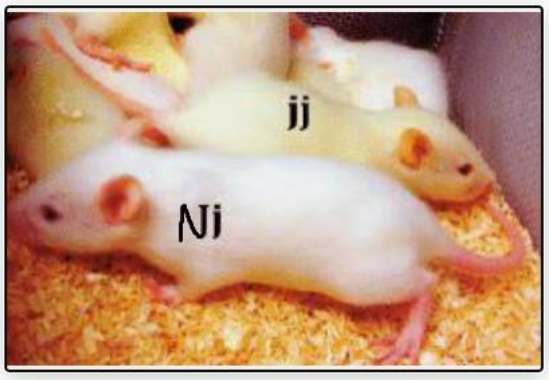

Figure 1.6 Gunn rats colony. Hyperbilirubinemic homozygous Gunn rats (jj) show jaundice (yellow hair) while normobilirubinemic heterozygous Gunn rats exhibit normal white hair (Nj).

Conversely, their heterozygous siblings (Nj) manifest only a short period of mild neonatal jaundice followed by bilirubin normalization for the rest of their lives (Iyanagi, 1991; Zelenka et al., 2016).

Zelenka et al. developed a highly sensitive method for quantitative determination of bilirubin in biological fluids and tissues from Gunn rats by HPLC analysis (Zelenka et al., 2008). Comparing the unconjugated bilirubin concentrations in various organs and tissues of the two Gunn rat genotypes, it is evident a substantially higher UCB level in hyperbilirubinemic adult Gunn rats (jj) compared to their normobilirubinemic heterozygous littermates (Nj) in all investigated organs and tissues (Table 1.1) (Zelenka et al., 2008).

Table 1.1 Bilirubin concentration in various organs and tissues of hyperbilirubinemic (jj or RHA/jj) and normobilirubinemic Gunn rats (Nj or RHA/Jj) (table from Zelenka, Lenicek et al. 2008).

Tissue	RHA/jj, $n=3$ (nmol/g) (median, 25–75% range)	RHA/Jj, $n=3$ (nmol/g) (median, 25–75% range)	Ratio (jj/Jj)
Liver–UCB	88 (73–91)	0.70 (0.65–0.75)	126
Liver–TBIL	N.D.	1.6 (1.4–1.7)	N.D.
Liver–CBIL	N.D.	0.87 (0.72–0.97)	N.D.
Brain	3.0 (2.7–3.2)	0.089 (0.08–0.09)	34
Myocardium	21 (20–24)	0.16 (0.15–0.18)	131
Visceral fat	12.1 (11.5–12.4)	0.047 (0.04–0.05)	255
Kidney	33 (31–43)	0.23 (0.19–0.24)	144
Spleen	16.0 (14.9–16.1)	2.9 (2.3–6.5)	5.5
Testis	11.7 (11.7–14.8)	0.32 (0.29–0.33)	37
Blood serum	179 (164–190)	0.46 (0.45–0.51)	389

The variability in unconjugated bilirubin (UCB) levels among tissues in hyperbilirubinemic homozygous rats is most likely due to differences in production, uptake, intracellular binding, conjugation, oxidation, and excretion of bilirubin. Bilirubin content in jj kidneys are 144 fold higher than that in Nj kidneys (Zelenka et al., 2008). Moreover, the comparison of metabolic parameters of 12-month-old hyperbilirubinemic Gunn rats and their normobilirubinemic heterozygous siblings delineates an interesting overview demonstrating how the total body weight and the gastrocnemius muscle weight are comparable, while the weight of the visceral body fat is significantly reduced in hyperbilirubinemic Gunn rats compared to normobilirubinemic ones (Zelenka et al., 2016). The weight of a visceral body fat is associated with pro-inflammatory effects and increased mortality (Finelli et al., 2013) and this difference correlates well with the lower serum leptin levels [ng/mL] in the Gunn rats (**table 1.2).**

Table 1.2 Comparison of metabolic parameters of 12-month-old hyperbilirubinemic Gunn rats and their normobilirubinemic heterozygous siblings (n=5 in each group).
Bilirubin concentration [μM] and visceral fat weight [gr] are not comparable between the two groups (table from Zelenka, Dvorak et al.2016)

Parameter	Normobilirubinemic	Gunn	p value (t-test)
Bilirubin (μM)	1.5 ± 0.4	75 ± 18	*0.001
Body weight (g)	309 ± 55	298 ± 33	0.67
Gastrocnemius muscle (g)	2.2 ± 0.2	2.0 ± 0.3	0.22
Visceral fat (g)	6.3 ± 2	3.2 ± 1	*0.01
Feed/day (g)	10 ± 2	10 ± 3	0.8

*Significant difference between normobilirubinemic and Gunn rats.

Lastly, it was demonstrated that the mildly elevated levels of bilirubin potently decrease the mitochondrial and cytoplasmic ROS levels, thus modulating the cellular ROS homeostasis in human and rat cells and this effect was associated with decreased accumulation of visceral fat, lower markers of chronic inflammation, better glucose tolerance, improved status of cellular senescence, and protection against mitochondrial dysfunction in aged hyperbilirubinemic animals (Zelenka et al., 2016).

1.2 Diabetic Nephropathy

Diabetic nephropathy (DN) is a complication of diabetes mellitus and it is the leading cause of end-stage renal disease, as well. Up to 40% of type II diabetic patients develop diabetic nephropathy and the incidence of this metabolic disorder is increasing rapidly worldwide (Slyne et al., 2015). Clinically, proteinuria (excess of serum proteins in the urine) is the main index of diabetic nephropathy; nevertheless it is not an accurate method to evaluate its severity or prognosis since many patients develop diabetic nephropathy and renal disorders without prior proteinuria (Qi et al., 2017). Diabetic nephropathy is also characterized by hypertension, renal failure leading to edema, and uremic symptoms (Bose et al., 2017).

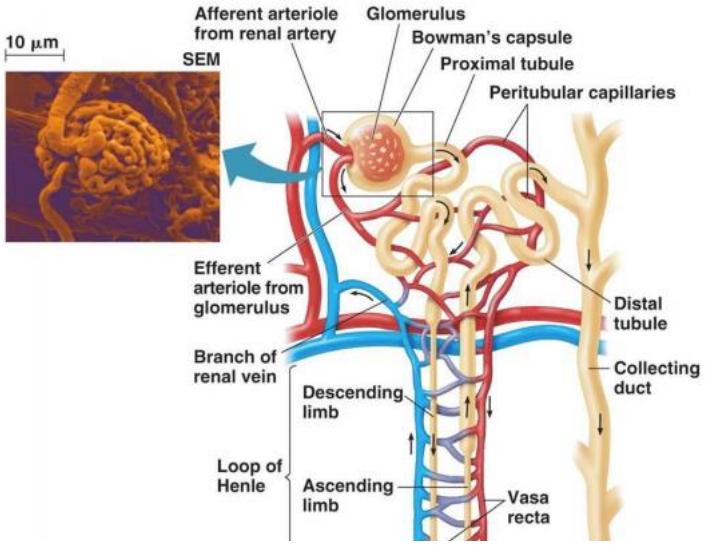

Figure 1.7 Schematic view of a nephron (picture from Pearson Education Inc 2008 – Pearson Benjamin Cummings)

The functional unit of the kidney is the nephron, consisting of glomerulus, proximal tubule, Henle's loop, and distal convoluted tubule (**Figure 1.7**). A fine circulatory system let blood to reach the glomeruli, where plasma is filtered into the Bowman's capsule. The human kidney can filter 180 liters of blood through its glomeruli and produce about 2 liters of urine daily (Mullins et al., 2016). In case of diabetic nephropathy, both tubular and glomerular elements of nephrons are affected leading to glomerulosclerosis, tubulointerstitial fibrosis (TIF), and tubular atrophy and resulting in the loss of normal renal architecture and renal filtration capacity (**Figure 1.8**) (Mullins et al., 2016).

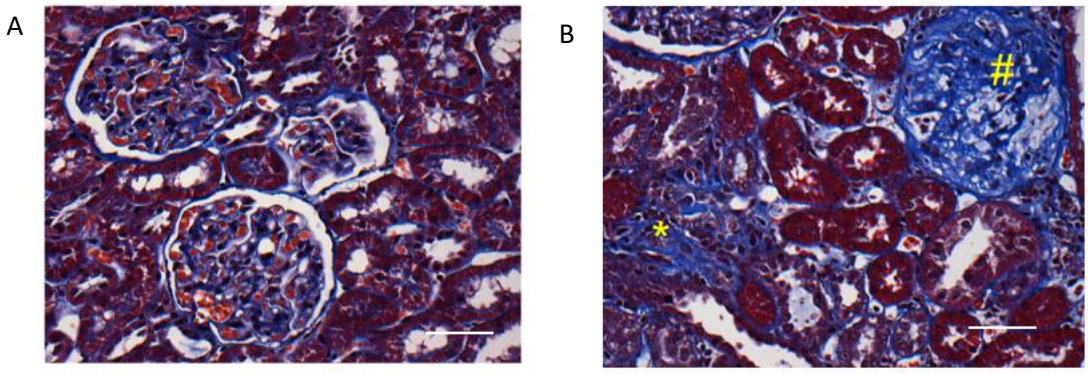

Figure 1.8. The pathophysiological processes linked to kidney disease. **A)** The glomerular and tubular architecture of a normal adult rat kidney**, B)** glomerulosclerosis (#) and tubulointerstitial fibrosis (*) in a 12-month-old rat exhibiting end-stage renal disease (picture from Mullins, Conway et al. 2016).

1.2.1 Mediators of Diabetic Nephropathy

Diabetes affects all kidney cells type including endothelial cells, tubular epithelial cells, and podocytes. The pathogenesis of diabetic nephropathy has been intensely investigated and the roles of various mechanisms has been established, including those of high glucose and advanced glycation end-product (AGEs) exposure, the polyol pathway activation, glomerular hyper-filtration, renin–angiotensin–aldosterone system (RAA) signaling, reactive oxygen species (ROS) increase, diacylglycerol (DAG)/protein kinase C (PKC) pathway activation and TGF-β signaling. The final effects of diabetic nephropathy involve endothelial injury, tubulointerstitial fibrosis, and podocytes detachment and apoptosis (**Figure 1.9**) (Maezawa et al., 2015).

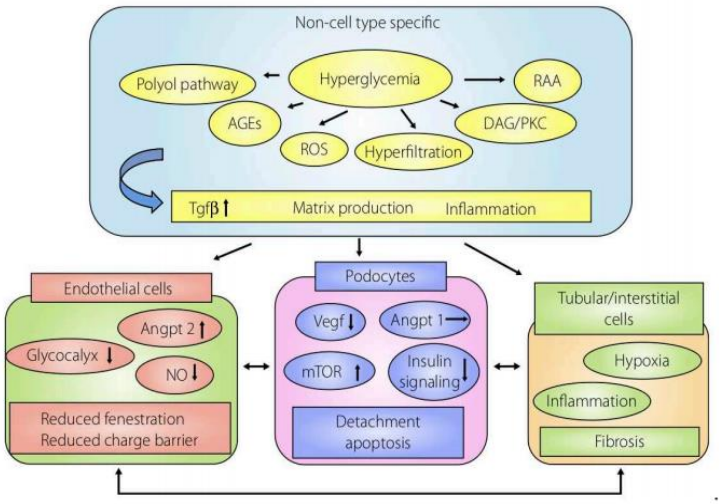

Figure 1.9 Schematic diagram on pathogenesis of diabetic nephropathy (picture from Maezawa, Takemoto et al.2015).

All these pathophysiological mediators have been commonly used in *in vitro* modeling of diabetic nephropathy (**Figure 1.10**) (Slyne et al., 2015).

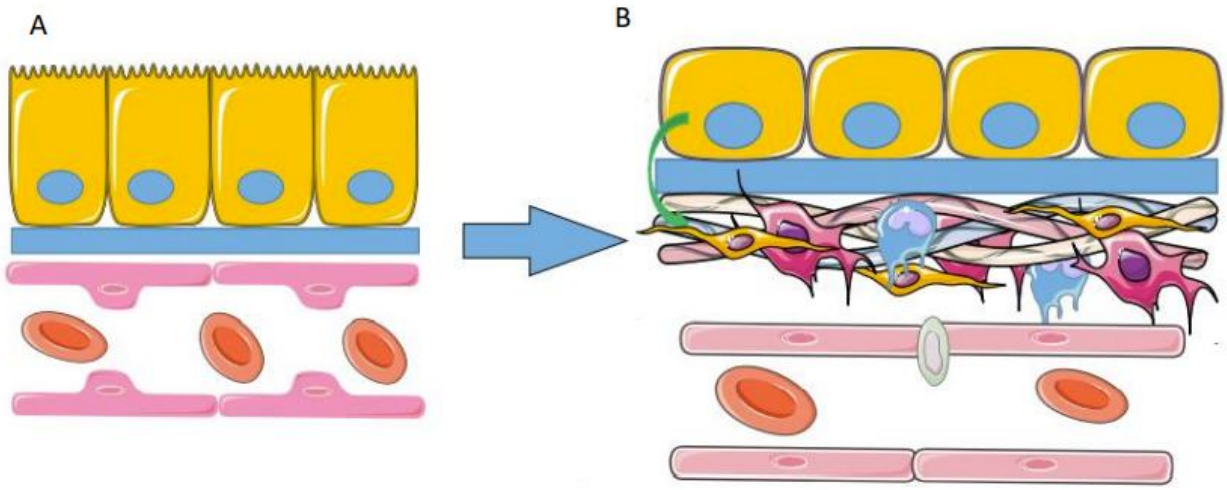

Figure 1.10 The pathophysiological processes linked to renal tubular dysfunction. A) The normal conditon with a well-organized epithelium and well defined basal membrane B) Tubulointerstitial fibrosis (TIF) is characterized by interstitial matrix deposition, inflammation, fibroblast activation and recruitment, microvascular rarefaction, flattened tubular epithelium, thickness of the tubular basement membrane, and tubular cell loss (picture modified from Mullins, Conway et al. 2016).

Angiotensin II signaling

On exposure to glucose, proximal tubular cells elaborate vasoactive hormones, including angiotensin II and injurious cytokines such as TGF-β, as well as extracellular matrix proteins. In turn, angiotensin II may further amplify the stimulus to fibrogenesis in the renal tubulointerstitium. In addition to these mostly direct influences, the renal tubule, particularly its proximal segment, is exposed to glomerular effluent. In this context, tubulointerstitial fibrosis is thought to be a coordinated and dynamic process (Gilbert and Cooper, 1999).

Advanced Glycation End Products (AGEs) signaling

Hyperglycaemia is a major factor involved into diabetic tubular damage. Among the many events occurring in diabetic nephropathy as a result of hyperglycaemia is the formation of advanced glycation end products (AGEs)(Slyne et al., 2015). AGEs constitute a diversified category of modified proteins, lipids, and nucleic acids formed by non-enzymatic glycation and oxidation processes, called Maillard reaction; the first steps of glycation and oxidation lead to the formation of Schiff bases and Amadori's products favoured at alkaline pH values and in presence of phosphate ions. Despite being relatively stable, the Amadori's products can undergo rearrangements generating AGEs stable products (Gallo et al., 2014)(Vistoli et al., 2013). AGEs have pathogenic importance in age-related chronic diseases due to contribution in promotion of oxidative stress, inflammation and apoptosis. Further, they have been proved as reliable markers in diabetes mellitus (Kheirouri et al., 2018). AGEs mediate their effects through two mechanisms:

on one hand, AGEs alter the functions and mechanical properties of tissues due to their accumulation and induction of crosslinks with intracellular and extracellular matrix proteins; on the other hand, through the binding with specific receptors (RAGEs), they induce the production of reactive oxygen species (ROS) and pro-inflammatory mediators (Gallo et al., 2014). AGEs exposure causes activation and increased expression of a wide number of mediators involved in diabetic nephropathy. For instance, the treatment of proximal tubular epithelial cell line (HK-2) with AGEs-albumin resultes in the significantly increase of proinflammatory cytokines IL-6 production, both at mRNA and protein level, and significantly increase of macrophage migration ability(Gallo et al., 2014).

1.2.2 Tubular dysfunction in diabetic nephropathy

Although glomerular components have been considered as the main leaders of the diabetic nephropathy, recent evidences are showing an important role of the tubular part in the progression of the disease. Given that the tubulointerstitial component represents up to 90% of the renal parenchymal, it is not surprising its crucial involvement (Slyne et al., 2015). Histologically, early diabetic kidneys show tubular hyperplasia which precedes TGF-1β mediated hypertrophy while, in the advanced renal disorder, tubulointerstitial atrophy and fibrosis are evident. Many evidences suggest that TIF is a good determinant of moderate - to severe renal injury and correlates with the progression of this disease better than the glomerular damage(Maezawa et al., 2015)(Slyne et al., 2015). In diabetic kidney the most significant damage at tubular epithelium level is related to massive pro-fibrotic and pro-inflammatory factors. Under long term chronic injury, such as unbalanced diabetes, tubular epithelial becomes flat, some cells arrest their cell-cycle leading atrophy of tubules and the tubular basal membrane becomes thicker. Hypoxia condition (mainly through HIF-1α signaling) and pro-fibrotic pathways (e.g TGFβ), and pro-inflammatory signals (e.g. IL-6) induce massive fibroblast activation and recruitment, extracellular matrix production and apposition, inflammatory cell infiltrate leading tubulointerstitial fibrosis. Moreover, injury activates endothelium and eventual capillary rarefaction leading increased apoptosis and hypoxia (Mullins et al., 2016) (**Figure 1.11).** The renal tubule in diabetes is subject to both direct and indirect pathogenetic influences as a consequence of its position in the nephron and its resorptive function. On exposure to glucose, proximal tubular cells elaborate vasoactive hormones, including angiotensin II and injurious cytokines such as TGF-1β, as well as extracellular matrix proteins. In turn, angiotensin II may further amplify the stimulus to fibrogenesis in the renal tubulointerstitium. In addition to these mostly direct influences, the renal tubule, particularly its proximal segment, is exposed to glomerular effluent. In this context, tubulointerstitial fibrosis is thought to be a coordinated and dynamic process (Gilbert and Cooper, 1999).

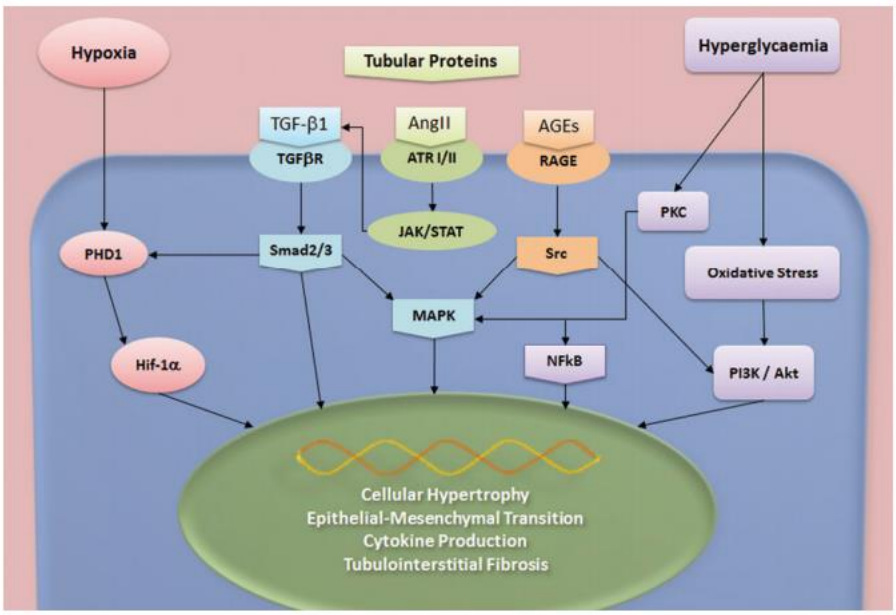

Figure 1.11 Illustration of possible pathways and interactions in mediating tubular dysfunction in diabetic nephropathy (picture from Slyne et al., 2015)

HIF-1α signaling in tubular fibrosis

A reduction in renal oxygenation occurs in most chronic kidney diseases (CKD) irrespective of etiology (Haase, 2012). Associated with this hypoxia condition, the increased expression of oxygen-sensitive α-subunit of hypoxia-inducible factor-1 (HIF-1) occurs in renal biopsy material from patients with chronic kidney diseases(Higgins et al., 2007). Hypoxia-inducible factor-1 is the key mediator of cellular responses to low oxygen; it is a heterodimeric transcription factor consisting of a constitutively expressed β subunit (also known as aryl hydrocarbon receptor nuclear translocator, ARNT) and an O2 sensitive α subunit. In conditions of normoxia, prolyl hydroxylase domain (PHD) enzymes hydroxylate HIF-1α and enable it to be targeted for proteasome degradation by the von Hippel-Lindau protein (pVHL), resulting in its ubiquitylation and subsequent proteasomal degradation (Higgins et al., 2007). In response to hypoxia, the hydration step does not occur and HIF-1α is stabilized. Once translocated to the nucleus, it dimerizes with HIF-1β to form the active heterodimeric factor, able to modify gene transcription by binding to specific DNA sequences, named hypoxia-response elements (HREs), and by recruiting transcriptional co-activators such as CBP/p300 (**Figure 1.12**)(Haase, 2012).

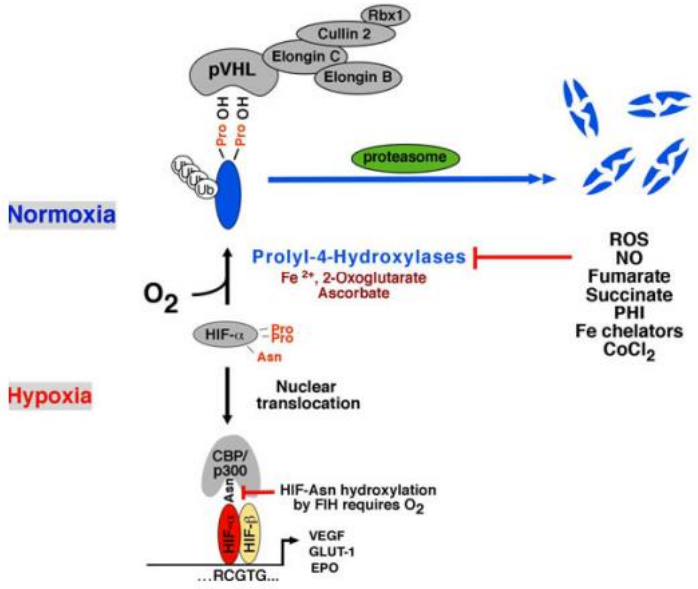

Figure 1.12 Overview of HIF signaling. Under hypoxic stimulation, HIF1-α can translocate into the nucleus and modify gene expression (picture from Haase 2012).

HIF-1α is continuously synthesized and rapidly degraded under normoxia, keeping HIF signaling at minimal levels when oxygen tension is in normal range (Haase, 2012). HIF-1α regulates biological processes relevant for wound healing, tissue repair and fibrogenesis, including extracellular matrix synthesis and turnover, cell adhesion and migration, and epithelial to mesenchymal transition (EMT) (Haase, 2012). Among the genes regulated by HIF signaling are phosphoglycerate kinase-1 (PGK), glucose transporter-1 (GLUT1), vascular endothelial growth factor (VEGF), erythropoietin (EPO), and tissue inhibitor of metalloproteinase-1 (TIMP-1) (Haase, 2006). As mentioned above, peritubular capillary loss due to glomerular injury reduces the oxygen supply leading to chronic interstitial and tubular cell hypoxia in chronic kidney diseases. HIF-1α is expressed throughout the kidney and plays a central role in this hypoxic response of tubular epithelial cells (Kimura et al., 2008).Prolongated activation of HIF-1α signaling in renal epithelial cells enhances maladaptive responses, inducing fibrosis and tissue destruction. Renal tubular fibrosis, as well as fibrosis occurring in other tissues, is characterized by excessive deposition of extracellular matrix (ECM), including different types of collagens, hyaluronic acid, fibronectin, and proteoglycans (Xiong and Liu, 2017). In experimental models of chronic kidney diseases, HIF-1α is thought to stimulate collagen accumulation and inflammatory cells recruitment showing pro-fibrotic ability. By comparing renal biopsy material from patients with different stages of diabetic nephropathy, a statistically significant correlation of disease stage with the percentage of HIF-1α expression was found in tubular epithelial cells. These data suggest a crucial role of HIF-1α in determining disease severity, extent of fibrosis, and disease progression (Haase, 2012). While on one hand HIF-1α would appear to exert a beneficial effect on renal tissues by stimulating the expression of vasculogenic genes to maintain oxygen delivery and to protect cells from ischemia, on the other hand HIF-1α up-regulates pro-fibrotic factors, leading tissue fibrosis acceleration (Kimura et al., 2008). Inactivation of HIF-1 in proximal tubule epithelial cells resultes in reduced accumulation of collagen and macrophage, supporting the notion that HIF-1 can act as pro-fibrotic

transcription factor under chronic injury conditions(Haase, 2012). In renal epithelial cells, hypoxia stimulates collagen I synthesis, decreases matrixmetallopeptidase 2 (MMP-2) expression, and increases PAI-1, tissue-inhibitor of metalloproteinase-1 (TIMP-1), and connective tissue growth factor (CTGF) expression through HIF mediated transcriptional responses (Haase, 2012). Fibrosis may be the results of up-regulation of ECM-modifying genes, such as LOX and PAI-1, co-operation with transforming growth factor (TGF-β1), modulation of renal inflammation, or promotion of epithelial to mesenchymal transition (EMT) (Haase, 2012). The epithelial mesenchymal transition is an important cellular process associated to tubulointerstitial fibrosis development. In the context of chronic kidney diseases, renal tubular epithelial cells acquire motility and a mesenchymal phenotype by loosingapicobasal polarity. This process enables cells to migrate into the interstitium, where they would produce ECM as myofibroblasts together with resident cells (Haase, 2012). Epithelial mesenchymal transition requires the downregulation of epithelial cell markers, such as Ecadherin (E-cad), and the acquisition of mesenchymal cell markers such as α-smooth muscle actin (α-SMA), the actin isoform typical of vascular smooth muscle cells (Xiong and Liu, 2017). Lysyl oxidase (LOX and LOXL2) are transcriptional targets of HIF-1 and although they are noted for their ability to cross-link collagen (I and III) and elastin to form the fibrillar collagen fibers, they carry out intracellular functions and display various biological activities those extend beyond extracellular matrix cross linkage (Schietke et al., 2010). LOX and LOXL-2 induction by HIF-1α is thought to be involved in migration of epithelial renal cells (Halberg et al., 2009). While hypoxia is the main stimulus for HIF activation, various signaling molecules with key role in chronic renal injury pathogenesis can activate this pathway, such as angiotensin II. In this context, recent studies in renal interstitial fibroblasts propose for HIF-1 some functions downstream of a pro-fibrotic signaling cascade stimulated by angiotensin II, leading EMT and excessive collagen apposition (Wang et al., 2011).

1.2.3 Podocytes dysfunction in diabetic nephropathy

Among the main histological changes correlated to diabetic nephropathy is the deep impairment of glomerular elements, including glomerular endothelial cells and podocytes, and the development of glomerulosclerosis (Maezawa et al., 2015). Podocytes are terminally differentiated cells specialized in encasing the glomerular basement membrane (GBM). The unique morphology of these cells consists in thick primary foot processes, supported by microtubule system, and fine secondary foot processes with a core of actin filaments. These last interdigitate with each other as well as with neighbouring podocytes by a specialized intercellular junction called slit diaphragm. Slit diaphragm consists of proteins including nephrin, podocin, Cd2-associated protein and actin binding proteins (Maezawa et al., 2015). These processes enable podocytes to form a charge and size-selective barrier for proteins allowing the flux only for proteins smaller than albumin and also contributing to charge selectivity where the proteins are phosphorylated (Bose et al., 2017).For this reason, podocytes play a crucial role in maintaining the glomerular filtration barrier and preventing protein loss into the urine, and any alteration or mutation of this mechanism leads to podocytes dysfunction resulting in defective glomerular filtration along with the onset of proteinuria (**Figure 1.13**) (Bose et al., 2017)(Haley et al., 2018).

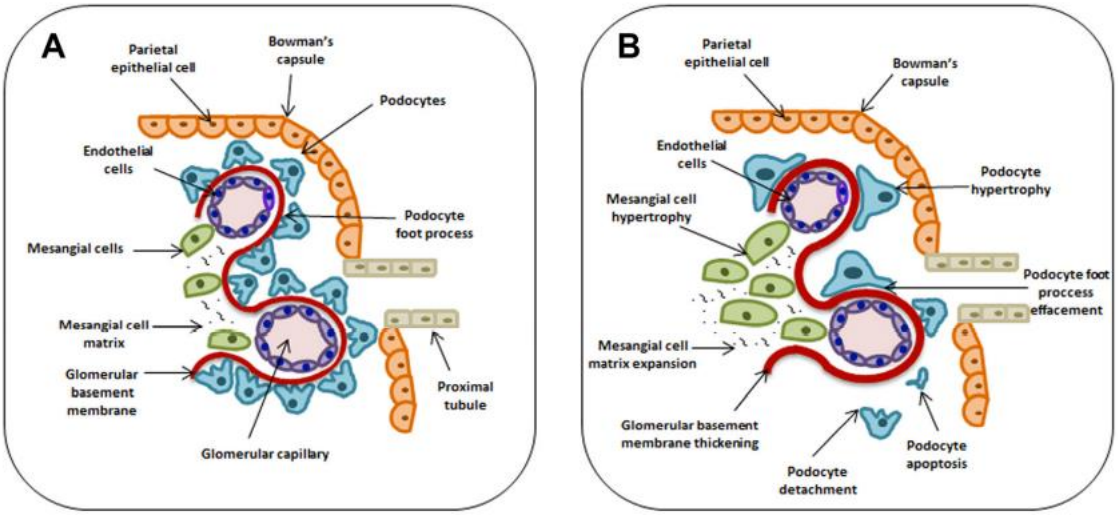

Figure 1.13 Illustration of structural elements of glomerulus. A) Normal glomerulus**; B)** glomerulus in diabetic nephropathy (picture from Bose, Almas et al.2017).

In diabetic nephropathy, the signaling of pathophysiological mediators (hyperglycaemia, advanced glycation end products (AGEs), TGF-β, and angiotensin II) affects podocytes number, structure, and functions leading to podocytes hypertrophy, podocytopenia, podocytes apoptosis, and flattening of foot processes (**Figure1.14)**(Bose et al., 2017)(Maezawa et al., 2015).Among the early key events in diabetic nephropathy is the loss of podocytes (podocytopenia).

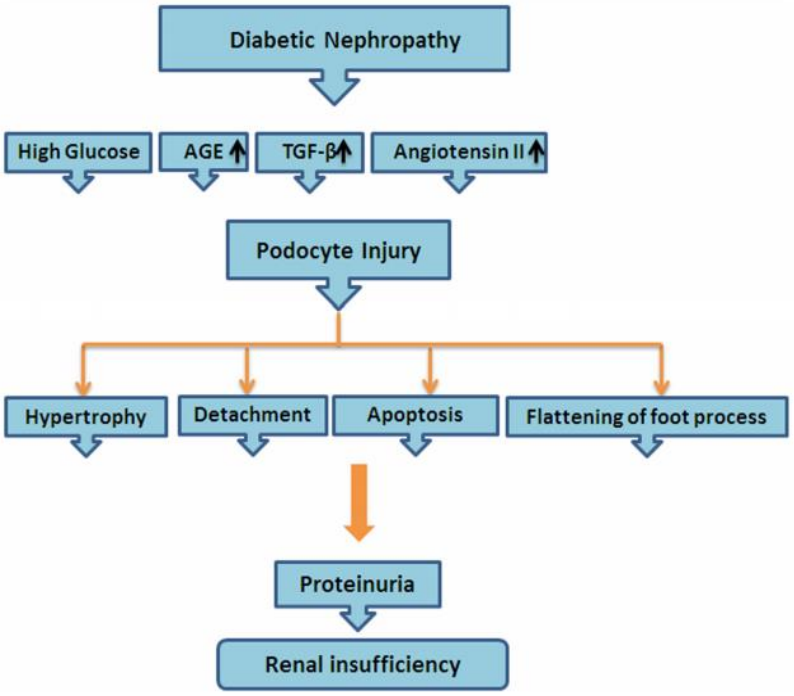

Figure 1.14 Podocyte injury and loss in diabetic nephropathy (picture from Bose, Almas et al.2017).

The mechanisms thought to cause podocytopenia are the flattening of foot processes, detachment, and apoptosis. Since podocytes does not have proliferative capacity even in normal conditions, these cells cannot oppose their loss(Maezawa et al., 2015)(Bose et al., 2017).Like tubular epithelial cells, podocytes undergo hypertrophy in order to compensate the kidney enlargement mainly due to long-term hyperglycaemia. However, unlike tubular epithelial cells, podocytes cannot proliferate and the hypertrophy seems to be the only way for these differentiated cells to compensate this process and podocytes hypertrophy is considered as a maladaptative attempt to cover denuded area of the glomerular basement membrane(Dai et al., 2017)(Lohmann et al., 2014). Podocytes apoptosis may have a crucial role in both early and late stages of diabetic nephropathy contributing to reduce further the podocytes number and the glomerular filtration capacity (Bose et al., 2017).All these changes are directly implicated in the development of proteinuria and glomerulosclerosis in diabetic nephropathy (Bose et al., 2017).Apoptosis or "programmed cell death" features include cytoplasmic shrinkage, accompanied by phosphatidylserine exposure, blebbing from the cell surface, and the formation of apoptotic bodies. Although cytoplasmic compartments display intact structure, the nucleus suffers chromatin condensation, initiated at sublamellar foci and frequently broadening to generate densely heterochromatic regions(Elmore, 2007). PARP, a 116 kDa nuclear poly (ADP-ribose) polymerase is is one of the main cleavage targets of caspase-3 *in vivo* (Nicholson et al., 1995)(Tewari et al., 1995). In human PARP, the cleavage occurring between aspartic ASP214 and glycine GLY 215 separates the PARP amino-terminal DNA binding domain (24 kDa) from the carboxylterminal catalytic domain (89 kDa) (Lazebnik et al., 1994)(Nicholson et al., 1995). PARP helps cells to maintain their viability; cleavage of PARP facilitates cellular disassembly and serves as a marker of cells undergoing apoptosis (Oliver et al., 1998).

Apoptosis in podocytes andCrosstalk between autophagy and apoptosis

Macroautophagy (simply referred to as autophagy hereafter) is a cellular process by which portions of cytoplasm, including proteins and organelles, are sequestered within doublemembrane vesicles named autophagosomes. Autophagosomes with their cargo fuse with a lysosome to form an autolysosome and the cargo is degraded by acidic lysosomal hydrolyses (**Figure 1.15**)(Zhang et al., 2014).

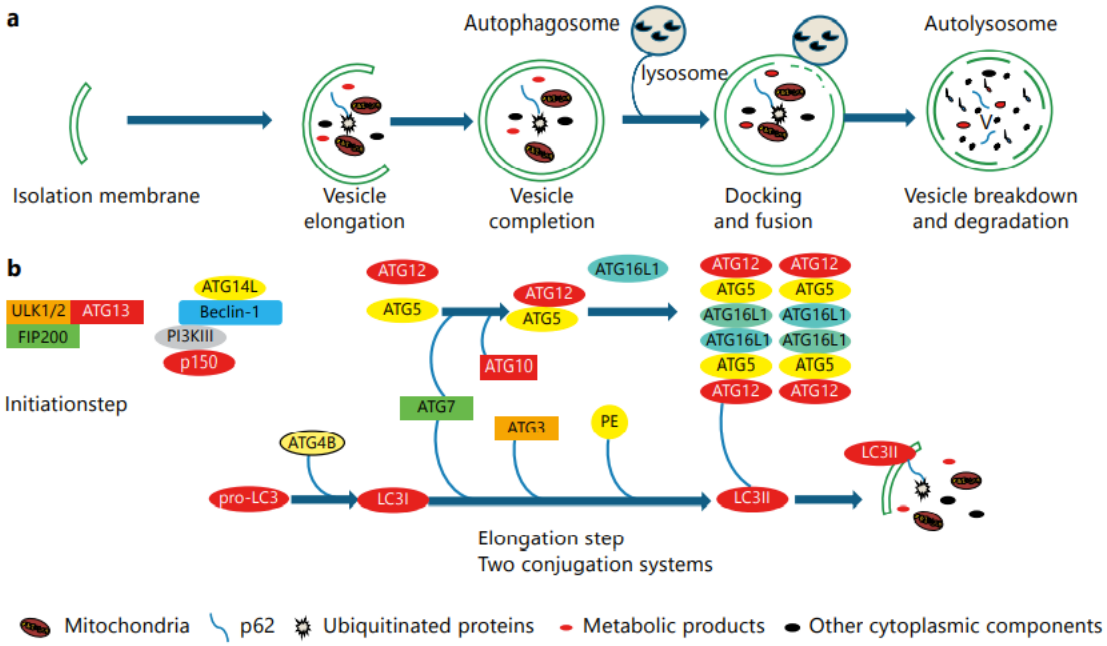

Figura 1.15 Molecular circuitry and signalling pathways regulating autophagy. a) The cellular events of autophagy proceed through several steps, including initiation/vesicle nucleation (formation of an isolation membrane or a phagophore), vesicle elongation, vesicle completion (autophagosome maturation and cargo sequestration), docking and fusion of the autophagosome with a lysosome to form an autolysosome, breakdown of the autophagosome inner membrane and degradation of the cargos inside the autolysosome for recycling**. b)** At the molecular level, Atg proteins form different complexes that function at multiple steps of autophagy. The precursor form of LC3 is cleaved by the protease ATG4B to generate LC3-I. Conjugation of PE to LC3-I forms LC3-II that is targeted into autophagosomal membrane. (picture from Zhang et al., 2014).

Podocytes homeostasis is maintained by a high level of basal autophagy under normal conditions whereas stress-induced autophagy primarily allows for an adaptive and defensive strategies (Liu et al., 2019).Podocytes are terminally differentiated and relatively long-lived cells with high levels of basal autophagy that may act synergistically with the proteasome pathway to maintain the structural and functional integrity of these cells(Zhang et al., 2014). In case of metabolic stress, the autophagic process generated amino acids and lipids useful to synthesize proteins and ATP, thus acting as a cell survival mechanism. On the other hand, despite its cytoprotective role, autophagy acts also as mechanism of death cell under some stimuli, and it is implicated in the pathogenesis of a increasing number of disease, including aging, metabolic disorders, and kidney disease (Zhang et al., 2014). Microtubule-associated protein 1A/1B-light chain 3 (LC3) is a soluble protein known as autophagosome marker and commonly used to monitory autophagy process in vivo. LC3 exists in two forms: the cytosolic form of LC3 (LC3-I) and the phospholipid associated protein (LC3-II), which is recruited to autophagosomal membranes and then degraded by lysosomal hydrolases. Thus, lysosomal turnover of the autophagosomal marker LC3-II reflects starvation-induced autophagic activity, and detecting LC3 by immunoblotting or immunofluorescence has become a reliable method for monitoring autophagy and autophagy-related processes (Hartleben et al., 2010)(Chen et al., 2010)(Tanida et al., 2008).Given that autophagy is a dynamic pathway, the number of autophagosomes is a function of the balance between the rate of their generation and the rate of their conversion into autolysosomes. In this context, autophagosome accumulation may represent either autophagy induction or a block in the autophagosome maturation or fusion with

lysosome. It is possible to distinguish among these possibilities by performing a "autophagic flux" assay (Mizushima et al., 2010). In normal adult rats, abundant LC3 protein was detected in glomeruli and in particular in podocytes (thanks to co-staining with podocalyxin, a podocyte marker) while it was much less in proximal tubules. Moreover, LC3-I was present mainly in mesangial and proximal tubular cells while LC3-II seemed to accumulate significantly in glomeruli and podocytes. Thus, podocytes display clearly high level of autophagy under basal conditions compared to tubular cells (Zhang et al., 2014). It is believed that autophagy is important in cell death decisions and could protect cells by preventing them from undergoing apoptosis (He et al., 2013)(Bhogal et al., 2012). Nevertheless, autophagy may also result in cell death called "autophagic cell death" through excessive self-digestion and degradation of essential cellular constituents under certain circumstances. Thus, it seems that the relationship between autophagy and apoptosis is complex (Maiuri et al., 2007). Recent studies highlight the renoprotective role of autophagy in podocytes in models of diabetic nephropathy; in one of these studies, it has been seen that the defective autophagy (in cultured mouse podocytes) induced by sustained high glucose is accompanied by podocytes injury, as indicated by reduced podocin expression and increased leakage of albumin (Fang et al., 2014). Furthermore, rapamycin induces autophagy on streptozocin (STZ)-induced type I diabetic mice inhibits apoptosis of podocytes (Xiao et al., 2014). Recent study demonstrated that Resveratrol (antioxidant compound) attenuates high glucose-induced apoptosis via activation of autophagy in db/db mice and podocytes (Huang et al., 2017).Fang et al. demonstrated that autophagy might act as a crucial regulatory mechanism of apoptotic cell death by modulating the balance between the pro-survival pathway and the pro-apoptotic pathway of endoplasmic reticulum stress, which might provide a novel mechanistic insight into the interface between autophagy and apoptosis in the progression of podocyte injury (Fang et al., 2014). Furthermore emerging evidences demonstrate that diabetes induces cardiomyocyte apoptosis and suppresses cardiac autophagy, indicating that the interplay between the autophagy and apoptotic cell death pathways is important in the pathogenesis of diabetic cardiomyopathy (Ouyang et al., 2014).

1.3 Atherosclerotic process in the arterial wall

Atherosclerosis is a chronic inflammatory disease caused by deposition of lipids in the medium and large arterial walls. It is one of the largest sources of morbidity and mortality in the developed world (Fazio et al., 1997). This process involves the uptake of modified lowdensity lipoprotein (LDL) cholesterol by macrophages and it is associated with a state of heightened oxidative stress and damage. It is caused by smoking, hypercholesterolemia, diabetes mellitus, hypertension, obesity, and high homocysteine levels (Stocker and Keaney, 2004). It is a silent process until the atherosclerotic lesion is destroyed by blood flow. This leads to thrombosis, which compromises oxygen supply to organs, such as the heart or the brain. Initial events are observed in the damage of the endothelium and in the accumulation and subsequent modification, aggregation, LDL-oxidation, in the intima of the arteries. Accumulation of LDL is caused by the increase in permeability of the endothelium but also by their bond to the constituents of the extracellular matrix of the intima, making longer, therefore, the stay in loco of the lipoproteins. The inflammatory response starts with the endothelium activation led by the recruitment of leukocytes in the damaged tissue. So, the endothelial dysfunction enhances the inflammatory response (Kang et al., 2014). Cytokines secretion induces a smooth muscle cell migration of the intima media. Here

they proliferate and change in the phenotype that synthesizes the extracellular matrix, with a subsequent advanced transformation of the lesion in the inflammatory reaction (**Figure 1.16**) (Kang et al., 2014). The earliest events in the development of atherosclerosis involve progressive modifications in the endothelial microenvironment. This endothelial cell activation, a complex of multi-step mechanisms, is characterized by increasing expression of adhesion molecules, which mediate the diapedesis (migration) of inflammatory and immunocompetent cells through the endothelial layer into the arterial wall. The two major subsets of adhesion molecules participating in these processes are the selectins (in particular E-selectin) and the immunoglobulin gene superfamily (in particular cell vascular adhesion molecule 1, VCAM-1, and intercellular adhesion molecule 1, ICAM-1). Nitric oxide (NO) is one of the pivotal factors involved in the prevention of atherosclerotic lesions of the endothelium. It has been demonstrated that NO plays a critical role also in vascular hyper-permeability through both NO synthases (NOSs) expression, the endothelial form (eNOS) and the inducible one (iNOS) *in* vitro (Mazzone et al., 2009). In pathological conditions, iNOS is regarded as a harmful enzyme and is proposed to be a major contributor to diseases of the cardiovascular system such as atherosclerosis (Lind et al., 2017). Bilirubin has a protective role against atherosclerosis as indicated by the blue arrows in Figure 1.4. The antioxidant effect of UCB might be exerted at multiple stages: preventing the peroxidation of lipoproteins in the intima, the oxidation of membrane phospholipids in the endothelial cells and macrophages inhibiting the trans endothelial vascular cell adhesion molecule (VCAM-1)-dependent migration of monocytes into the subendothelial space that occurs early in atherogenesis (Rigato et al., 2005).

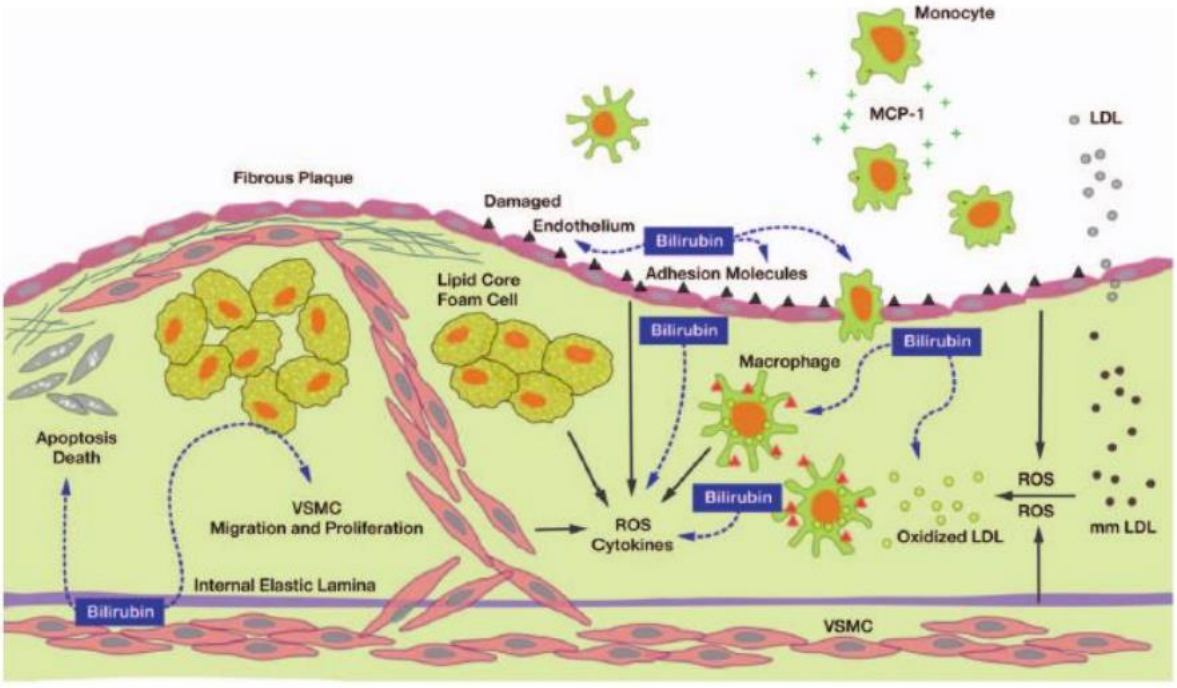

Figure 1.16 Mechanism of atherosclerotic process in arterial wall and protective role of bilirubin against atherosclerosis (Kang et al., 2014).

1.3.1 Involvement of Oxidative stress, ER-stress-inflammation axis in endothelial cells

Oxidative stress, inflammation and ER-stress are closely related events and they are associated with MetS manifestations, including pathogenesis of atherosclerosis, diabetes (T2DM), and other different cardiovascular diseases (CVD) (Roberts and Sindhu, 2009). Oxidative stress occurs when production of oxidants or reactive oxygen species (ROS) exceeds local antioxidant system. ROS include free radicals such as superoxide (O_2^-), hydroxyl (·OH), peroxyl (·RO2), and not radical species such as hydrogen peroxide (H_2O_2) and hydrochlorous acid (HOCl). It is important to point out that there are also reactive nitrogen species produced from similar processes, which include the radicals nitric oxide (·NO) and nitrogen dioxide (·NO2 $^-$), as well as the not radical peroxynitrite ($ONOO^-$), nitrous oxide (HNO_2), and alkyl peroxynitrates (RONOO). Among the cytosolic sources of ROS, is worth to note that, within the kidney, various subunits of NAD(P)H oxidase are increased in experimental diabetic nephropathy(Gorin et al., 2005). NAD(P)H oxidase is a cytosolic enzyme complex composed of five subunits comprising a membrane-associated p22phox and a gp91phox (Nox-4 in the kidney) subunit and at least four cytosolic subunits: p47phox, p67phox, p40phox, and GTPase rac1 or rac2. In response to excess ROS production during cellular respiration and metabolism, mammals have evolved numerous antioxidant systems including free radical scavengers and enzymes (**Figure 1.17**). Glutathione (GSH) is regarded as the principal endogenous intracellular small molecule antioxidant cytoprotectant. Studies on cells depleted of GSH or bilirubin indicate that bilirubin is of comparable, or greater, importance to GSH in cytoprotection (Baranano et al., 2002) since bilirubin is one of the most abundant endogenous antioxidants in mammalian tissues (Gopinathan et al., 1994). The first and perhaps most important of these antioxidant enzymes is superoxide dismutase (SOD), which exists in three major cellular forms: copper zinc (CuZnSOD, SOD1), manganese (MnSOD, SOD2), and extracellular (SOD3). These enzymes are responsible for the detoxification of superoxide radicals to hydrogen peroxide and water in different cellular compartments. Glutathione peroxidase (GPx) and catalase are other antioxidant enzymes that catalyze the conversion of hydrogen peroxide to water (Forbes et al., 2008). Decreases in expression, and in some instances the activity of each of these antioxidant enzymes, has been previously reported in diabetic microvascular disease (Ceriello et al., 2000). Indeed, the overexpression of CuZnSOD protects against end organ damage in models of type 2 diabetic nephropathy (DeRubertis et al., 2007).Chronic activation of ER stress and UPR pathways in endothelial cells leads to increased oxidative stress and inflammation, and often results in cell death. Because endothelial cells play a pivotal role in maintaining vascular homeostasis, various pathological conditions interfering with this homeostasis including homocysteinemia, hyperlipidimia, high glucose, insulin resistance, disturbed blood flow, and oxidative stress can lead to endothelial dysfunction in part through the activation of ER stress (Lenna et al., 2014).

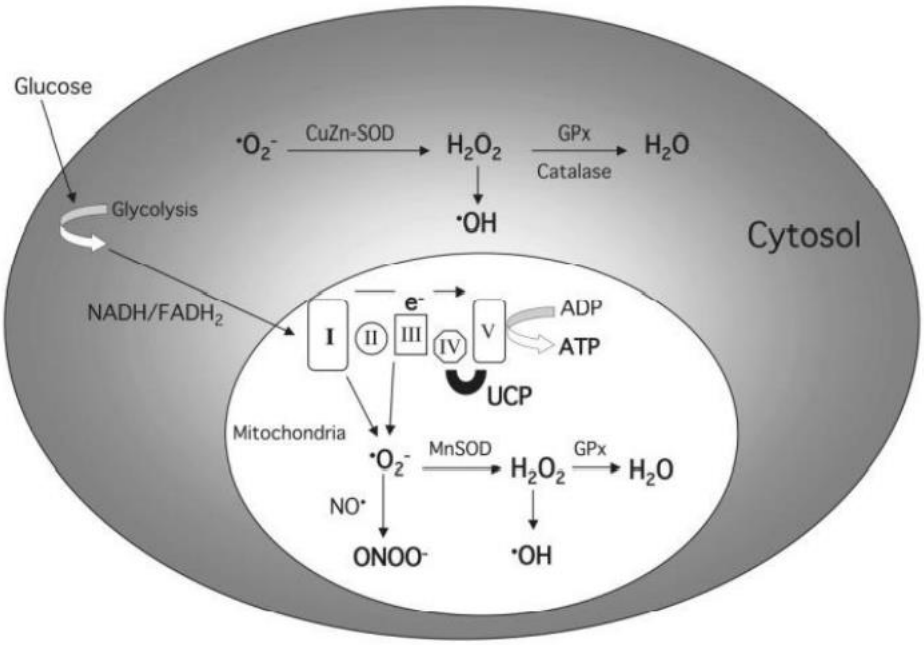

Figure 1.17 Major ROS generated within renal cells in diabetic milieu and the classic antioxidant pathways for their detoxification (Forbes et al., 2008).

Generally, in the eukaryotic cells, the endoplasmic reticulum (ER) is involved in the secretion and in the fold of the majority proteins. Proteins enter in the ER as unfolded polypeptides and their folding depends by the necessity of the cells. The accumulation of unfolded proteins is detected by a transmembrane sensors that activate transcriptional and translational pathways such as the unfolded protein response (UPR) (Mozzini et al., 2017). ER-stress condition affects different sensors: protein kinase-like ER kinase (PERK), inositol requiring kinase 1 (IRE1) and the transcriptional factor activating transcription factor 6 (ATF6) that are normally inactivated by glucose-regulated protein (GRP78/BiP). Under conditions of ER stress, in order to deal with the increasing load of ER proteins, GRP78 dissociates from PERK, ATF6 and IRE1 leading to their activation. BiP triggers UPR (Bertolotti et al., 2000). If not chronic, UPR activation is adaptive and helps the cell recover to normal health. If ER stress cannot be alleviated or the UPR is prolonged, the cell dies by a mechanism known as ER-stress-induced apoptosis (Szegezdi et al., 2006). The most studied mechanism of cell death triggered by ER stress, involved the transcription factor C/EBP homologous protein (CHOP) indution. CHOP down-regulates the xpression of anti-apoptotic Bcl-2 and up-regulates the pro-apoptotic genes (e.g. PUMA, NOXA, and BAX) (Rutkowski and Kaufman, 2004; Urra et al., 2013). However, several studies showed hat CHOP $^{-}$ / $^{-}$ cells are modestly resistant to ER-stress-induced apoptosis (Zinszner et al., 1998; McCullough et al., 2001). This sustained ER stress is implicated in many disease processes and has been linked to Type II diabetes, cardiovascular disease, Alzheimer's disease, as well as atherosclerosis (Bertolotti et al., 2000). Diabetic-induced ER stress mechanisms for Endothelial dysfunction and atherosclerosis are complex and there is an interplay among different mechanisms and pathways. These pathways not only interact with ER stress signaling but also affect each other. For example, promotes ER stress, while ER stress also induces oxidative species production. ER stress enhances ROS/RNS inflammation, while chronic inflammation further promotes ER stress (Dong et al., 2017). IRE1 is considered the connection between the ER-stress and inflammation (Kaneko et al.,

2003). Sure enough, activated IRE1 encodesXbox binding protein (XBP) 1. XBP1 increases the transcription of chaperones and other UPR-related proteins and enhances the degradation of the misfolded proteins. Eventually, IkB kinase is activated followed by IkB kinase-mediated suppression of the inhibitor of kB protein and the induction of the nuclear factor (NF)-kB (Mozzini et al., 2017). The UPR is involved in the generation of reactive oxygen species (ROS) through ER-oxido-reduction and protein di-sulphide isomerase.

1.4 Obesity and Metabolic Syndrome

Obesity is generally recognized as an increasingly important cause of morbidity worldwide and is a contributor to chronic diseases such as type 2 diabetes and cardiovascular disease (Nathan and Moran, 2008). With the global rise in obesity, metabolic syndrome is becoming a global epidemic as well (Sigit et al., 2020).

MetS is defined as clustering of several cardiovascular and metabolic risk factors. Clinical diagnosis is made on the basis of the presence of 3 of 5 conditions: high triglyceride level, low high-density lipoprotein (HDL) cholesterol level, high fasting blood glucose level, presence of central obesity (ie, high waist circumference), and high blood pressure (Camhi et al., 2008)(Grundy et al., 2004).

In recent years some studies have reported a higher prevalence of MetS in the Mediterranean basin, in comparison with published average levels for Europe (Ottevaere et al., 2011). Behavioral factors such as poor dietary habits, a sedentary lifestyle, and a social environment which encourages unhealthy behaviors are closely correlated with the prevalence of obesity and MetS (Huang et al., 2007). During adolescence, developmental physiologic changes in body composition, lipid profile, blood pressure, insulin secretion and number of body fat cells occur as a result of higher levels of sex and growth hormones (Park et al., 2010). This results in increased insulin resistance that is associated with MetS. Therefore, the convergence of hormonal changes associated with adolescence and unhealthy lifestyle behaviors can predispose this group to MetS and obesity and a risk of adverse CVD events later in life (Huang et al., 2007).

1.4.1 Children obesity, Mets and NAFLD

Children and adolescents overweight and obesity prevalence has tremendously increased in recent years (Ng et al., 2014). As in adults, also in childhood and adolescence, obesity plays a central role in the development of the MetS (Weiss et al., 2004; Calcaterra et al., 2008), an important clustering of metabolic abnormalities and anthropometric characteristics entailing an increased risk for mortality from cardiovascular and all causes in adults (Ford et al., 2004; Ford, 2005), as well as an increase in type-2 diabetes and early cardiovascular disease in juvenile age (Nathan and Moran, 2008b). Using the criteria of the definition of the MetS in children and adolescents (Zimmet et al., 2007), the overall prevalence among the obese adolescents in Italian cohorts was between 17 and 31% (Viggiano et al., 2009; Lafortuna et al., 2010; Brufani et al., 2011; Santoro et al., 2013).

Non alcoholic fatty liver disease (NAFLD) is a spectrum of disease ranging from simple steatosis (NAFL) to nonalcoholic steatohepatitis (NASH), which can progress to advanced fibrosis and cirrhosis, culminating in HCC (Sherif, 2019). NAFLD is presently considered a manifestation of the

metabolic syndrome (Marchesini et al., 2003; Neuschwander-Tetri and Caldwell, 2003). There is increasing evidence that obesity, hyperglycemia and insulin resistance are risk factors for NAFLD also in children (Kawasaki et al., 1997; Schwimmer et al., 2003, 2005). Pooling data from studies performed mainly in tertiary medical centers, the prevalence of NAFLD in obese children has been reported to range from 20 to 77% (Chan et al., 2004).

The pathogenesis of MetS and NAFLD are incompletely understood. NAFLD requires an accumulation of hepatocyte lipid in the form of free fatty acids and triglycerides. Progression to NASH involves increased hepatocyte susceptibility to oxidative stress, generation of reactive oxygen species, and subsequent lipid peroxidation (Harrison and Neuschwander-Tetri, 2004). By-products of oxidative stress and lipid peroxidation are powerful chemoattractants of neutrophils and stimulate the hepatic stellate cells responsible for fibrosis, along with the release of inflammatory cytokines, including TNF-α (Sundaram et al., 2009). TNF-α, a pro-inflammatory cytokine, promotes insulin resistance, is pro-apoptotic and is important in white blood cell recruitment. It is increased in patients with NAFLD and the MetS (Sundaram et al., 2009).

1.5 Bilirubin protective role

Bilirubin has been regarded as a powerful endogenous anti-oxidant and anti-inflammatory agent. Therefore, higher TBili levels may be protective against the autoimmune pathology related to the type 1 diabetes inflammation and the oxidative physiologic stress related to the development of type 2 diabetes (Cheriyath et al., 2010). The set of data provided by Chariyath et al. and the National Health and Nutrition Examination Survey (NHANES), show that a higher level of serum TBili is related to the possibility of a lower incidence of Diabetes Mellitus (DM). This findings support the hypothesis that the antioxidant nature of TBili, with its protective effect against the risk of stroke, atherosclerosis, and vasculitis, may be extended to DM risk, too. Furthermore, research has pointed out that higher levels of TBili increase glucose mobilization within the cells, enhancing a more effective and biological glucose utilization. Current studies also suggest that physiological levels of TBili block the production of various free radicals that might hinder the inhibitory responses of the cell to take up the high glucose (Chen et al., 2008). Furthermore, it is shown that they prevent the vascular endothelial activation due to the oxidative stress in the vessels. Results from several experimental and clinical studies suggest that oxidative stress plays a major role in the pathogenesis of both type of DM (Maritim et al., 2003). A recent study reveals that expression level and polymorphism in HO-1 gene promoter is associated with the prevalence of T2DM (Song et al., 2009). Recently, the relationship between serum bilirubin and Chronic kidney disease in patients with diabetes mellitus (DMCKD) has been demonstrated in Japanese patients with DM (Fukui et al., 2008). This cross-sectional study evaluated albuminuria according to the ratio of albumin to creatinine from random urine samples and Estimated Glomerular Filtration Rate (eGFR) with the Modification of Diet in Renal Disease (MDRD) study equation. The results showed that serum bilirubin had an inverse correlation with albuminuria and a positive correlation with eGFR(Fukui et al., 2008)(Han et al., 2010). The interesting thing is that GS patients have improved adipocyte function and vascular protection. In this study, for the first time bilirubin is shown to bind directly in order to activate PPARα that increases target genes to reduce adiposity. The ability of bilirubin to act as an activator of nuclear hormone receptors such as

PPARα is a new function and it may explain the beneficial effects of moderate rises in plasma bilirubin levels that have been observed in patients with GS.

The association between serum bilirubin and chronic kidney disease (CKD) is explained through different mechanisms. One of these is based on antioxidant properties of bilirubin: Oxidative stress and renal reactive oxygen species are known to induce renal vasoconstriction, sodium retention, and kidney damage leading to CKD. Another suggested mechanism highlights the negative association between hyperbilirubinemia and insulin resistance, which is a reported risk factor for CKD. Bilirubin is also famous for its anti-complement properties that protect against inflammation. Some studies indicate that systemic low-grade inflammation is a possible mechanism that relates serum bilirubin with CKD development thanks to its negative association with the inflammatory marker C-reactive Protein (CRP) (Mortada, 2017). This association is explained with several studies. A longitudinal cohort study on Korean males examines the association between serum bilirubin level and the prevalence of DM and DMCKD in a Korean population. The clinical parameters investigated are age, sex, weight, height, waist circumference and history of hypertension and diabetes mellitus, ever-smoking, and ever-consuming alcohol. Results show that the increases in serum bilirubin were associated with decreased levels of insulin resistance and inflammatory markers, serum insulin, and CRP (Mortada, 2017). Another prospective cohort study of 1458 adult patients with primary IgA nephropathy shows that elevated serum bilirubin (≥0.6 mg/dL) was associated with a reduced incidence of end stage renal disease incidence (Chin et al., 2009). The results of a post-hoc analysis of the RENAAL trial with independent replication in the Irbesartan Diabetic Nephropathy Trial (IDNT), demonstrated an independent inverse association of bilirubin levels with progression of diabetic nephropathy (Riphagen et al., 2014). In diabetic patients, serum bilirubin showed a positive correlation with eGFR, with lower serum bilirubin level, a risk factor for the development of albuminuria (Okada et al., 2014). There are also prospective studies that report negative correlations between serum bilirubin levels and different disorders such as CVD and metabolic syndrome (Choi et al., 2013). In addiction, subjects with hyperbilirubinemia had several reduced CVD risk factors including body mass index ($p = 0.003$), low-density lipoprotein ($p = 0.0005$) and total cholesterol ($p = 0.0002$) (Oda et al., 2013).

UCB also has antioxidant properties in Gunn rat animal models (Oh et al., 2013). They have recently shown that the administration of bilirubin reduces tubular renal damage after the induction of nephropathic cyclosporine in Gunn rats and HK-2 cells thanks to its protective effects from oxidative stress and apoptosis. Cyclosporine treated rats show damage markers of kidney visibly reduced and histopathological examinations show an improvement in arteriolopathy, interstitial tubular fibrosis, and tubular damage associated with cyclosporine - controlled control rats (Fujii et al., 2010). The pre-treatment in Gunn rats downregulates the activity of NADPH-oxidase in streptozotocin-induced diabetic nephropathy (Oh et al., 2013) highlighting the decrease of intracellular ROS production and the inhibition of apoptosis thanks to the regulation of bcl-2 and the downregulation of Bax expression in bilirubin-treated rats (cyclosporine-induced).

A lot of studies demonstrate the linkage between serum bilirubin levels and metabolic syndrome and supported the beneficial impacts of mild hyperbilirubinemia on in human health. Circulating total bilirubin has been consistently shown to be inversely and independently associated with

adverse cardiometabolic outcomes such as cardiovascular disease, hypertension and type 2 diabetes in most of observational and prospective epidemiological studies (Vítek, 2012; Kunutsor et al., 2015, 2017; Nano et al., 2016; Kwon et al., 2017).

Not surprisingly, bilirubin concentrations have been negatively associated with risk factors of MetS, such as central obesity, insulin resistance, dyslipidemia, and hypertension that together culminate in the manifestation of T2DM and CVD (O'Neill and O'Driscoll, 2015). Kwal et al. also demonstrated that the prevalence of non-alcoholic fatty liver disease decreased steadily as the serum bilirubin leel increased (Kwak et al., 2012).

In line with these negative relationships between serum bilirubin levels and metabolic syndrome, a negative association between bilirubin levels and abdominal obesity per se has been shown in several recent studies (Bhuiyan et al., 2008; Wu et al., 2011; Choi et al., 2013). Since weight reduction is known to reduce several cardiovascular risk factors, it is important to note that each one percent decrease in weight loss was associated with a linear increase in serum bilirubin concentration (Andersson et al., 2009). The close relationship between serum bilirubin levels and the UGT1A1 gene promoter variants, responsible for manifestation of Gilbert syndrome in Asians, and the risk of non-alcoholic fatty liver disease (a condition commonly associated with obesity and metabolic syndrome) was recently demonstrated in Taiwanese children (Lin et al., 2009).

Not only MetS per se but also the NAFLD (Kwak et al., 2012) and NASH (Salomone et al., 2013) seems to be negatively associated with serum bilirubin concentrations. Puri at al showed, in a cohort of children with biopsy proven NAFLD that 67% had evidence of NASH. On multivariable analysis, higher bilirubin levels were significantly associated with a decreased likelihood of a histological diagnosis of NASH on biopsy (Puri et al., 2013). Despite these evidence, the relationship between circulating total bilirubin and incident non-alcoholic fatty liver disease (NAFLD) is uncertain. Recently two different studies performed in China (Puri et al., 2013) and Neatherlands (Kunutsor et al., 2020) aimed to assess the association of total bilirubin with the risk of new-onset NAFLD and investigate any causal relevance to the association using a Mendelian randomization approach. Multivariate analysis showed that elevated levels of total bilirubin were not causally associated with decreased risk of NAFLD.

Chapter 2
Aim of the thesis

2. AIM OF THE THESIS

Unconjugated bilirubin (UCB) is a metabolic end-product of heme catabolism. Bilirubin's behavior in a human body has two faces similar to Janus Bifrons. Elevated serum/plasma UCB concentration exposes babies to the risk of neurotoxicity. Conversely, mildly elevated systemic bilirubin concentrations such as in Gilbert syndrome (GS) protect against various oxidative stress-mediated and metabolic diseases including cardiovascular diseases (CVD), diabetic nephropathy (DN) and Metabolic syndrome (MetS).
The main aim of the present thesis work is to discriminate between protective and toxic bilirubin concentration and then unravelling the molecular mechanism involved in the protective impact of bilirubin, both *in vitro* and *in vivo*. The work was divided in 3 aims, corresponding to the three parts of the thesis (task 1, 2 and 3).

Aim 1 was focused to determine the UCB threshold for its anti- and pro-oxidant activity. The corresponding task 1 is an *in vitro* comparative study, performed on four different immortalized cell lines coming from different organs. It is based on the evaluation of the effects of increasing concentration of bilirubin on redox balance.

Aim 2 was focused to understand if life-long hyperbilirubinemia and bilirubin-priming might significantly contribute protecting against atherosclerosis and DN at the cellular level. ER-stress and inflammation activation were evaluated on primary aortic endothelial cells exposed to PA to mimic atherosclerosis. Cell death by apoptosis was studied on primary podocytes exposed to Ang II to mimic diabetic nephropathy. Results were also validated on immortalized cell lines pre-treated with UCB (bilirubin-priming) and then exposed to damage.

Aim 3 was focused to study the clinical association between serum bilirubin levels and the development of Non-alcoholic fatty liver disease (NAFLD) and MetS. In task 3, thanks to the collaboration of Prof. Sartorio of Istituto Auxologico Italiano, we investigated this association in a retrospective cross-sectional study in a cohort of extremely obese Italian children and adolescents.

Chapter 3
Material and Methods

3. MATERIAL AND METHODS

3.1 *Cell cultures*

3.1.1 HepG2 human hepatoblastoma cells

HepG2 human hepatoblastoma cells were maintained in DMEM high glucose supplemented with 10% FBS, 1% penicillin/streptomycin solution (penicillin G (100 U/mL), streptomycin (100 mg/mL), and L-glutamine (2 mmol/L). The cell culture medium was changed every 48 hours and the cells were cultured at 37°C in 5% CO_2 humidified atmosphere in 25 cm^2 culture flasks. HepG2 cells were used between passages 20th and 30th and, once they reached 75-80% of confluence, HepG2 cells were sub-cultured and treated with an incrising doses of UCB and used in studies as described in the task 1.

3.1.2 SH-SY5Y human neuroblastoma cells

SH-SY5Y human neuroblastoma cells (ATCC-CRL-2266) were maintained in EMEM/F12 1:1 supplemented with 15% fetal bovine serum (FBS), 1% penicillin/streptomycin solution (penicillin G (100 U/mL), streptomycin (100 mg/mL), L-glutamine (2 mmol/L)(Euroclone S.p.A., Italy), and 1% non-essential amino acids (Sigma-Aldrich, MO, USA). The cell culture medium was changed every 48 hours and the cells were cultured at 37°C in 5% CO_2 humidified atmosphere in 25 cm^2 culture flasks. SH-SY5Y cells were used between passages 10th and 20th and were sub-cultured once they reached 75-80% of confluence. When 80% of confluence was achieved, the cells were treated with an incrising doses of UCB and used in studies as described in the task 1.

3.1.3 H5V Murine heart endothelial cells

H5V, murine heart endothelial immortalized cells (kindly provided by Istituto Mario Negri, Milan, Italy), were grown in DMEM low glucose containing 10% (v/v) FBS, 1% penicillin/streptomycin solution (penicillin G (100 U/mL), streptomycin (100 mg/mL), and L-glutamine (2 mmol/L). The cell culture medium was changed every 48 hours and the cells were cultured at 37°C in 5% CO_2 humidified atmosphere in 25 cm^2 culture flasks. H5V cells were used between passages 10th and 20th and were sub-cultured once they reached 75-80% of confluence. When 80% of confluence was achieved, the cells were treated with an incrising doses of UCB and used in studies as described in the task 1. Cells were used also in studies as described in the task 2 as *in vitro* model for atherosclerosis. In this case, cells were treated with selected doses of Palmitic Acid or with UCB pre/post treatment (Li et al., 2013; Wu et al., 2014).

3.1.4 HK2 Tubular interstitial epithelial cells

HK2, an immortalized human proximal tubular epithelial cell line (kindly provided by Prof. R. Bulla, Department of Life Sciences, University of Trieste), was cultured in DMEM low glucose, Ham's F12 media (1:1) supplemented with decomplemented 5% (v/v) FBS, 1% penicillin/streptomycin solution (penicillin G (100 U/mL)), streptomycin (100 mg/mL), L-glutamine (2 mmol/L), bovine insulin (5 mg/mL), holo-transferrin (5 mg/mL), sodium selenite (5 ng/mL), hydrocortisone (5 ng/mL), EGF (10 ng/mL), T3 (5 pg/mL), and PGE (15 pg/mL).
These cells grow in monolayer showing large granular deposits typical of glycogen (Ryan et al., 1994). The cell culture medium was changed every 48 hours and the cells were cultured at 37°C in 5% CO_2 humidified atmosphere in 25 cm^2 culture flasks. HK2 cells were used between passages 10th and 20th and were sub-cultured once they reached 75-80% of confluence. When 80% of confluence was achieved, the cells were treated with an incrising doses of UCB and used in studies as described in the task 1. Cells were used also in studies as described in the task 2 as *in vitro*

model for diabetic nephropaty. In this case, cells were treated with selected doses of Angiotensin II and AGEs or with UCB pre/post treatment (Slyne et al., 2015).

3.1.5 Primary cultures of rat

Rats used in the project were born in animal facility of Area Science Park, Trieste (Italy) and animal handling was approved (NO1487BEL19) by the Ethics Committee for Animal Experimentation (OPBA) of the University of Trieste in compliance with the Italian regulation (D.L.vo 26/2014) and the Directive 2010/63/EU of the European Parliament. Rats were anesthetized via intraperitoneal injection of Zoletin (60 mg/Kg) and Xylazine (40 mg/Kg) and successively sacrificed through decapitation. We did not distinguish between male and female and used animal at the weight of 180-250 gr.

3.1.5.1 Primary cultures of rat aortic endothelial cells: isolation and characterization

The aorta was extracted and conserved in Human Endothelial serum-free medium GIBCO (Life Technologies, Monza, Italy). The aorta was cleaned from fat tissue, cut into two halves, and digested by collagenase (Worthington Industries, OH, USA). After collagenase treatment, endothelial cells removed from the aorta were collected by centrifugation and suspended in Human Endothelial medium GIBCO (Life Technologies, Monza, Italy) supplemented with 10% FBS, EGF (10 ng/ml), bFGF 20ng/ml, and 1% penicillin/streptomycin solution (penicillin G (100 U/mL) in wells of 6-multiwell coated with gelatin. After 1h of incubation at 37°C, the supernatant containing endothelial cells was re-seeded in another well. Then aortic endothelial cells were isolated and characterized by magnetic beads coated with CD31 (BD Biosciences, San Jose, CA), a characteristic marker for endothelial cells (Liu and Shi, 2012). The cell culture medium was changed every 48 hours and the cells were cultured at 37°C in 5% CO_2 humidified atmosphere in 25 cm^2 culture flasks. Cells were used between passages 2th and 4th and were sub-cultured once they reached 75-80% of confluence. When 80% of confluence was achieved, the cells were treated with selected doses of pamitic acid (Li et al., 2013) and used in studies as described in the task 2.

3.1.5.2 Primary cultures of rat podocytes: isolation and characterization

The kidneys were extracted and conserved in D-glucose (5.5 mM) Dulbecco's Modified Eagle's Medium (DMEM) and Ham's F12 medium (EuroCloneS.p.a., Italy) in the ratio 1:1 on ice; Bowman's capsule was removed by pliers and the cortical of the organ was cut into thin strips. Using filters with different sizes (respectively 80, 100, and 300 mesh) and a pestle, glomeruli were collected and then centrifuged at 136 g for 3 minutes; the pellet was seeded in the 25 cm^2 culture flasks pre-coated with collagen type IV (Sigma-Aldrich, MO, USA). The lyophilized powder of collagen type IV was reconstituted in sterile 0.5 M acetic acid to reach a concentration of 1 mg/mL and then diluted 1:2 in sterile Phosphate buffered saline (PBS). The final concentration resulted 0.5 mg/ml in 0.25 M acetic acid and it was stored at -20°C. After 30 min of coating, collagen type IV was removed, the flask was let to dry for 15 min and was rehydrated with podocytes medium (5 min) before using. Glomeruli were left in the incubator at 37°C in 5% CO_2 humidified atmosphere in presence of a medium composed by D-glucose (5.5 mM) Dulbecco's Modified Eagle's Medium (DMEM) and Ham's F12 medium in the ratio 1:1 (EuroCloneS.p.a., Italy), decomplemented 10% (v/v) fetal bovine serum (FBS), penicillin/streptomycin solution (100 U/mL penicillin, 100 mg/mL streptomycin), 2 mmol/L L-glutamine, 0.12 U/m insulin from bovine pancreas, 5 μg/mL holo-transferrin, 5 ng/mL sodium selenite, and 5 ng/mL hydrocortisone (Sigma-Aldrich, MO, USA) (Zennaro et al., 2014). After four/five days of incubation, it was possible to appreciate podocytes coming from glomeruli and when cells reached 70-80% of confluence, they were detached using

trypsin-EDTA (EuroCloneS.p.a., Italy), a scraper, and 40 mesh. Lastly, collected podocytes were centrifuged at 136 g for 5 minutes and seeded in the 25 cm^2 culture flasks pre-coated with collagen type IV (Sigma-Aldrich, MO, USA). The cell culture medium was changed every 48 hours and the cells were cultured at 37°C in 5% CO_2 humidified atmosphere. Cells were used at the first passage treated with selected doses of Angiotensin II or AGEs and used in studies as described in the task 2.

3.2 Histology

Rat aorta and kidneys were harvested and immediately fixed in 20 mL of 10% neutral buffered formalin pH 7.2 (equivalent to an aqueous solution of 4% formaldehyde p/v and methanol 0,1% v/v) in containers of Klessidra (Bio-Optical) by using a specimen / fixative ratio of 1:20 (volume). The principal of the technique is based on Aqueous formaldehyde property to form methylene glycol and react with amines on proteins and nucleic acids to form methylene bridge crosslinks. Methanol additive stabilizes formaldehyde and prevents the formation of the paraformaldehyde. The fixation was performed at room temperature. Tissue sections were cut at a thickness of 3.5 μm and before tissue staining with Hematoxylin & Eosin (H&E) can occur, the paraffin wax was removed (deparaffinization step) by using xylene. Due to its insolubility with water, clearant was followed by anhydrous alcohol and then diluted alcohols (95%, 70%) before going to water. The hematoxylin solution, because its basic properties, stains the nuclear chromatin and possibly other acidic cellular elements, thus vesicular nuclei exhibit stained nuclear membrane, well-defined chromatin and unstained nucleoplasm. Slides were stained with hematoxylin for 3 min. An alcoholic differentiation step was performed to remove non specific hematoxylin stain and the tissue was then exposed to a bluing solution, which an alkaline pH, to change the alum hematoxylin stained nuclei from a reddish to blue-purple appearance. Before staining in the cytoplasmic counterstain the alkaline bluing solution was removed, and alcohol rinses was used after the eosin stain to dehydrate the tissue section, prepare the slide for cover-slipping, and obtain the proper eosin intensity (2 min) by pulling excess eosin from the tissue section, as well. The more aqueous the alcohol rinse, the more eosin that is extracted from the tissue section, decreasing the eosin shade (Siddiqui et al., 2016). Complete dehydration with anhydrous alcohol was required before going into a clearant (xylene) and slides were mounted with DPX mounting media (Marin, Rosso et al. 2016). Photomicrographs and image digitising were performed using D-Sight, Menarini Diagnostics. Histological analysis was realized in collaboration with Anatomia Patologica Department, Cattinara Hospital (Trieste).

3.3 Treatments

3.3.1 Bilirubin manipulation

Unconjugated bilirubin (UCB) (Sigma-Aldrich, MO, USA) was purified as described in literature (McDonagh and Assisi, 1972;Ostrow and Mukerjee, 2007). An aliquot of purified unconjugated bilirubin was dissolved in Dimethyl sulfoxide (DMSO) (33 μL of DMSO per 100 μg of UCB) and its concentration was measured spectrophotometrically at 458 nm in growth medium with Bovine Serum Albumin (BSA) 30 μM. UCB was diluted with growth medium in order to reach the final concentrations used in the experiments. Expected free bilirubin concentration was reported in table 3.1, thanks to the previous work of Roca et al. (Roca et al., 2006).

Table 3.1 Bf concentration corresponding to UCB concentration in presence of BSA 30 μM

TOTAL UCB in the presence of BSA 30 μM	Bf
<2.5 μM	<15 nM
2.5 μM	15 nM
5 μM	30 nM
10 μM	60 nM
20 μM	120 nM
25 μM	200 nM
>25 μM	>200 nM

3.3.2 Bilirubin treatment

UCB (Sigma-Aldrich, MO, USA) was dissolved in DMSO (6 mM) and added to the cell medium for 24h in the presence of BSA (30 μM) to reach a range of final concentration from 0.4 to 30 μM performing serial dilution. DMSO (0.5%) was used to treat control cells.

3.3.3 Palmitic acid treatment

Palmitic acid (PA) 0.1 M stock solution was prepared by dissolving fatty acid-free (FFAs) in DMSO. Since albumin played a crucial role in determining the FFAs available concentration, the BSA concentration was kept fixed at 75μM. The medium containing a final BSA concentration of 75μM was aliquoted to set up various BSA/PA ratios (1:1, 1:2, 1:3, 1:4, 1:5, 1:6). DMSO solution was used as control and its final concentration never exceeded 0.1%. Primary aortic andothelial cells and immortalized murine heart endothelial cells (H5V) were treated with selected doses of PA in the presence of BSA 75 μM for 24 h.

3.3.4 Angiotensin II treatment

Human Angiotensin II (Sigma-Aldrich, MO, USA), provided as powder, was reconstituted with Phosphate Buffered Saline (PBS) at the concentration of 1 mg/ml. The stock solution was then aliquoted and blanketed with an inert gas (nitrogen) and stored desiccated in the dark at –20 °C to avoid proteolytic degradation. When required, an aliquot was reconstituted in PBS to 1 mg/ml. The range of Angiotensin II concentration used in the experiments was from 0.01 μM up to 10 μM and all treatments required 24 hours (Chen et al., 2017) on primary podocytes and human proximal tubular epithelial cells (HK2).

3.3.5 AGEs-BSA preparation and treatment

Advanced glycation end products - BSA (AGEs–BSA) preparation was conducted in agreement with literature (Gallo, Cocchietto et al. 2014) starting from D-glucose. 50 mg/mL of BSA were incubated with D-glucose 0.5 mol/L in a 0.2 mol/L Phosphate Buffered Saline containing azide (0.2 M Na2HPO4; pH 7.4) at 37°C for six weeks in the dark. Moreover, 50 mg/ml of BSA were incubated under the same condition but without D-glucose and used as control. In presence of D-glucose, the solution started to assume a yellow-brown color and it showed the typical fluorescent spectrum of advanced glycation end products. At the end of the incubation time, the preparation was extensively dialyzed against phosphate buffer (pH 7.4) to remove free glucose and a cellulose

membrane (Sigma-Aldrich, MO, USA) with cut-off of 10 kDa was used for this step. After the dialysis process, protein concentration was assessed by bicinchoninic acid assay (BCA). Fluorescence characteristics of AGE-BSA were inspected by the EnSpire® Multimode Plate Reader (PerkinElmer®) by setting the excitation wavelength at 370 nm and the emission wavelength at 440 nm. Glycated Bovine Serum Albumin (BSA) showed a 300% increase in fluorescence compared to control one. The solution was finally aliquoted and stored at -20°C. Human proximal tubular epithelial cells (HK2) were treated with AGE 20 μM for 24 h

3.3.6 Bilirubin Pre- and Post-treatment

Immortalized murine heart endothelial cells (H5V) and Immortalized human proximal tubular epithelial cells (HK-2) were expose to damage after (UCB pre-treatment) or before (UCB-post-treatment) being exposed to UCB.2.5 μM or UCB 1.25 μM in BSA 30 μM. DMSO 0,1% was used as control. In pre-treatment, cells were at first treatment with bilirubin for 16 hours (UCB 1.25 μM or UCB 2.5 μM or just DMSO 0,1% in presence of BSA 30 μM) and then exposed to the damage agent. On the contrary, in post-treatment, cells were at first exposed to damage agent and later they were treated with bilirubin for 16 hours (UCB 1.25 μM or UCB 2.5 μM or just DMSO 0,1% in presence of BSA 30 μM).

UCB was diluted with DMSO and then with Growth Medium in order to reach the two final concentrations used in the following experiments: UCB 2.5 μM and UCB 1.25 μM corresponding to free bilirubin (Bf) ≤ 15 nM (see**Table 3.1).**

3.4 Intracellular UCB determination

HepG2, H5V, HK2 and SH-SY5Y cells at 80 % of confluence were incubated with different UCB concentrations (from 0.4 to 30 μM) for 24 h, or 0.5 % DMSO. After treatment time, the cells were collected by centrifugation and washed three times in PBS. The intracellular UCB level was quantified using an LC-MS/MS method as described previously (Jašprová et al., 2020).

Briefly, the cells after being mixed with internal standard (mesobilirubin), were lysed and deproteinated by 0.5% ammonium acetate in methanol. Finally, this suspension was sonicated and centrifuged. After the final centrifugation steps, 100 μL of supernatant were pipetted into glass vials with the inert insert (suitable for liquid chromatography-tandem mass spectrometry (LC-MS) analysis), and 2 μL was directly injected into the LC-MS apparatus. The LC-MS/MS analyses were performed using high-performance liquid chromatography (Dionex Ultimate 3000, DionexSoftron GmbH, Germany) equipped with a Poroshell 120 EC-C18 column (2.1 μm, 3.0 × 100 mm; Agilent, CA, USA). For a gradient elution, the phase was prepared by mixing 1 mM of NH_4F (Honeywell, International Inc., Morris Plains, NJ, USA) in water and methanol (BiosolveChimie SARL, France). The analytes were detected by mass spectrometer (TSQ Quantum Access Max with a HESI-II probe, Thermo Fisher Scientific, Inc., USA) operating in a positive SRM mode: bilirubin [585.3→299.1 (20 V); 585.3→271.2 (18 V)]; MBR [589.3→301.1 (20 V); 589.3→273.2 (44 V)]. Protein concentration in the cell suspension was determined by DC Protein Assay (Bio-Rad Laboratories, CA, USA) and results were expressed as nmol/mg of protein. All steps were performed at dim light.

3.5Viability and cytotoxicity assay

3.5.1 MTT assay

Cell viability was determined by assessing the reduction of 3(4,5-dimethylthiazolyl-2)-2,5 diphenyl tetrazolium (MTT) to formazan by succinate dehydrogenase, a mitochondrial enzyme (Twentyman and Luscombe 1987). The stock of MTT (Sigma-Aldrich, MO, USA) was dissolved in Phosphate Buffered Saline pH 7.4 at 5 mg/mL and later diluted in the growth medium at the final concentration of 0.5 mg/mL. HepG2 cells were seeded in 96-well plates at the concentration of 18.000 cell/cm², H5V cells at concentration of 10.000 cell/cm², HK-2 cells at concentration of 8000 cell/cm² whileSH-SY5Y cells at concentration of 15.000 cell/cm². Primary rat aortic endothelial cells were seeded in 96-well plates at the concentration of 10.000 cell/cm² while primary podocytes were seeded in 48-well plates at the concentration of 12.000 cell/cm² and cultured at 37°C in 5% CO_2 humidified atmosphere for 24 hours. After treatment time, the cells were incubated with the MTT solution for at least 60 min at 37°C. After incubation, the medium containing the MTT was removed and the formazan crystals were dissolved in 100 μL of DMSO by shaking gently the samples for 10 min. The absorbance value at 562 nm was determined by the EnSpire® Multimode Plate Reader (PerkinElmer®). Cells cultured just in Growth Medium were considered as control (100% viability) and the results were compared to this value.

3.5.2 Propidium Iodide fluorescence assay

Propidium Iodide (PI) is a fluorescent agent able to penetrate only into cells with damaged membranes (non-viable cells) so that it can be used for selective labelling of dead cells (mortality assay). PI binds to double stranded DNA by intercalating between the bases with little or no sequence preference, forming complexes that increase the fluorescence capacity. While in aqueous solution the dye has excitation/emission maxima of 493/636 nm, once the dye is bound its fluorescence is enhanced resulting in an excitation maximum at 535 nm and fluorescence emission maximum at 617 nm. According to the literature (Dengler, Schulte et al. 1995), HepG2 cells were seeded in 96-well black plates at the concentration of 18.000 cell/cm², H5V cells at concentration of 10.000 cell/cm², HK-2 cells at concentration of 8000 cell/cm² while SH-SY5Y cells at concentration of 15.000 cell/cm². Primary rat aortic endothelial cells were seeded in 96-well black plates at the concentration of 10.000 cell/cm² while primary podocytes were seeded in 48-well black plates at the concentration of 12.000 cell/cm² and cultured at 37°C in 5% CO_2 humidified atmosphere for 24 hours. After culturing time, growth medium was discard and PI (Sigma-Aldrich, MO, USA) was solubilized in PBS in order to reach a final concentration of PI 50 μg/mL. After 60 min of incubation at 37°C in the dark, the fluorescence detection by the EnSpire® Multimode Plate Reader (PerkinElmer®) allowed the assessment of the number of non-vital cells in the population (first measurement). The second measurement allowed to assess the number of the total cells population considering both the non-viable cells (already detected in the first measurement) and the viable cells. In order to let PI solution enter any cells and bind double stranded DNA, all cell population was incubated with Triton x-100 1.5% and PI 50 μg/mL (ratio 1:1.5) on ice for at least 60 min in the dark. The fluorescence was read by the EnSpire® Multimode Plate Reader (PerkinElmer®). The percentage of dead cells was calculated as the proportional fluorescence intensity of dead cells to that of total cells.

3.6 ROS determination by fluorescence dye

The intracellular ROS accumulation after UCB treatment was determined using the 2'7'-dichlorofluorescein diacetate (H_2DCFDA) compound (Molecular Probes, Carlsbad, CA, USA), which is a non-polar compound converted into a non-fluorescent polar derivative (H_2DCF) by a cellular esterase after incorporation into cells. H_2DCF is membrane impermeable and it rapidly oxidizes into the highly fluorescent 20, 70-dichlorofluorescein (DCF) in the presence of intracellular ROS. HepG2 cells were seeded in 96-well black plates at the concentration of 18.000 cell/cm², H5V cells at concentration of 10.000 cell/cm², HK-2 cells at concentration of 8000 cell/cm² while SH-SY5Y cells at concentration of 15.000 cell/cm² and cultured at 37°C in 5% CO_2 humidified atmosphere for 24 hours. At the end of the treatment, the cells were washed with PBS, and post-treated for 1h with 10 μM H_2DCF-DA diluted in serum free medium without phenol red. The cells needed another wash in PBS before being incubated in fresh PBS solution to read the fluorescence at an excitation wavelength of 505 nm and emission wavelength of 525 nm by EnSpire2300 (PerkinElmer). Then the cells were incubated with Triton X100 0.2% in PBS to lyse them and the Fluorescence detection was repeated. Cells treated with H_2O_2 1 mM were used as positive control.The time with the highest peak of ROS increase both by UCB and by H_2O_2 1 mM (used as positive control) was chosen for each cell line (90 min for HepG2 cells, 120 min for SH-SY5Y and HK2 cells, and 360 min for H5V cells). Results were reported as relative to ROS intracellular accumulation of control cells considered as one.

3.7 Anti Oxidant Power 1 (AOP1)

HepG2 cells were seeded in 96-well plates at the concentration of 75.000 cell/well, H5V cells at concentration of 30.000 cell/well, HK-2 cells at concentration of 20.000 cell/well while SH-SY5Y cells at concentration of 20.000 cell/well and cultured at 37°C in 5% CO_2 humidified atmosphere. Cells were incubated with UCB (9 concentrations obtained by serial $\log_2$ dilutions) in the cells growth medium in the presence of FBS plus BSA to reach BSA final concentration of 30μM. Cells were treated for 24 h at 37 °C in the presence of 5% CO_2. At least three independent experiments were performed each on triplicate wells. AOP1 assay is based on the Light Up Cell System (LUCS) Technology which measures the ability of an antioxidant to neutralize oxidative stress and the effect is measured by a delay in the kinetic evolution of fluorescence emission according to Gironde et al. (Gironde et al., 2020). Briefly, after 24 h of incubation, the cells were treated with the fluorescent biosensor thiazole orange (4 μM, Sigma Aldrich) for 1 h and Relative Fluorescence Units (RFU) at 535 nm was recorded (Varioskan, Thermo Fisher Scientific) after a recurrent (20 iterations) 480 nm LED application procedure (24 mJ/cm²)(Gironde et al., 2020) of the whole 96-well plate. Kinetic profiles were recorded and dose-response curves were calculated. Prooxidant/cytotoxic effect is revealed at the initial time course by a fluorescence intensity higher than control value (Derick et al., 2017). The antioxidant cell index (AOP index) used for sigmoid fit modelling was calculated as previously described (Gironde et al., 2020).

3.8 Gene expression

3.8.1 RNA extraction

Total RNA was isolated using EuroGOLDRNAPure (EuroClone, Italy) according to the manufacture's suggestions. Each sample was homogenized and incubated for 5 minutes at +15 to +25°C to ensure the complete dissociation of nucleoprotein complexes; 200 μl of chloroform for each 1ml RNA Pure Isolation Reagent (required in the initial homogenization) was added and samples were incubated on ice (or at 4°C) for 5 minutes. To separate the solution into three phases, the samples were centrifuged at 12,000 x g for 15 minutes at 4°C; the aqueous phase was transferred in a fresh tube while the lower organic phase and the interphase were discarded because of DNA and proteins content. For RNA precipitation step, an equal volume of isopropanol was added to each sample before a centrifugation at 12,000 x g for 15 minutes at 4°C in order to make the pellet visible at the bottom of the tube. Lastly, RNA pellets were washed with 75% ethanol, re-suspended in RNase-free water, and stored at -80°C until use. The total RNA concentration and purity were quantified by the EnSpire® Multimode Plate Reader (PerkinElmer®); the A260/A280 ratio was used as criteria to determine the RNA purity, considering acceptable between 1.6 and 2.0 as a good RNA quality for each sample analyzed.

3.8.2 Retrotranscription and Real Time PCR

cDNA was obtained from 1 μg of purified RNA using the High Capacity cDNA Reverse Transcription Kits (Applied Biosystems, USA) according to the manufacture's suggestions. The reaction was run in a thermal cycler (Gene Amp PCR System 2400, Perkin-Elmer, Boston, MA, USA) according to the reaction protocol proposed by the manufacturer. Real time PCR was performed according to the iQ5 SYBR Green Supermix (Bio-Rad Laboratories, Hercules, CA, USA) protocol. PCR amplification was carried out in 20 μL reaction volume containing 25 ng of cDNA, 1x iQ SYBR Green Supermix (100 mMKCl; 40 mMTris-HCl; pH: 8.4; 0.4 mM each dNTP; 40 U/mL iTaq DNA polymerase; 6 mM MgCl2; SYBR Green I; 20 mM fluorescein; and stabilizers) (Bio-Rad) and 250 nM of gene 32 specific forward and reverse primers. The reaction was run in IQ5 real time PCR system (Bio-Rad). Primer sequences were obtained using Beacon Designer 8 software (PREMIER Biosoft International, Palo Alto, CA, USA) for the detection of the desired gene and were listed in **Table 3.2.**

Table 3.2 List of forward and reverse primers used for detection of human target genes

Gene	Accession number	Forward primer 5′-3′	Reverse primer 5′-3′
HIF-1α	NM_001530	CAGCAGTTACTCATGGAATA	AACCATACAGCATTTAAGAATC
GAPDH	NM_002046	TCAGCCGCATCTTCTTTTG	GCAACAATATCCACTTTACCAG
HPRT	NM_000194	ACATCTGGAGTCCTATTGACATCG	CCGCCCAAAGGGAACTGATAG

Standard curves were generated by serial dilution of an abundant cDNA sample and a melting curve was made in order to analyze the specificity of the amplification process and calculate the efficiency. Cycling parameters were determined and the results were analyzed by using the comparative Ct method as the means of the relative quantification, normalized to two references genes and expressed as $2^{-\Delta\Delta CT}$ (Rao et al., 2013). In each experiment two housekeeping genes were used to normalize the expression level of the genes analyzed. In order to determine the

relative expression of the mRNA for the same sample (Sample or Control), the Ct of the target gene has been normalized on the Ct of the housekeeping genes (Rao et al., 2013). The expression of the gene of interest in the sample is expressed as relative to that of the control that is always considered one. The formula used for computing the relative expression (**Figure 3.1**) also takes into account the amplification efficiency of the primers: Etarget for the gene of interest and E_{ref} for gene house keeping.

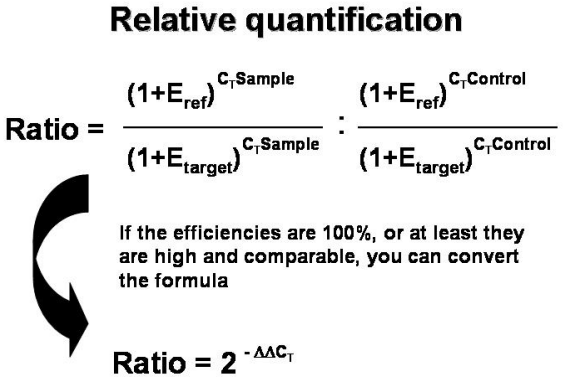

Figure 3.1 Formula to calculate the relative expression of the mRNA of a sample in analogy with a sample selected as control. Eref is the efficiency of the housekeeping gene and Etarget is the the efficiency of the gene of interest; CT sample is the Ct value of the sample in question; CT Control is the Ct value of the sample chosen as a control.

Various sample dilutions will be associated with Ct values that are represented. To evaluate the efficiency of primers for each gene, it was necessary to construct a standard curve that is generated by scalar dilutions of a sample cDNA that expresses the gene of interest. according to the concentration in a graph Ct / log (concentration). Experiments were accepted if the correlation coefficient of the straight lines obtained was ≥ 0.99. The slope of the straight line is directly related to the efficiency of the reaction by the formula:

$$\text{Efficiency} = [10(-1/\text{slope})] - 1$$

3.9 Protein expression

3.9.1 Total protein extraction and quantification

At the end of treatment, cells were collected in Cell Lysis Buffer 10 X (Cell Signaling Technology) using a scraper. The protein lysate was centrifuged for 10 minutes at 14000 x g at 4°C, the supernatants were collected and stored at -80 C°. Total protein concentration in the lysate was determined by the Bicinchoninic Acid Protein Assay (BCA). The assay was performed in 96-well plate and the absorbance was detected at 562 nm. To determine the protein concentration, a standard calibration curve was built by using increasing concentrations (2.5 μg/ml, 5 μg/ml, 10 μg/ml, 20 μg/ml) of BSA dissolved in MilliQ water. The final volume of 50 μL was reached adding water to each well. A solution of Bicinchoninic Acid (containing Na_2Co_3, $NaHCO_3$, Sodium Tartrate, Bicinchoninic Acid in solution of 0.1M of NaOH) and 4% of Cu_2So_4 (ratio 50:1) was prepared and 100 μL was added to each well in order to trigger the reaction. All samples were analyzed in triplicate. The samples were incubated for 30 minutes at 37°C and a purple colored reaction product was formed by the chelation of two molecules of BCA with one cuprous ion. The BCA/Copper complex is water soluble and exhibits a linear absorbance at 562 nm over a broad range of protein concentrations. The absorbance value is directly proportional to the protein concentration. The blank absorbance value was subtracted to each sample one and the protein concentration of each sample was determined considering the standard calibration curve.

3.9.2 Western Blot

Equal amounts of proteins were separated by 8%, 10% or 12% sodium dodecyl sulphatepolyacrylamide gel electrophoresis (SDS-PAGE). Molecular weight standards (10-180 kDa, ThermoFisher) were used as visible race markers. Each sample was properly diluted with loading Buffer 5X (250 mMTris-HCl; pH 6.8; 10% SDS; 30% (v/v); Glycerol; and 0,05% (w/v) Bromophenol Blue) and added to 10% β-mercaptoethanol before loading step. The SDS-PAGE was run at 80 Voltage for 30 minutes and only when proteins migrate into the running gel, the Voltage was increased at 180 for 1 hour. The race was performed in presence of Electrophoresis Buffer 1X (25 mMTris-Base; 0,25mM Glycine; SDS 0,1%). After SDS-PAGE, proteins were electrophoretically transferred onto polyvinylidene fluoride (PVDF) membrane (0,2 m; Bio-Rad Laboratories, Hercules, CA, USA) by a semidry blotting system at 100 V for 60 min in a 1X Transfer Buffer (25 mMTris-Base; 192 mM Glycine; 0,1% SDS, and 20% methanol). In order to evaluate the transfer efficiency onto the membrane, both the gel and the PDVF membrane were stained with Comassie (Brilliant) Blue and Ponceau Solution in 5% v/v of Acetic Acid, respectively. The membrane was blocked in 4% MILK or 4% BSA in TBS-T (0,2 % Tween 20; 20 nMTris; and 500 mMNaCl; pH 7.5) for 1 hour at room temperature according to the primary antibody. Subsequently, the membrane was incubated overnight at 4°C with a primary antibody diluted in the same blocking solution used in the previous step. After the incubation, the primary antibody was removed, the membrane was washed three times with blocking solution (4% MILK or 4% BSA in TBS-T) and incubated with peroxidase conjugated (HRP) anti rabbit or anti mouse secondary antibody (1:2000 dilution) for 1 hour at room temperature (**Table 3.3**). After properly washings (Blocking solution; TBS; and TBS-T), the chemiluminescent horseradish substrate was added (ECL Plus Western Blot detection reagents, GEHealthcareBioSciences, Italy) and visualized by the C-DiGit® Blot Scanner (LI-COR Inc., Lincoln, Nebraska, USA). The relative intensities of protein bands were analyzed using the Image Studio™ Lite software (LI-COR Inc., Lincoln, Nebraska, USA). α-actin was used as internal control for protein normalization.

Table 3.3 List of Antibodies used in Western Blot

PrimaryAntibody	SecondaryAntibody
Anti-HIF-1α antibody (GTX127309) Dilution 1:1000 in blocking solution MILK 4% in TBS-T	Goat anti-Rabbit (P0448, Dako Laboratories, Denmark) Dilution 1:1000 in blocking solution MILK 4% in TBS-T
Anti-LOXl2 antibody (CSB-PA013041LA01MO) Dilution 1:1000 in blocking solution MILK 4% in TBS-T	
Anti-α-Actin antibody (Sigma A2066) Dilution 1:2000 in blocking solution MILK 4% in TBS-T	
Anti-PARP antibody (CST#9542) Dilution 1:250 in blocking solution MILK 4% in TBS-T	
Anti-LC3B antibody (PA1-16930) Dilution 1:1000 in blocking solution MILK 4% in TBS-T	
Anti-CHOP antibody (GADD 153 (N1C3)_GTX112827) Dilution 1:1000 in blocking solution MILK 4% in TBS-T	
Anti-Caspase 3 antibody (MA5-11516) Dilution 1:50 in blocking solution BSA 4% in TBS-T	Rabbit anti-Mouse (P0260, Dako Laboratories, Denmark) Dilution 1:1000 in blocking solution BSA 4% in TBS-T

3.10 Immunofluorescence

Podocytes were seed into appropriate glass coverslips pre-coated with Poly-L-lysine (P7890, Sigma Aldrich, USA) while primary aortic endothelial cells were seed into glass coverslips pre-coated with gelatinin a humid chamber and fixed with 4% paraformaldehyde in 1x PBS for 20 minutes at room temperature under laminal hood. A permeabilization step was performed with 0.5% Triton X-100 in PBS for 5 minutes followed by an incubation with blocking solution of 5% Bovine Serum Albumin (BSA) in PBS-T + 0.1% Tween 20 for 60 minutes at room temperature. After blocking step, podocytes on glass coverslips were incubated overnight at 4°C with the specific primary antibody (**Table 3.4**). The excess of primary antibody was removed by three washes with PBS and cells were incubated with the secondary antibody goat anti-rabbit Alexa Fluor 546 at a 4 μg/mL dilution (#A-11035, Invitrogen, USA) for 1 hour at room temperature in the dark. After appropriate washes in PBS-T and PBS, cell nuclei were stained by Hoechst 33328 1μM (Sigma Aldrich, USA) for 2 minutes at room temperature. Cells were mounted with Fluorescent Mounting Media (Calbiochem, US and Canada) and images were acquired by using a Leica DM 2000 microscope equipped with a appropriate filter to cover both the excitation and the emission wavelength of Alexa Fluor 546 and Hoechst 33328. The fluorescence intensity was quantified using ImageJ and displayed in corrected total cell fluorescence (CTCF). The corrected total cell fluorescence (CTCF) has been calculated using the following equations:

CTCF = Integrated Density – (Area of selected cell X Mean fluorescence of background readings)

Table 3.4 List of Antibodies used in Immunofluorescence

PrimaryAntibody	SecondaryAntibody
Anti-nephrin antibody (#PA5-20330) 10 μg/mL dilution 1:50 in blocking solution	Goat anti-rabbit Alexa Fluor 546 (#A-11035) 4 μg/mL dilution in blocking solution
Anti-Caspase-3 antibody (E-AB-63602) Dilution1:50 in blockingsolution	

Anti-ERG antibody (E-AB-63602) Dilution1:100 in blockingsolution

3.11 Enzymatic activity

3.11.1 Catalase activity

The Catalase activity was measured according to Aebi(Aebi, 1984). Catalase is an enzyme which catalyzes the following reaction: $2\ H_2O_2 \rightarrow 2\ H_2O + O_2$

The decomposition of H_20_2 can be followed directly by the decrease in absorbance at 240 nm (e240 = 0.00394 --- 0.0002 litersmmol -I mm-I). The difference in absorbance (ΔA240) per unit time is a measure of the catalase activity.

Bovine liver catalase (Sigma-Aldrich, MO, USA) was diluted with 0.05 M phosphate buffer (pH 7.0). Varying quantities of catalase, ranging from 0.01 to 2.00 units, were added to a 96-well flat-bottom UV-transparent microtiter plate (Thermo Scientific, Ottawa Ontario). Hydrogen peroxide was diluted in 0.05 M phosphate buffer (pH 7.0) to a final concentration of 5 mM. A volume of 250 μL of substrate solution was added to each well of the microtiter plate rapidly, using a repeating pipette. The plate was then immediately scanned by the EnSpire® Multimode Plate Reader (PerkinElmer®) at λ = 240 nm every 10 sec for 5 min at 22°C. Catalase activity was calculated based on the rate of decomposition of hydrogen peroxide, which is proportional to the reduction of the absorbance at λ = 240 nm. The catalase activities of cells were normalized to total cellular protein in the lysate and are expressed as units per mg of protein.

3.11.2 SOD activity

The superoxide dismutase (SOD) activity was measured according to Ewing and Janero (Ewing and Janero, 1995). SOD activity was measured using an NBT/NADH/PMS system. The non-enzymatic phenazinemethosulfate-nicotinamide adenine dinucleotide (PMS/NADH) system generates superoxide radicals that reduce nitro blue tetrazolium (NBT) into a purple-colored formazan. One SOD activity unit was defined as the amount of an enzyme required to cause 50% inhibition of the NBT photoreduction rate. Cell lysates were added to a reaction mixture containing 50 mM potassium phosphate, pH 7.0, 166 μM NADH, 43 μM NBT. The reaction was initiated with the addition of 50 μL freshly prepared PMS 0.75 μM. The absorbance (considered as an index of NBT reduction) was monitored at 560 nm over 5 min every 30′ using a multiplate reader (EnSpire 2300, PerkinElmer) in the kinetic mode. The change in absorbance at 560 nm was plotted as a function of time. The slope obtained in the absence of SOD (the activity control) should be maximal and it wastaken as the 100% value; all other slopes generated with SOD standards or cell tissue extracts were compared to this slope. The % inhibition of the rate of increase in absorbance at 560 nm is calculated as follows:

$$\% \text{ Inhibition} = \frac{(\text{Slope of 1X SOD Buffer Control} - \text{Slope of Sample}) \times 100}{\text{Slope of 1X SOD Buffer Control}}$$

IC_{50} values of the samples were determined by plotting percentage inhibition *vs.* the quantity (mg of total proteins) of the cell extract. The SOD activity was expressed in terms of units/mg of protein considering that one SOD activity unit was defined as the amount of enzyme required to cause 50% inhibition of the NBT photoreduction rate.

Bovine SOD Cu,Zn-SOD (SOD1) (Sigma-Aldrich, MO, USA) was used as an internal control to generate a standard curve of the SOD activity.

3.12 GSH total determination

Total Glutathione (GSH) concentration was determined using a GSH Colorimetric Detection Kit (Invitrogen, CA, USA). The kit uses a colorimetric substrate that reacts with the free thiol group on GSH to produce a highly colored product. The cells were cultured in 6-well plate at different concentrations according to the cell size. When a confluence of around 80% was reached, the cells were treated with different bilirubin concentrations. Afterward, the cells were washed with ice-cold PBS, suspended in ice-cold 5% aqueous 5-sulfosalicylic acid dehydrate, and sonicated to lyse cells. The dilution and assay were conducted as indicated by the kit instructions (the end-point method). Total GSH concentrations (μM) were obtained by interpolation on the standard curve. Results were normalized per 100,000 seeded cells at control condition.

3.13 TUNEL assay

TUNEL assay is based on the incorporation of modified dUTPs by the enzyme terminal deoxynucleotidyl transferase (TdT) at the 3'-OH ends of fragmented DNA, a hallmark as well as the ultimate determinate of apoptosis (Grasl-Kraupp et al., 1995). Detection is based on a copper catalyzed covalent reaction between an Alexa Fluor™488 picolyl azide dye and an alkyne and it can be directly observed under a fluorescent microscope. For this purpose cells were seeded on chamber slides, treated with Ang II 0.01 μM, 0.1 μM, and 1 μM for 24 h and then subjected to the TUNEL test using the Click-iT ™ Plus TUNEL assay following the manufacturer's protocol (Thermo Fisher Scientific, MA, USA). Control experiments were carried out where untreated cells were grow up in complete growth medium (to test the background level o f apoptosis). Also, as a positive control for the TUNEL assay, untreated cells were permeabilized with 1 unit of DNase I (Thermo Fisher Scientific, MA, USA) for 30 minutes at room temperature. Cells were counterstained with Hoechst 33328 stain by incubation with a 1μM (Sigma Aldrich, USA) for 2 minutes at room temperature. Cells were mounted with Fluorescent Mounting Media (Calbiochem, US and Canada) and images were acquired by using a Leica DM 2000 microscope equipped with a appropriate filter to cover both the excitation and the emission wavelength of Alexa Fluor 488 and Hoechst 33328.

3.14 IL-6 ELISA

The supernatants of H5V and Aortic endothelial primary cells were collected and subjected to ELISA analysis using Mouse IL-6 ELISA KIT (Diaclone, Besançon, Francia) and Rat IL-6 ELISA KIT respectively (Thermo Fisher Scientific, MA, USA). H5V cells were seeded into plates at a density of 10.000 cells/cm^2 and they were pre- or post- treated with UCB 1.25 or 2.5 μM or DMSO 0.1% (as control) in the presence of BSA 30 μM for 16 h and treated with PA 300 μM for 24 h as decribed in the section 3.3.6. Aortic endothelial primary cells at concentration of 10.000 cell/cm^2 were treated with PA 300 μM for 24 h.Using the method of ELISA we tested the amounts of IL-6 of cell culture supernatants. 100μl of supernatant were added to each well and ELISA tests ware performed according to the manufacturer's instructions. The absorbance was detected at 450 nm by the EnSpire® Multimode Plate Reader (PerkinElmer®).

3.15 Statistical analysis

GraphPad Prism 5 software (GraphPad, San Diego, CA, USA) was used to perform statistical analysis. A statistically significant difference between two data sets was assessed by unpaired two-tailed Student's t-test. Data were obtained from at least three independent experiments and were expressed as mean ± SD. Analysis was performed using student's t test considering $P < 0.05$ as statistically significant. Significance : * $P < 0.05$, ** $P < 0.01$, *** $P< 0.001$.

3.16 Retrospective cross-sectional study

3.16.1 Study design

A retrospective cross-sectional study was performed on 1672 consecutive children and adolescents followed at our Pediatric Obesity Clinic between January 2009 and March 2014. They were admitted to the clinic to undergo a shortterm structured multidisciplinary weight-loss program. The inclusion criteria for the present study were: 1)age ≥5 and age ≤18 years; 2) body mass index (BMI) ≥95th percentile for age and sex using Italian growth data (Cacciari et al., 2006); 3) absence of any drug treatment; 4) abstinence from alcohol; 5) absence of serological markers of hepatitis B (HBV) and hepatitis C (HCV). The study was approved by the Ethical Committee of the IstitutoAuxologicoItaliano (Acronym: BILOB) and was conducted in accordance with the 1975 Declaration of Helsinki, as revised in 2008. The parents or the legal guardians of the subjects or the subjects themselves when aged 18 years gave the written informed consent to participate to the study.

3.16.2 Clinical and anthropometric assessment

Pubertal status was classified in five stages according to Tanner (Tanner and Whitehouse, 1976). Weight and height were measured following standard procedures (Lohman et al., 1988). BMI was calculated as weight (kg)/squared height (m2). Standard deviation scores (SDS) of weight, stature, and BMI were calculated using Italian growth data (Cacciari et al., 2006).Waist circumference was measured at the midpoint between the last rib and th eiliac crest using an anthropometric tape (Organization, 2011).

3.16.3 Laboratory and ClinicalMeasurements

HBV surface antigen and antibodies against HCV were measured to exclude hepatitis B and C (46). Alanine aminotransferase (ALT), aspartate aminotransferase (AST), gamma-glutamyl-transferase (GGT),Alkaline phosphatase, total bilirubin, total cholesterol, high-density lipoprotein (HDL)-cholesterol, low-density lipoprotein (LDL)-cholesterol, triglycerides were measured by the same internal laboratory using standard laboratory methods.C-Reactive protein (CRP) was measured using a immunoturbidimetric assay (CRP RX, Roche Diagnostic, Indianapolis, IN, USA).Blood pressure was measured using asphygmomanometer following international guidelines (The recommended method of measurementof blood pressure remained the same during the study period). The metabolic syndrome (MetS) wasdiagnosed using the criteria of the International Diabetes Federation (IDF)(Alberti et al., 2009).

3.16.4 Liver ultrasonography

Liver ultrasonography was performed by the same radiologistusing the standard criteria(Saverymuttu et al., 1986; Sartorio et al., 2007).Mild steatosis was defined as slightly increased liver echogenicity with normal vessels and absent posterior attenuation; moderate steatosis as moderately increased liver echogenicity with partial dimming of vessels and early posterior attenuation; and severe steatosis as diffusely increased liver echogenicity with absence of visible vessels and heavy posterior attenuation. Normal liver was defined as the absence ofliver steatosis or other liver abnormalities. Nonalcoholic fatty liver disease (NAFLD) was operationally defined as any degree of liver steatosis in the absence of HBV and HCV infection and alcohol intake. Normal liver was defined as the absence of fatty liver. Alcohol consumption was determined by interview with the children and/or their parents

3.16.5 Statistical analysis

Most continuous variables were not Gaussian-distributed and all were reported as median (50th percentile) and interquartile range (IQR, 25th and 75th percentiles). Discrete variables were reported as the number and proportion of subjects with the characteristic of interest. Linear regression models were used to quantify the association of continuous outcomes (age, BMI SDS, waist:height ratio, insulin, homeostatic model assessment (HOMA) and CRP) with bilirubin.Logistic regression models were used to quantify the association of binary outcomes (fatty liver, MetS, large waist circumference, high blood pressure, high triglycerides, impaired fasting glucose and low HDL-cholesterol) with bilirubin (Zimmet et al., 2007).Anunivariable ordinal generalized linear model (OGLM) was used to quantify the association between fatty liver degree (0 = none; 1 = light; 2 = moderate; 3 = severe) and bilirubin (Nano et al., 2016).We used fractional polynomials to test whether the association between the continuous and binary outcomes and bilirubin was linear and found it to be so in all cases (Kunutsor et al., 2017). Statistical analysis was performed using Stata 16.0 (Stata Corporation, College Station, TX, USA).

Chapter 4
Results

4. RESULTS

The results are divided in three tasks according to the development of the project.

4.1 Task 1: The extent of intracellular accumulation of bilirubin determines its anti- or pro-oxidant effect

4.1.1 UCB cytotoxicity

The four cell lines were exposed to a dose-dependent UCB treatment for 24 h and cytotoxicity was assessed by the propidium iodide (PI) test (**Figure 4.1**).

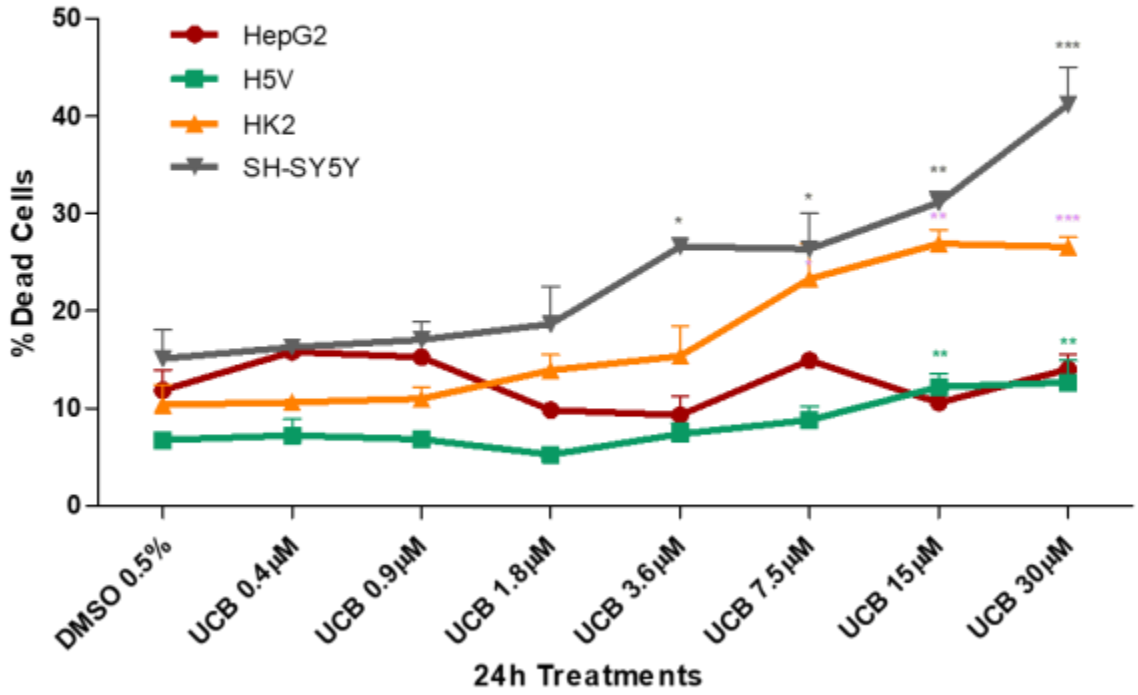

Figure 4.1 The effect of UCB treatment on cell death. The cell lines were exposed to increasing UCB concentration (from 0.4 to 30 µM in the presence of 30 µM BSA) or 0.5% DMSO for 24 h and then treated with PI. The percentage of dead cells was calculated as the proportion of fluorescence intensity of dead cells to that of total cells. Data were expressed as mean ± SD of at least four independent experiments. *p<0.05, **p<0.01, ***p<0.001.

UCB cytotoxicity showed three levels of susceptibility among the cell lines. HepG2 cell line was less sensitive, while the neuronal cells appeared to be the most sensitive. HK2 and H5V showed an intermediate dose-dependent cytotoxicity behavior. The first significant increase of dead cells was detected at UCB concentration of 3.6 µM for SH-SY5Y, 7.5 µM for HK2, and 15 µM for H5V. No changes were observed in HepG2.

4.1.2 UCB metabolic activity

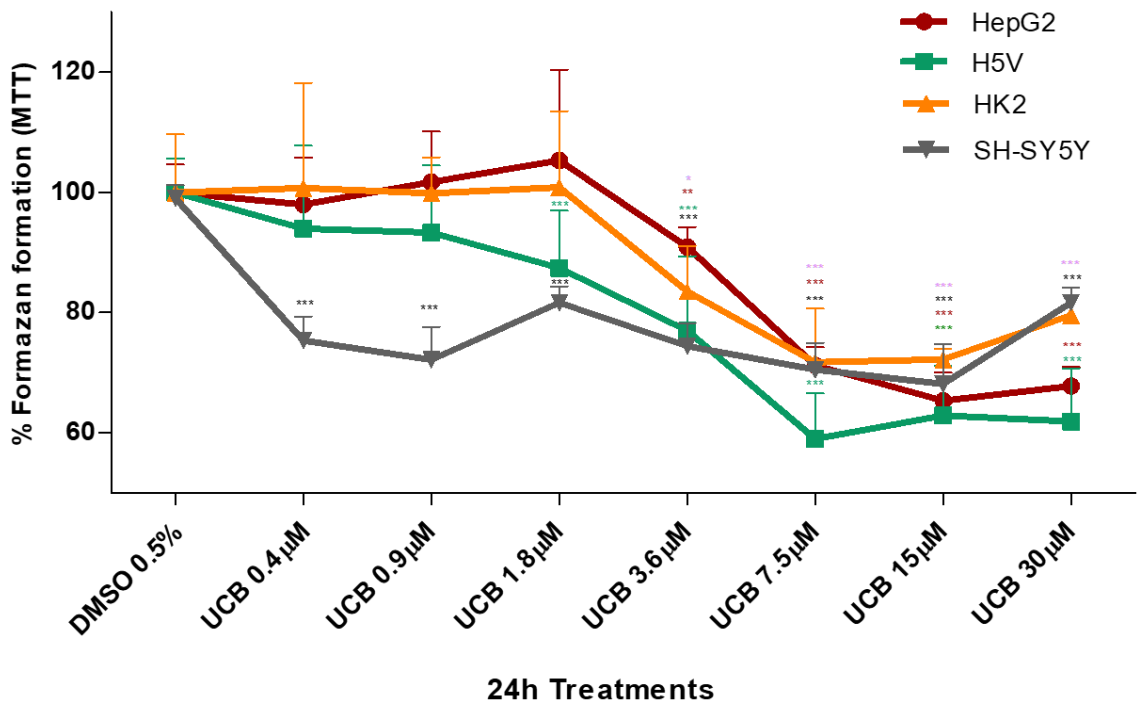

Figure 4.2 The effect of UCB treatment by MTT assay. The cell lines were exposed to increasing UCB concentration (from 0.4 to 30 µM in the presence of 30 µM BSA) or 0.5% DMSO for 24 h. Cells treated with vehicle (DMSO 0.5%) are considered 100% of viability. Data were expressed as mean ± SD of at least four independent experiments. *p<0.05, **p<0.01, ***p<0.001.

The four cell lines were exposed to a dose-dependent UCB treatment for 24 h. The metabolic activity measured by MTT was also substantially affected upon the same UCB exposure (**Figure 4.2**). In HepG2 cells, the formazan generation was reduced by 30% upon exposure to increasing UCB concentrations, and similar data were obtained also in H5V and HK2 cells. However, the SH-SY5Y cells were substantially more sensitive showing a reduction of formazan generation to 75% upon exposure to as low as 0.4 µM UCB concentrations.

4.1.3 The effect of UCB exposure on intracellular UCB concentration

All four cell lines were exposed for 24 h to increasing UCB concentrations, and then the intracellular bilirubin concentrations were determined (**Table 4.1**).

The intracellular bilirubin concentrations differed substantially among the cell lines: HepG2 cells were found to be the most resistant. Intracellular UCB concentration in this cell type remained comparable to the control level until UCB 15 µM exposure also showing a four-fold increase at 30 µM treatment when its value reached 20 ng/mg. SH-SY5Y, HK2, and H5V cells showed a significant dose-dependent intracellular bilirubin content though the extent differed among the three cell lines: SH-SY5Y resulted in the most sensitive cells, having one order of magnitude higher intracellular concentrations comparedtoHepG2 cells (p= 0.0014).

Table 4.1 The effect of UCB exposure to intracellular UCB concentrations. The cell lines were exposed for 24 h to the increasing UCB concentrations (from 0.4 to 30 μM in the presence of 30 μM BSA) or 0.5% DMSO. Data were expressed as mean±SD of three independent experiments and UCB concentrations were recalculated per mg of protein. P-values represent comparison to control cells.

	HepG2		H5V		HK2		SH-SY5Y	
Treatment	**Mean ± SD** (ng/mg)	**P-value**(vs Ctrl)	**Mean ± SD** (ng/mg)	**P-value**(vs Ctrl)	**Mean ± SD** (ng/mg)	**P-value**(vs Ctrl)	**Mean ± SD** (ng/mg)	**P-value**(vs Ctrl)
Control	5.0 ± 1.8		0.0 ± 0.0		0.0 ± 0.0		0.0 ± 0.0	
UCB 0.4 μM	4.1 ± 1.5	0.735	0.0 ± 0.0		1.8 ± 0.2	0.014	3.34 ± 1.06	0.503
UCB 0.9 μM	5.1 ± 2.0	0.984	1 ± 1.09	0.546	3.5 ± 0.4	0.013	7.5 ± 2.0	0.309
UCB 1.8 μM	2.4 ± 0.7	0.311	3.4 ± 3.51	0.415	3.0 ± 0.6	0.037	13.0 ± 3.0	0.163
UCB 3.6 μM	2.0 ± 0.5	0.245	4.7 ± 0.6	0.018	6.7 ± 0.1	0.000	25.5 ± 5.4	0.043
UCB 7.5 μM	4.6 ± 2.3	0.900	7.5 ± 1.6	0.042	13.4 ± 0.9	0.004	29.5 ± 6.3	0.043
UCB 15 μM	5.4 ± 0.7	0.874	42.4 ± 4.5	0.011	40.1 ± 9.5	0.052	79.1 ± 8.4	0.011
UCB 30 μM	21.3 ± 2.4	0.033	122.3 ± 2.8	0.001	123.8 ± 11.5	0.009	303.3 ± 11.2	0.001

4.1.4 The effect of UCB exposure on intracellular ROS

To test the pro-oxidant ability of UCB, the intracellular ROS production was measured (**Figure 4.3**).

UCB did not result in any significant increase in intracellular ROS production in HepG2 cells. On the contrary, in SH-SY5Y cells, UCB concentrations higher than 3.6 μM (corresponding to intracellular bilirubin concentration of 25 ng/mg) resulted in a 3-fold increase in intracellular ROS production. In H5V and HK2 cells, UCB treatments higher than 15 μM (corresponding to intracellular bilirubin concentration of 40 ng/mg) doubled the intracellular ROS concentration.

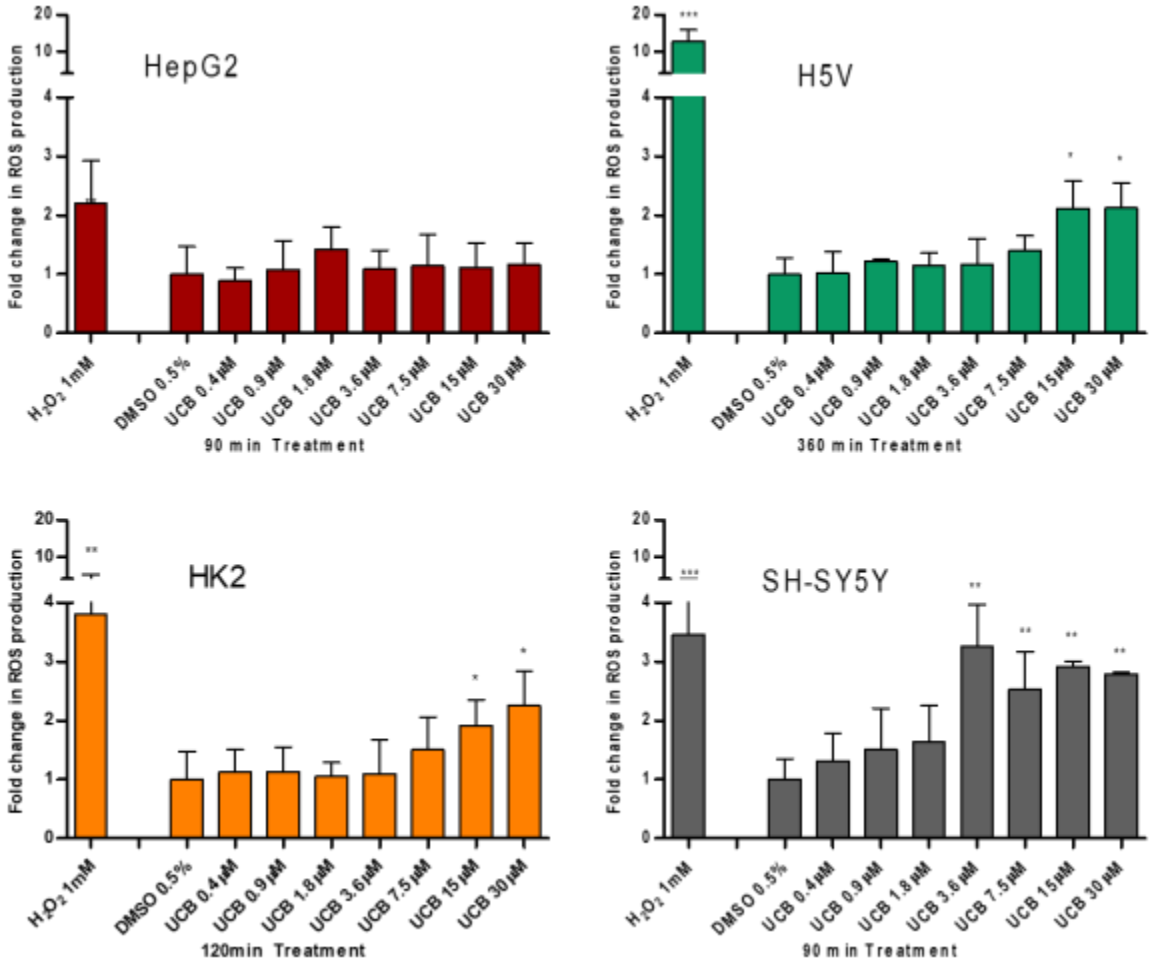

Figure 4.3 The effect of UCB treatment on intracellular ROS production. The cell lines were exposed to increasing UCB concentration (from 0.4 to 30 μM in the presence of 30 μM BSA) or 0.5% DMSO for the time indicated on the x-axis. The time of exposure to UCB was defined by a time course performed in each cell line. The time with the highest peak of ROS increase by H_2O_2 1 mM (used as positive control) was chosen for each cell line (90 min for HepG2 cells, 120 min for SH-SY5Y and HK2 cells, and 360 min for H5V cells). Fluorescence results reflecting the ROS production were normalized to the total protein content and compared to DMSO-treated cells. Data were expressed as mean±SD of three independent experiments. *p<0.05, **p<0.01, ***p<0.001.

4.1.5 The antioxidant effect of UCB on live cells measured by Anti Oxidant Power 1 (AOP1)

Having assessed the pro-oxidant capacity of bilirubin by evaluating intracellular ROS accumulation, we tested possible antioxidant effects of UCB by using the Light-Up Cell System (LUCS) technology (**Figure 4.4**). LUCS assay measures the ability of a condition to neutralize free radicals produced at the intracellular level by a photo-induction process (Derick et al., 2017). When applied on a dose-response mode, the assay allows to evaluate the EC_{50} of intracellular antioxidant effect of a compound (Gironde et al., 2020).

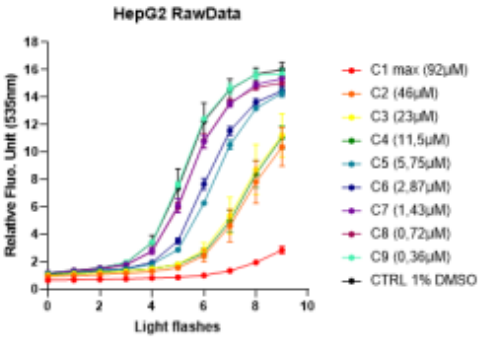
HepG2 RawData
Relative Fluo. Unit (535nm)
Light flashes
C1 max (92µM)
C2 (46µM)
C3 (23µM)
C4 (11,5µM)
C5 (5,75µM)
C6 (2,87µM)
C7 (1,43µM)
C8 (0,72µM)
C9 (0,36µM)
CTRL 1% DMSO

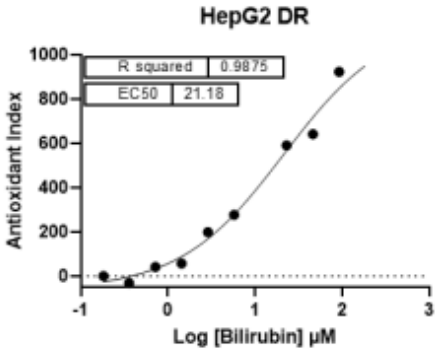
HepG2 DR
R squared 0.9875
EC50 21.18
Antioxidant Index
Log [Bilirubin] µM

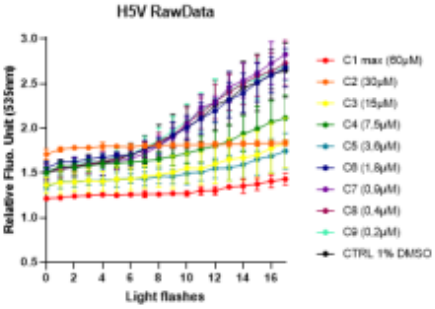
H5V RawData
Relative Fluo. Unit (535nm)
Light flashes
C1 max (60µM)
C2 (30µM)
C3 (15µM)
C4 (7,5µM)
C5 (3,6µM)
C6 (1,8µM)
C7 (0,9µM)
C8 (0,4µM)
C9 (0,2µM)
CTRL 1% DMSO

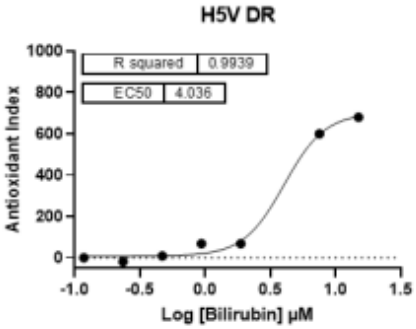
H5V DR
R squared 0.9939
EC50 4.036
Antioxidant Index
Log [Bilirubin] µM

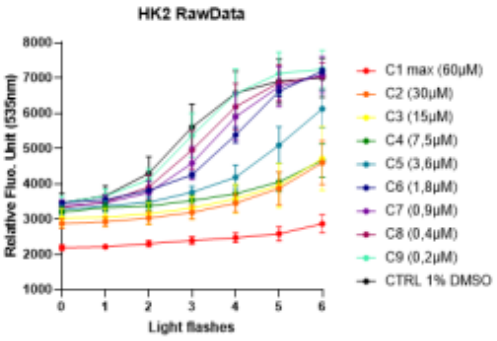
HK2 RawData
Relative Fluo. Unit (535nm)
Light flashes
C1 max (60µM)
C2 (30µM)
C3 (15µM)
C4 (7,5µM)
C5 (3,6µM)
C6 (1,8µM)
C7 (0,9µM)
C8 (0,4µM)
C9 (0,2µM)
CTRL 1% DMSO

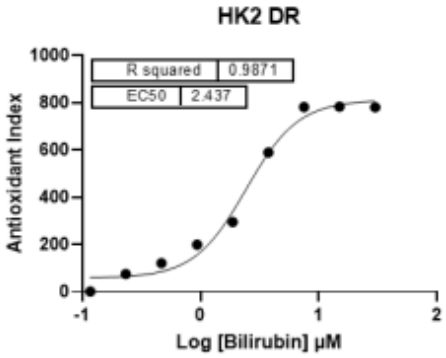
HK2 DR
R squared 0.9871
EC50 2.437
Antioxidant Index
Log [Bilirubin] µM

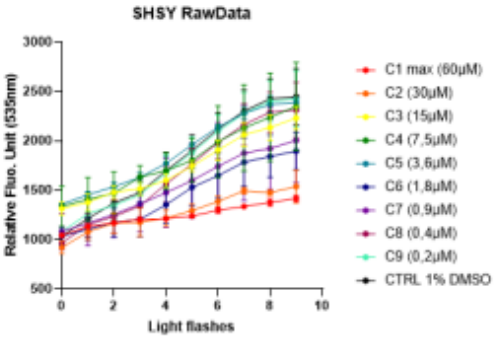
SHSY RawData
Relative Fluo. Unit (535nm)
Light flashes
C1 max (60µM)
C2 (30µM)
C3 (15µM)
C4 (7,5µM)
C5 (3,6µM)
C6 (1,8µM)
C7 (0,9µM)
C8 (0,4µM)
C9 (0,2µM)
CTRL 1% DMSO

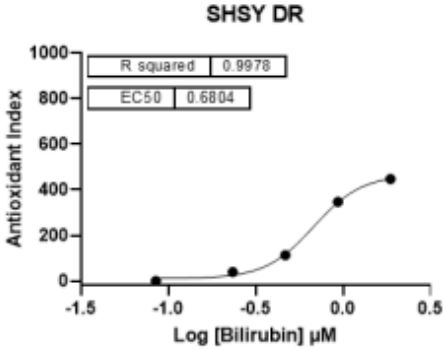
SHSY DR
R squared 0.9978
EC50 0.6804
Antioxidant Index
Log [Bilirubin] µM

Figure 4.4 The antioxidant and cytotoxic effects of UCB.
Each cell line was incubated for 24 h with indicated UCB concentrations and then treated with the fluorescent biosensor for 1 h. The left panel reports the kinetic profiles recorded for each cell line. Relative Fluorescence Units (RFU) were measured at exc/em 501/535 nm according to a recurrent 480 nm LED flash application (20 iterations). The antioxidant effect is measured as a delay (right shift) in fluorescence intensity increase in comparison to negative control profile. Fluorescence intensities higher than negative control at t=0 (before light application) indicate pro-oxidant/cytotoxic effects (as described in (Derick et al., 2017). Error bars represent SD values from triplicates. Right panel reports dose-response curves obtained after integration of normalized kinetic data. R2s represent determination coefficients obtained by fitting data with a sigmoid regression analysis. Unexpected concentrations C4 (HepG2 cells) and C5 (H5V cells) were removed from the regression analysis. Each series of data corresponds to an experiment representative of at least three experiments.

A direct antioxidant activity of lower UCB concentrations was detected in all the four cell lines even if it differed significantly among cell lines. In HepG2 cells, the dose-effect curve showed an EC_{50} of antioxidant effect of approximately 21.2 μM (corresponding to an intracellular UCB concentration of 5.4 ng/mg). In SH-SY5Y cells, the antioxidant effect was evident at 0.68 μM (corresponding to an intracellular UCB concentration between 3.3 and 7.5 ng/mg), whereas in H5V and HK2 cells, the antioxidant effect occurred at intermediate UCB concentration. EC_{50} of antioxidant effect was at 4 μM and 2.4 μM respectively, corresponding to and intracellular UCB concentration between 5 and 7 ng/mg in both cell lines.
LUCS is a dedicated approach to discriminate between pro-oxidant/cytotoxic and antioxidant effects (Gironde et al., 2020). Indeed, pro-oxidant/cytotoxic effect is revealed at the initial time course by a fluorescence intensity higher than control value (Derick et al., 2017). No cytotoxic effect was seen on HepG2 and HK2 cells, while it was present at low concentration on SH-SY5Y (treatment of 3.6 μM corresponding to an intracellular UCB concentration of 25 ng/mg) and at high concentrations (treatment of 30 μM corresponding to an intracellular UCB concentration of 122 ng/mg) on H5V cells. **Table 4.2** reports the intracellular UCB concentration (ng/mg protein) corresponding to the EC_{50} or cytotoxic effect in each cell line.

Table 4.2 The intracellular UCB concentrations corresponding to antioxidant (EC_{50}) or cytotoxic effects.

Cell Lines	Antioxidant EC_{50}		Cytotoxic effect	
	UCB Treatment	Intracellular UCB content (ng/mg total protein)	UCB Treatment	Intracellular UCB content (ng/mg total protein)
HepG2	21.2 µM	between 5.4 and 21.3 ng/mg total protein		
H5V	4.04 µM	between 4.7 and 7.5 ng/mg total protein	>30 µM	>122.3 ng/mg
HK2	2.44 µM	between 3 and 6.7 ng/mg total protein		
SH-SY5Y	0.68 µM	between 3,3 and 7.5 ng/mg total protein	>3.6 µM	>25.5 ng/mg

4.1.6 Intracellular UCB pro-oxidant and anti-oxidant thresholds

Considering the intracellular UCB (iUCB) concentration regardless of the UCB concentration treatment, we observed that all cell lines have a similar intracellular UCB threshold for antioxidant and pro-oxidant effects. **Figure 4.5** summarizes all the results previously presented and demonstrates the proposed intracellular UCB threshold. An intracellular UCB concentration around 7 ng/mg acts as an antioxidant, while an intracellular concentration higher than 25 ng/mg is associated with pro-oxidant and cytotoxic effects.

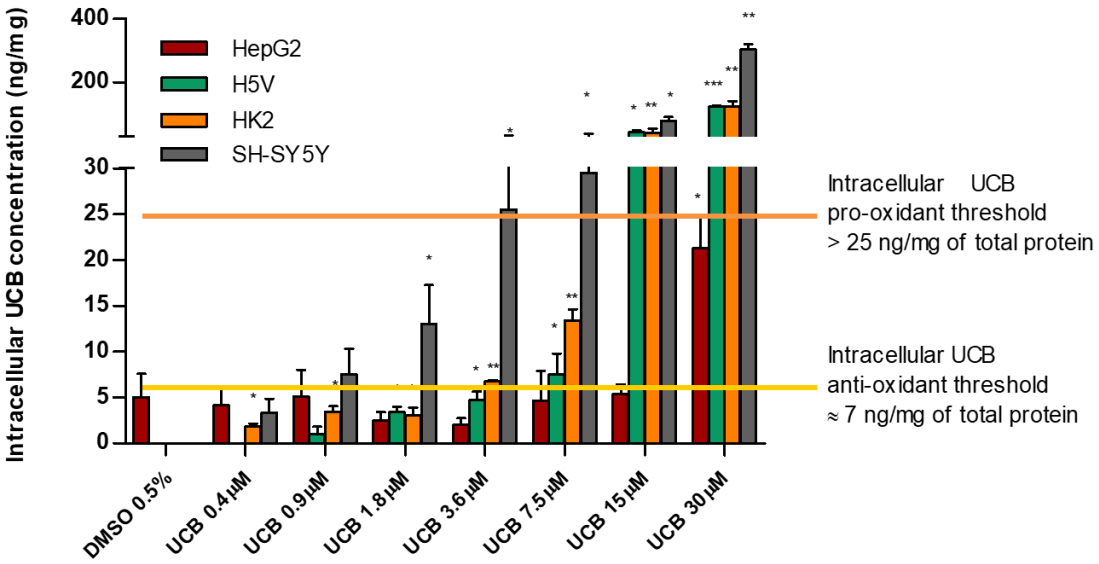

Figure 4.5 Intracellular UCB pro-oxidant and antioxidant thresholds. The cell lines were exposed for 24 h to the increasing UCB concentration (from 0.4 to 30 µM in the presence of 30 µM BSA) or 0.5% DMSO. Data are expressed as mean±SD of three independent experiments, UCB concentration were recalculated per mg of protein. P-values represent comparison with control cells. *p<0.05, **p<0.01, ***p<0.001.

4.1.7 The effect of UCB on total GSH

Since the cells use multiple systems to protect against ROS overproduction, we measured total GSH concentrations (**Figure 4.6**) in all four cell lines exposed for 24 h to increasing UCB concentrations.

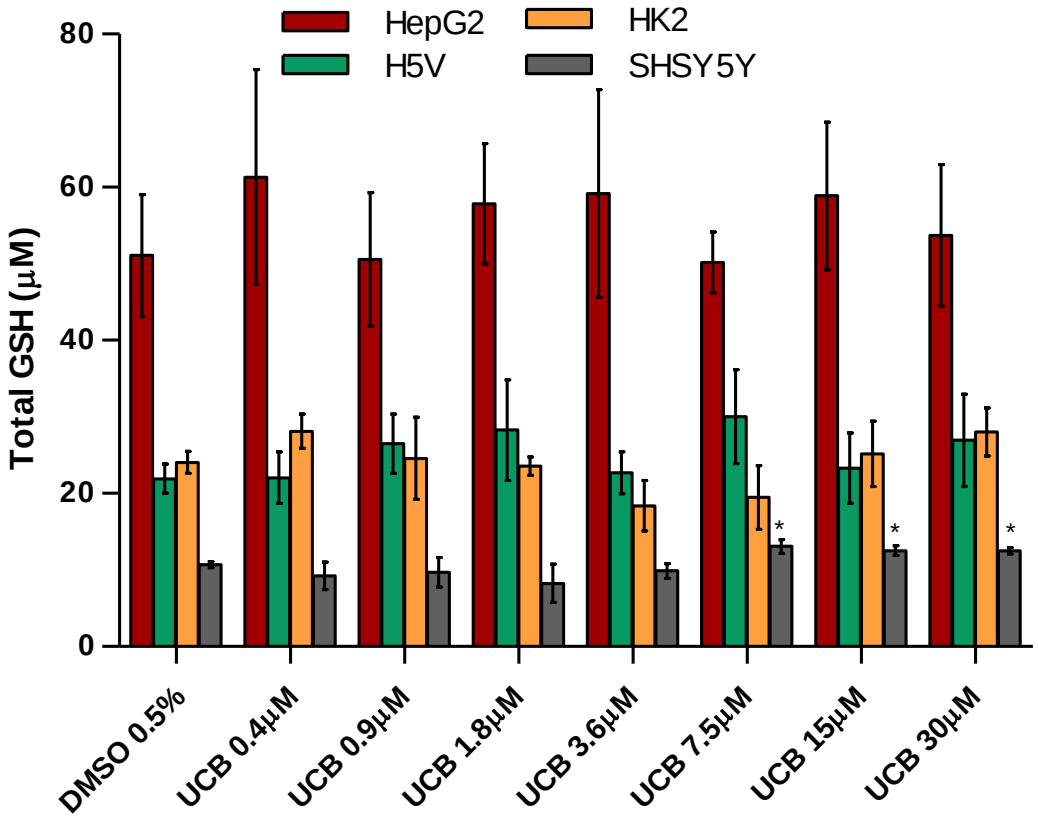

Figure 4.6 The effect of UCB exposure on intracellular glutathione (GSH) concentrations. The cell lines were exposed to increasing UCB concentrations (from 0.4 to 30 μM in the presence of 30 μM BSA) or 0.5% DMSO for 24 h and then total GSH concentration was measured. Data were expressed as mean ± SD of three independent experiments. * $p < 0.05$.

The basal level of GSH was higher in HepG2 cells. GSH concentration was not affected by UCB treatment. The only exception was represented by the SH-SY5Y cells, in which GSH concentrations increased at UCB treatment higher than 7.5 μM (corresponding to an intracellular bilirubin content of 30 ng/mg of total protein).

4.1.8 The effect of UCB on antioxidant enzymes activity

We tested the effect of increasing UCB concentrations on SOD and Catalase activity. Both SOD and Catalase activities were not affected by UCB treatment in HepG2 cells. SOD induction was observed in other cell lines at UCB pro-oxidant/cytotoxic concentrations (**Figure 4.7**).

In SHSY5Y cells, UCB concentrations higher than 3.6 μM (corresponding to intracellular bilirubin concentration of 25 ng/mg) increased SOD activity by approximately 30.000 mU/mg total protein, that means a significant induction compared to control cells (2000mU/mg total protein). In H5V and HK2 cells, treatments with UCB concentrations higher than 7.5 μM (corresponding to intracellular bilirubin concentration of 7.5 ng/mg) and 15 μM (corresponding to intracellular bilirubin concentration of 40 ng/mg) significantly increased the SOD activity.

It is important to note that the basal SOD activity on HepG2 cells is around 8000mU/mg total protein, higher than in the basal state of other cell lines considered.

On SHSY5Y cells, Catalase activity was induced in UCB dose-dependent manner and reached significativity compared to control at UCB concentration higher than 7.5 μM (corresponding to intracellular bilirubin concentration of 30 ng/mg). On H5V, Catalase activity was significantly lower than that control at UCB concentration higher than 7.5 μM. At the same time, in HK2 cells UCB concentrations ≤ 3.6 μM showed a significant 3 folds induction of catalase activity compared to the control (**Figure 4.8).**

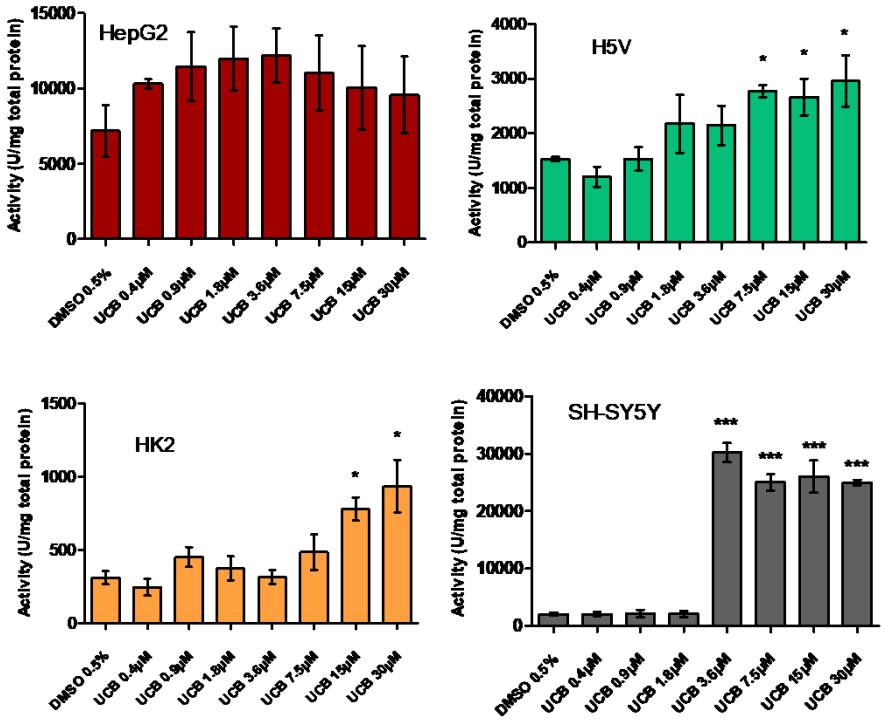

Figure 4.7 The effect of UCB exposure on SOD activity. The cell lines were exposed to increasing UCB concentrations (from 0.4 to 30 μM in the presence of 30 μM BSA) or 0.5% DMSO for 24 h and then total GSH concentration was measured. Data were expressed as mean±SD of three independent experiments. *p<0.05, **p<0.01, ***p<0.001.

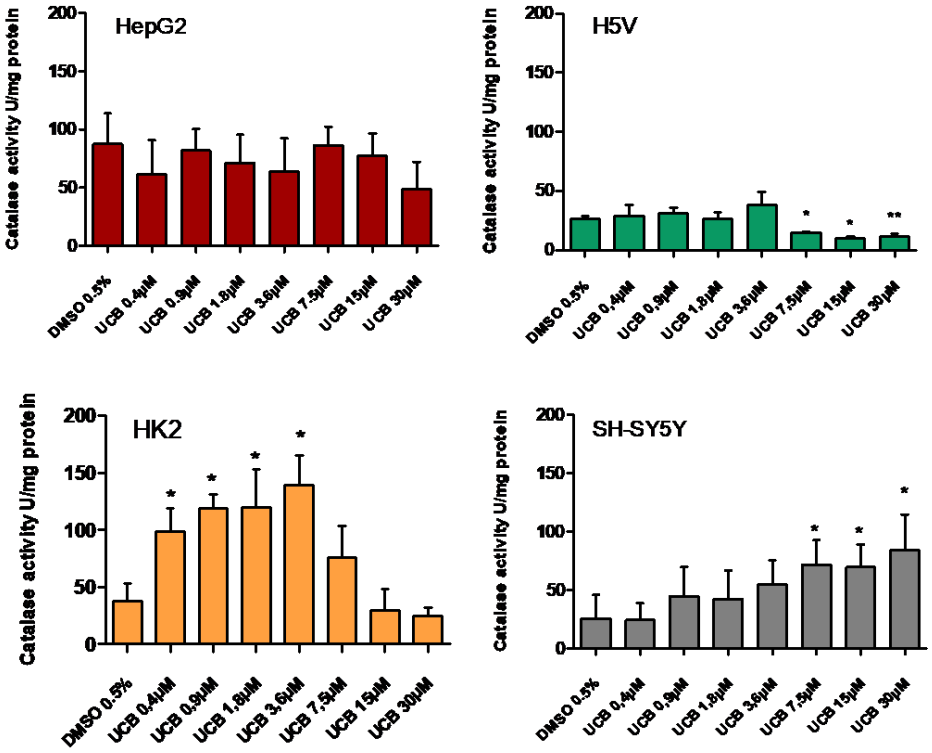

Figure 4.8 The effect of UCB exposure on Catalase activity. The cell lines were exposed to increasing UCB concentrations (from 0.4 to 30 μM in the presence of 30 μM BSA) or 0.5% DMSO for 24 h and then Catalase activity was measured. Data were expressed as mean±SD of three independent experiments. *p<0.05, **p<0.01, ***p<0.001.

4.2 Task 2: Life-long bilirubin exposure and UCB-priming prevent *in vitro* cellular metabolic damage

4.2.1 Gunn rat primary cells characterization

4.2.1.1 Histological analysis: comparison between Wistar and Gunn rats

Histological details of H&E aorta and kidneys revealed no macroscopical difference among Wistar rat organs, normobilirubinemic heterozygous Gunn rats Nj, and hyperbilirubinemic homozygous Gunn rats jj ones (**Figure 4.9 and 4.10**).

Regarding the aortic tissue, three layers or tunica were distinguished: tunica intima characterized by the presence of very pronounced nuclei, the tunica media and the tunica adventitia. The relaxed collagen in antique pink and the wisteria-colored curled elastin were distinguished. Around the section of the aorta, brown adipose tissue was detected, indicating the young age of the rat.

The arcuate arteries were clearly visualized on the cortico-medulla border as darker thin lines and cortical glomeruli could be easily identified at 20x magnification as oval violet elements, in which Bowman's capsule and parietal layer were evident (Siddiqui et al., 2016). The high number of petechiaes showed in photomicrographs of all kidneys were probably due to the anesthetic techniques, White spots (ectasia, cells with nuclei and without cytoplasm) visible in kidneys were attributed to fixation step.

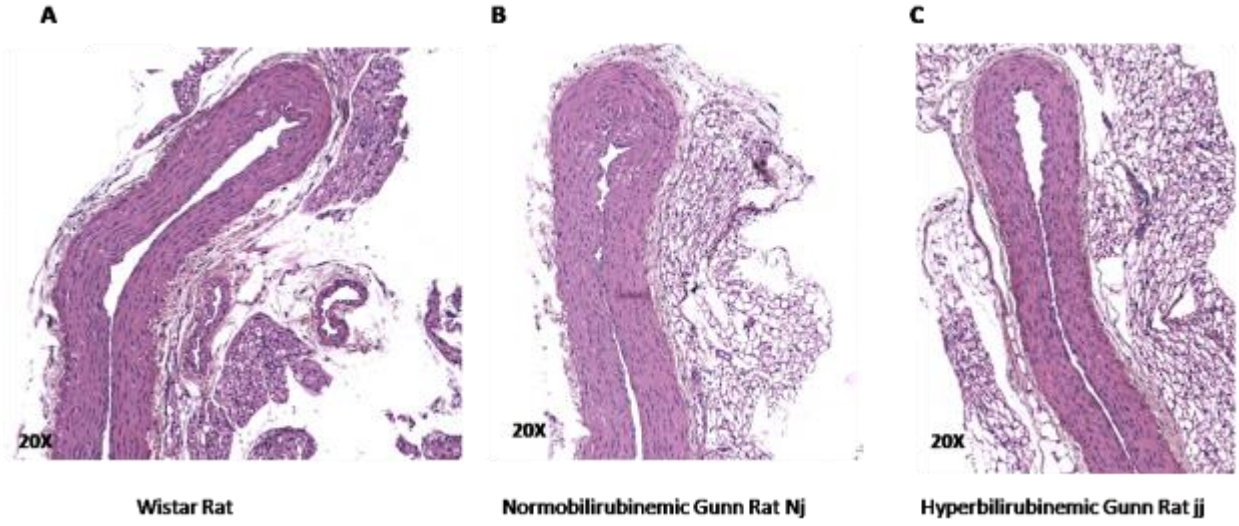

Figure 4.9 Visualization of normal rat aorta with Hematoxylin-eosin staining. A) H&E-stained Wistar rat aorta (20x). **B)** H&E-stained normobilirubinemic Gunn Nj rat aorta (20x). **C)** H&E-stained hyperbilirubinemic Gunn jj rat aorta (20x).

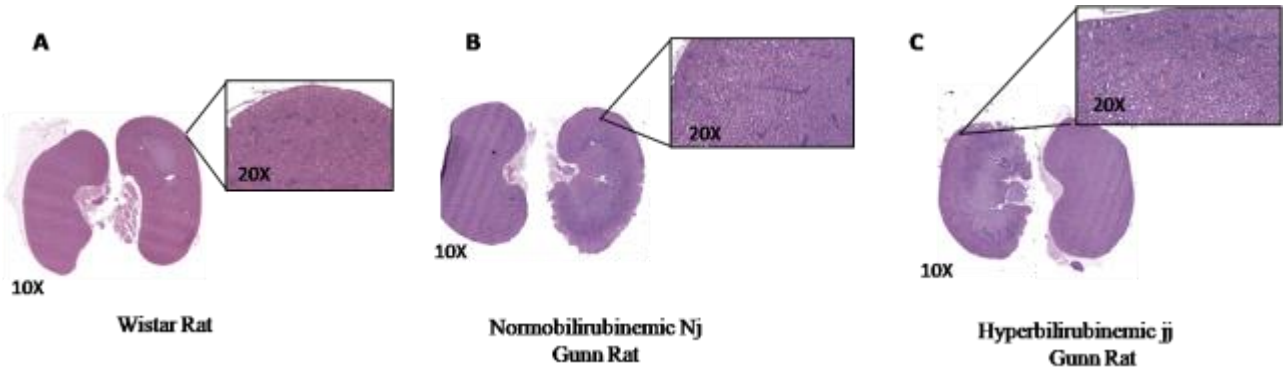

Figure 4.10 Visualization of normal rat kidneys with Hematoxylin-eosin staining. **A)** H&E-stained Wistar rat kidney (10x) and cortical histology section at higher magnification showed Bowman's capsule, cortical glomeruli (20x). **B)** H&E-stained normobilirubinemic Gunn (Nj) rat kidney (10x) and cortical histology section at higher magnification showed Bowman's capsule, cortical glomeruli (20x). **C)** H&E-stained hyperbilirubinemic Gunn (jj) rat kidney (10x) and cortical histology section at higher magnification showed Bowman's capsule, cortical glomeruli (20x).

4.2.1.2 Primary aortic endothelial cells characterization: ERG immunofluorescence

Immunofluorescence analysis indicated that only CD31 positive cells was also positive for ERG specific marker (**Figure 4.11)**.

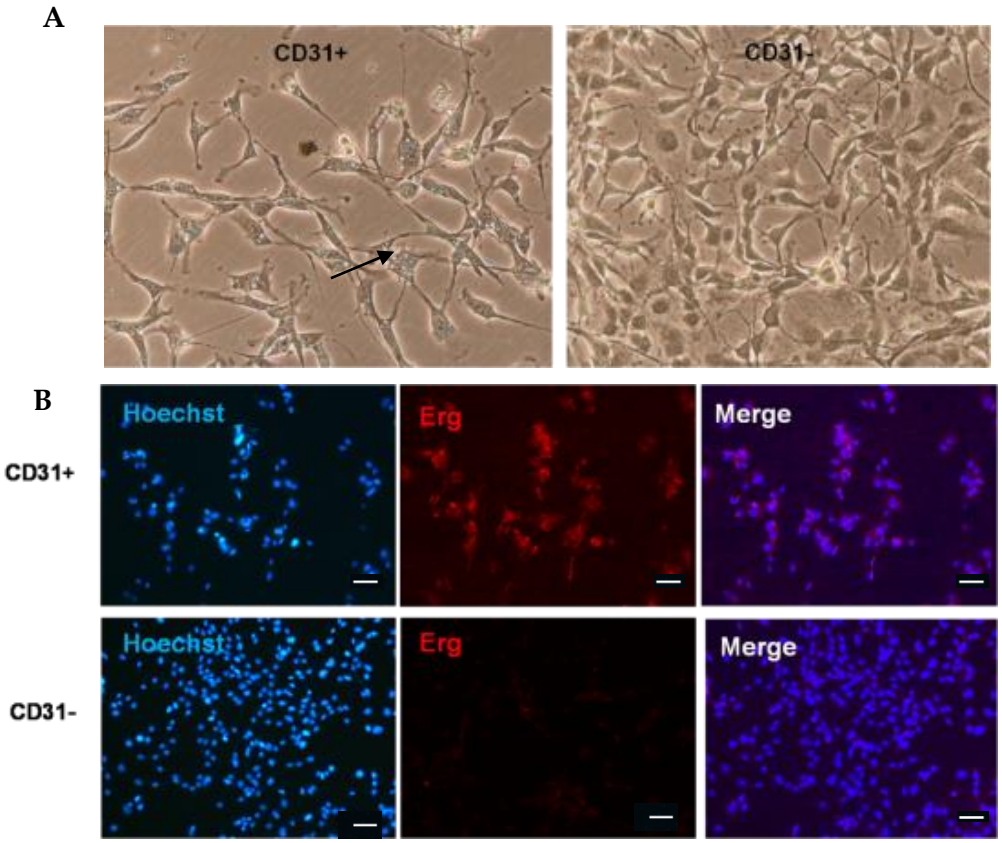

Figure 4.11 Purification of rat aortic endothelial cells. A) These representative immunofluorescence images shown the selected CD31+/CD31-cells isolated by using a positive selection with CD31+ magnetic beads indicated with an arrow. Fluorescence images were taken at imaged at cell passage 2. The magnification used was 40X**. B)** Rat aortic endothelial cells were characterized based on staining for cell surface marker Erg (red). Nuclei were stained with Hoechst (blue). The magnification used was 10X**.** Scale bar 50µm.

4.2.1.3 Primary podocytes characterization: Nephrin immunofluorescence

Immunofluorescence analysis indicated that both glomeruli and podocytes isolation expressed a high level of nephrin protein. Nephrin showed plasma membrane and perinuclear localizations (**Figure 4.12**).

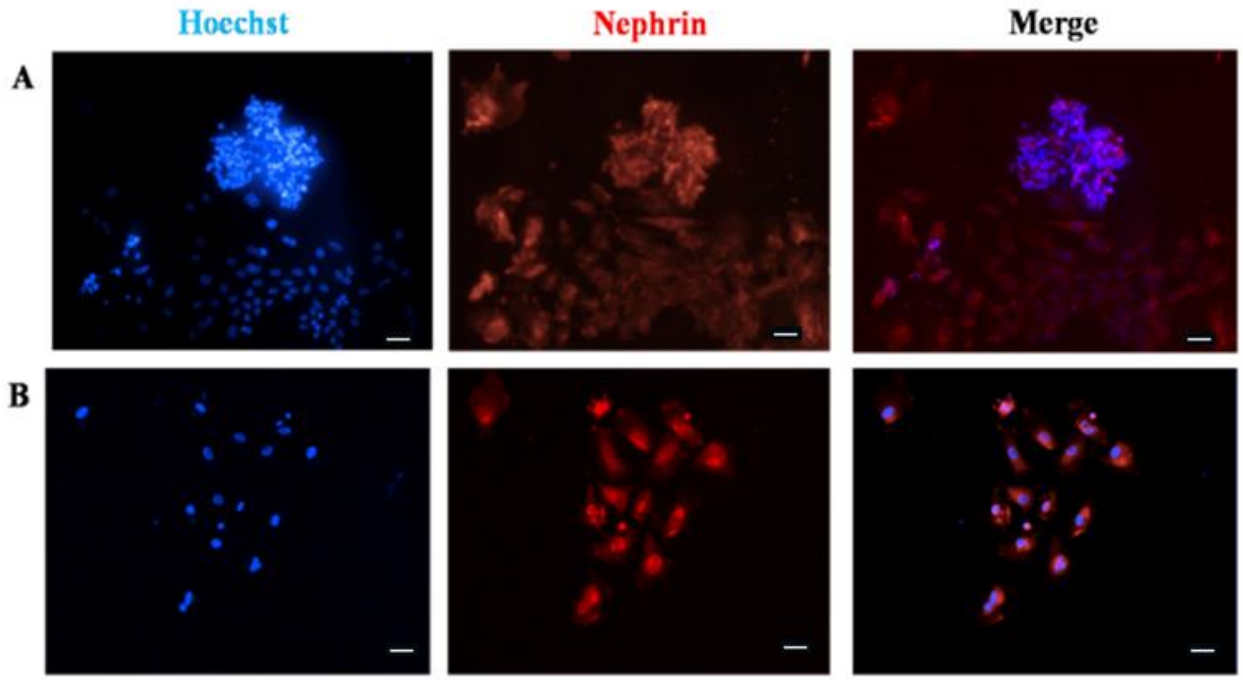

Figure 4.12 Localization and expression of podocyte-specific protein nephrin. Indirect immunofluorescence staining was used to identify podocytes. Specific podocyte marker protein nephrin stained positively, showing red fluorescence; the nuclei were stained with blue nuclear counterstain (Hoechst). **A)** Glomeruli immunofluorescence. 20x magnification. **B)** Podocytes immunofluorescence. 20x magnification. Scale bar 50µm**.**

4.2.2 Impact of UCB on cell viability upon different stimuli of damage

4.2.2.1 PA and Angiotensin II impact on Nj and jj primary cells

Aortic endothelial cells harvested from Nj and jj Gunn rats were treated with increasing doses of PA ranging from 75 μM up to 450 μM in the presence of BSA 75 μM for 24 h. As shown in the **Figure 4.13**, the viability of Nj cells decreased by 30% upon PA 75 μM while jj cells showed a lower reduction of their viability. Moreover, the viability of cells from jj rats resulted significantly higher than that of cells from Nj rats at any PA concentration.

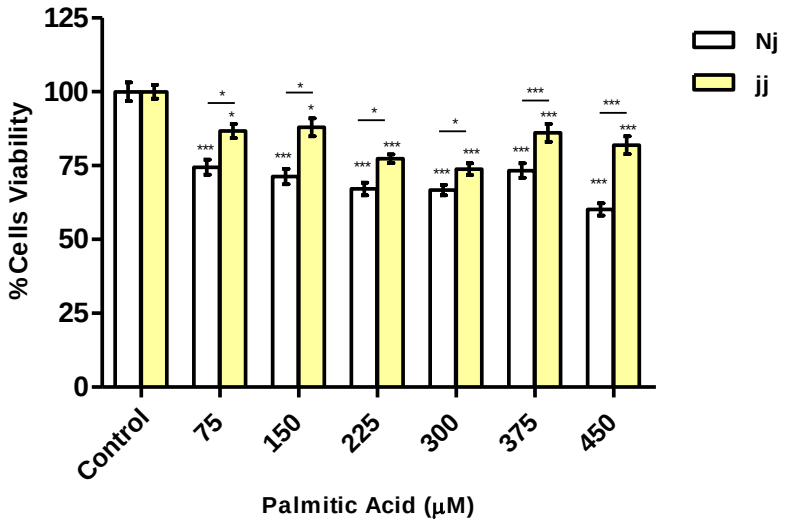

Figure 4.13 Effect of PA treatments on cell viability (MTT test) in Nj and jj primary cells. Aortic endothelial primary cells were exposed to increasing PA concentrations (from 75 to 450 μM in the presence of 75 μM BSA) for 24 h. Cells treated with complete growth medium were considered 100% of viability. Data were expressed as mean ± SD of three independent experiments. *p<0.05, **p<0.01, ***p<0.001.

Primary podocytes were exposed to Ang II 0.01, 0.1, and 1 μM for 24 h and the viability was measured by MTT test. Podocytes viability was reduced significantly upon all Ang II concentrations (20-25% in podocytes from Nj rats and 10-15% in cells from jj rats)(**Figure 4.14**). Importantly, at Ang II 0.1 μM and 1 μM cell viability of podocytes from jj rats was significantly higher than of podocytes from Nj rats.

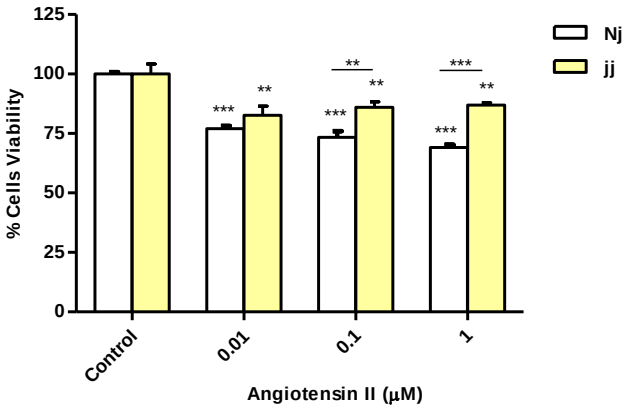

Figure 4.14 Effect of Ang II treatments on cell viability (MTT test) in Nj and jj primary cells. Primary podocytes were exposed to the Ang II 0.01 μM, 0.1 μM, and 1 μM for 24 h. Cells treated with complete growth medium were considered 100% of viability. Data were expressed as mean ± SD of three independent experiments. *p<0.05, **p<0.01, ***p<0.001.

4.2.2.2 PA effect on cell viability in UCB-treated H5V cells

H5V were exposed to PA, after (UCB pre-treatment) or before (UCB post-treatment) UCB treatment. As shown in **Figure 4.15 A and B,** PA treatment reduced cell viability (approximately 50%) and increased cell death (up to 20%), while UCB pre-treatment reduced PA effects by increasing cell viability and reducing cell death rate. On the contrary, UCB post-treatment did not change cell viability and cell death behavior induced by PA (data not shown).

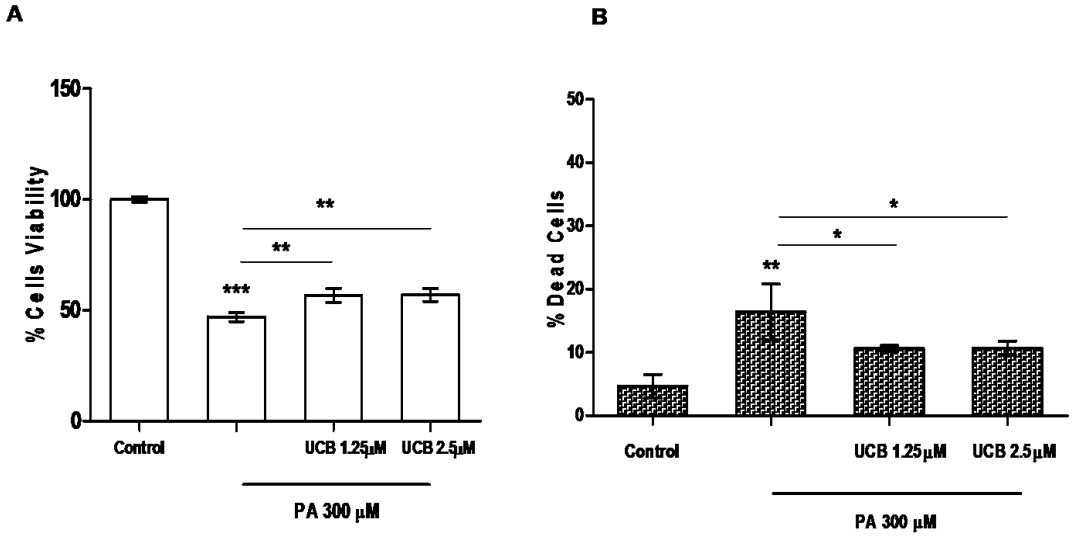

Figure 4.15 The effect of UCB pre-treatment in PA-induced damage on immortalized H5V cells. H5V cells were pre-incubated with UCB 1.25 or 2.5 μM or DMSO 0.1% (as control) in the presence of BSA 30 μM for 16 h. At the end of incubation, UCB was removed and H5V cells were treated with PA 300 μM for 24 h. **A)** UCB effect on cell viability was measured by MTT. Viability of control cells was considered 100%. **B)** UCB effect on cell death detected by PI assay. The percentage of dead cells was calculated as the proportion of fluorescence intensity of dead cells to that of total cells. Data were expressed as mean ± SD of at least three independent experiments. *p<0.05, **p<0.01, ***p<0.001.

4.2.2.3 Angiotensin II effect on HK2 cell viability

HK-2 were exposed to Ang II in a dose-dependent manner by using concentration ranging from 0.01 μM to 10 μM for 24 hours. Angiotensin II treatments did not reduce cells viability or cells mortality compared to control cells (**Figure 4.16 A and B**). For this reason, we did not perform UCB pre- and post- treatments as we did for H5V cells (seeparagraph4.2.2.2).

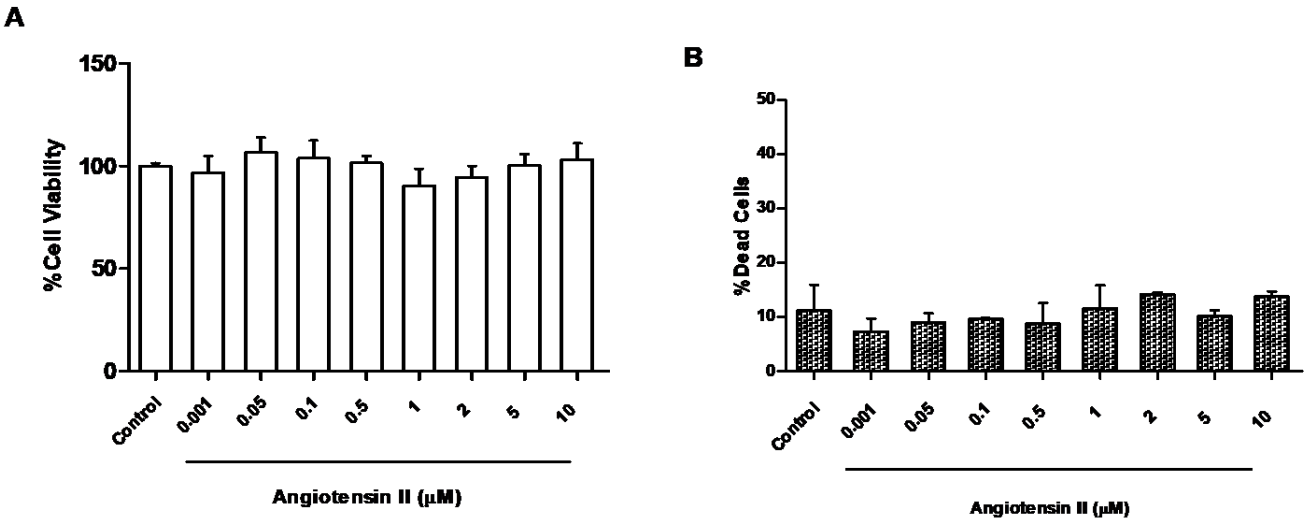

Figure 4.16 Angiotensin II effects on HK2 cells viability and mortality. HK-2 cells were exposed to a dose dependent Ang II treatment or cell medium (control) for 24 hours. **A)** MTT assay was used to assess cells viability. **B)** PI assay was used to assess cells viability. Results were reported as average ±SD of at least three independent experiments.

4.2.3 Impact of UCB on ER-stress-inflammation axis in endothelial cells

4.2.3.1 PA effect on CHOP activation and IL-6 release in Nj and jj aortic endothelial primary cells

Primary endothelial Nj and jj cells were treated with PA 300 μM and 450 μM for 24 h. A significant up-regulation of CHOP protein was observed after 24 h of incubation with PA 300 μM and 450 μM only in Nj aortic endothelial cells. Conversely, the same treatment on jj aortic endothelial cells showed a significant decrease in CHOP protein level (**Figure 4.17 A and B**). A major boost in IL-6 production upon PA 300 μM and PA 450 μM treatments was observed only in Nj cells, while cells from jj rats showed a significant decrease in IL-6 release. The IL-6 release in the cell medium by cells from jj rats was significantly lower than that released by cells form Nj rats (**Figure 4.17 C**).

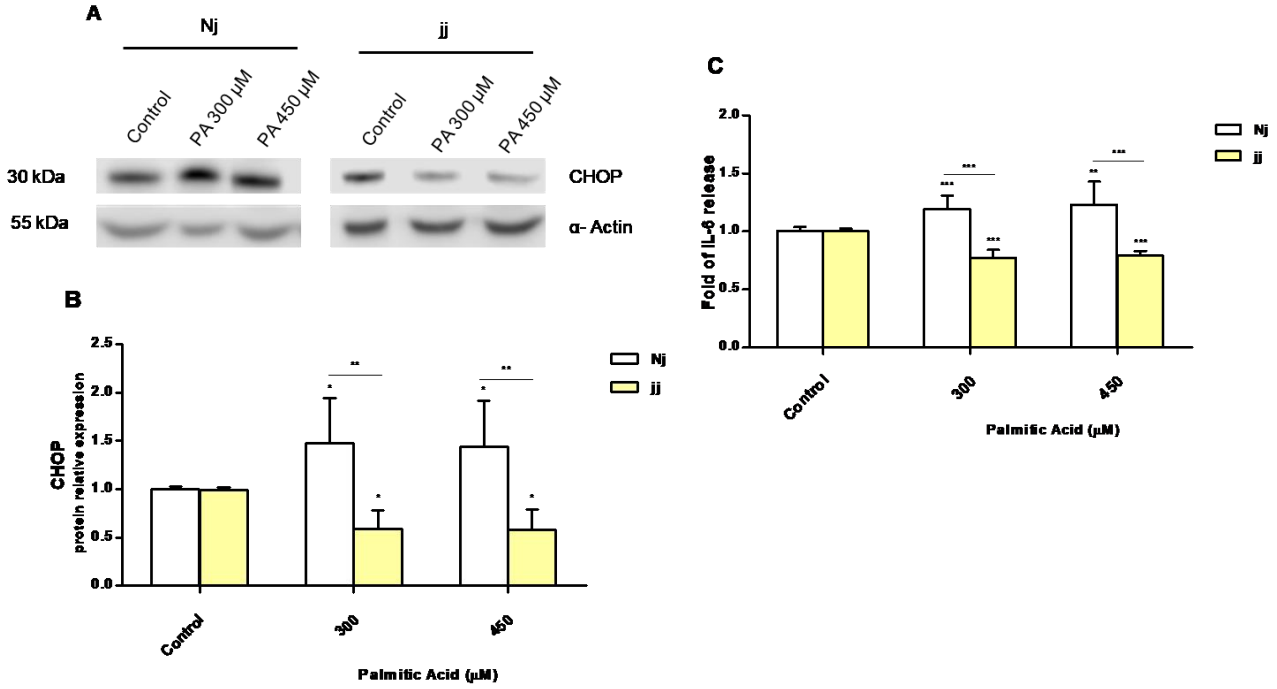

Figure 4.17 PA impact on CHOP activation and IL-6 release in Nj and jj aortic endothelial primary cells. Aortic endothelial cells were treated with PA 300 or 450 μM or DMSO (as control) in the presence of BSA 75μM for 24 h. **A)** Representative Western Blot for CHOP and α-Actin. **B)** The optical density of each band was normalized to α-Actin and represented as relative to control cells. **C)** ELISA quantification of IL-6 release in the cell medium. Results were expressed as relative to control cells release, considered as one. Data were expressed as mean ± SD of at least three independent experiments. Significativity was calculated compared to the control or between samples indicated with bars at each sampling concentration point. *p<0.05, **p<0.01, ***p<0.001.

4.2.3.2 UCB effect on CHOP activation and IL-6 release in PA- treated H5V cells

Murine heart endothelial cells (H5V) were exposed to PA, after (UCB pre-treatment) or before (UCB post-treatment) UCB treatment. PA 300 μM treatment significantly increased the expression level of CHOP protein while UCB pre-treatment restored it to control level **(Figure 4.18 A and B).** Similarly, UCB pre-treatment significantly reduced the 4-fold increase of IL-6 release due to PA 300 μM exposure **(Figure 4.18 C).** Whereas UCB post-treatment did not show an effect on CHOP protein and on IL-6 released induced by PA 300 μM **(Figure 4.18 D, E and F).**

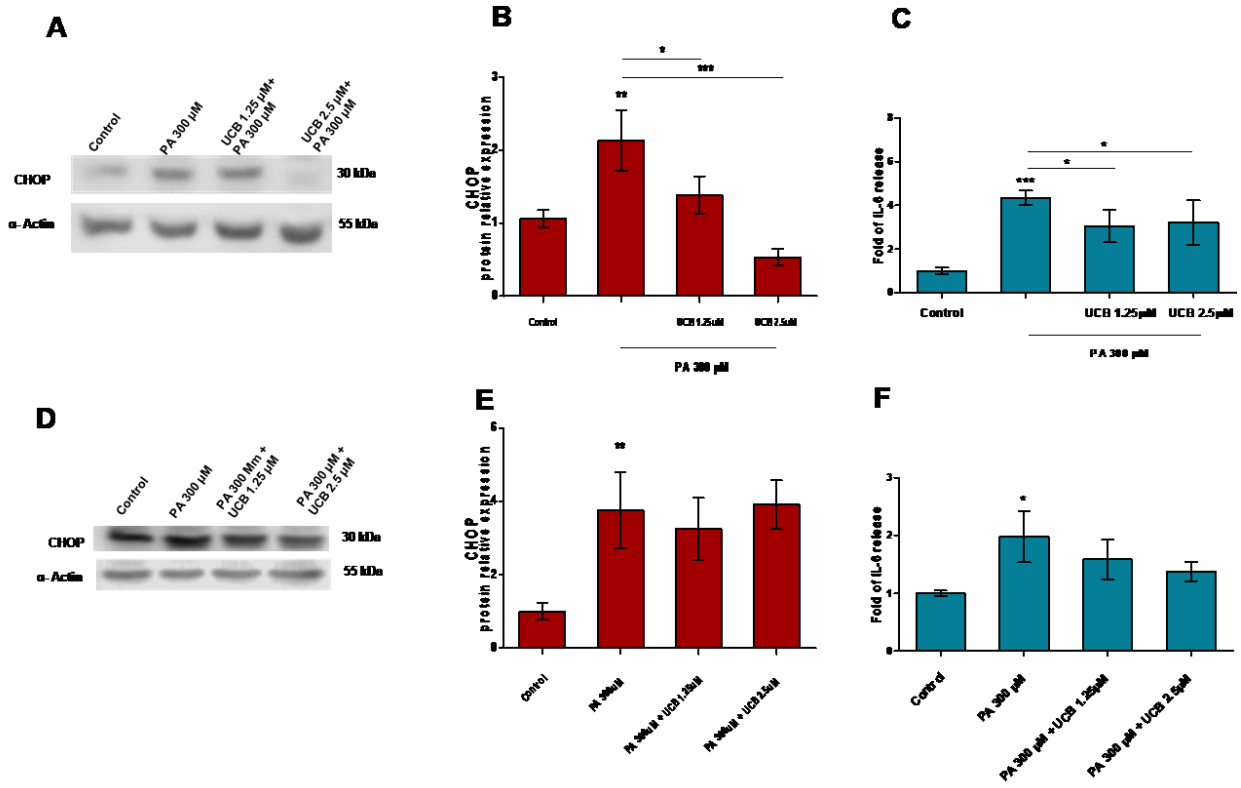

Figure 4.18 The effect of UCB pre- or post-treatment in PA-induced damage on immortalized H5V cells. H5V cells were pre-incubated with UCB 1.25 or 2.5 μM or DMSO 0.1% (as control) in the presence of BSA 30 μM for 16 h. At the end of incubation, UCB was removed and H5V cells were treated with PA 300 μM for 24 h. In UCB post-treatment, H5V cells were incubated with PA 300 μM for 24 h and then post-treated with UCB 1.25 or 2.5 μM or DMSO 0.1% (as control) in the presence of BSA 30 μM for 16 h. **A)** Representative Western Blot for CHOP and α-Actin in UCB pretreatment. **B)** The optical density of each band was normalized to α-Actin and represented as relative to control cells in UCB pretreatment. **C)** ELISA quantification of IL-6 release in the cell medium in UCB pretreatment. Results were expressed as relative to control cells release, considered as one. **D)** Representative Western Blot for CHOP and α-Actin in UCB post-treatment. **E)** The optical density of each band was normalized to α-Actin and represented as relative to control cells in UCB post-treatment. **F)** ELISA quantification of IL-6 release in the cell medium in UCB post-treatment. Results were expressed as relative to control cells release, considered as one. Data were expressed as mean ± SD of at least three independent experiments. *p<0.05, **p<0.01, ***p<0.001.

4.2.4 Impact of UCB on podocytes apoptosis upon Ang II treatment

4.2.4.1 Ang II effect on podocytes apoptosis in Nj and jj podocytes primary cells

Treatment with Ang II 0.01, 0.1, and 1 μM for 24 h showed a significant increase in the number of apoptotic podocytes in both genotypes, as detected by TUNEL assay (**Figure 4.19 A**). However, the extent of Ang II induced apoptosis was higher in podocytes harvested from Nj rats compared to the podocytes harvested from jj rats at each Ang II concentration tested (**Figure 4.19 B**).

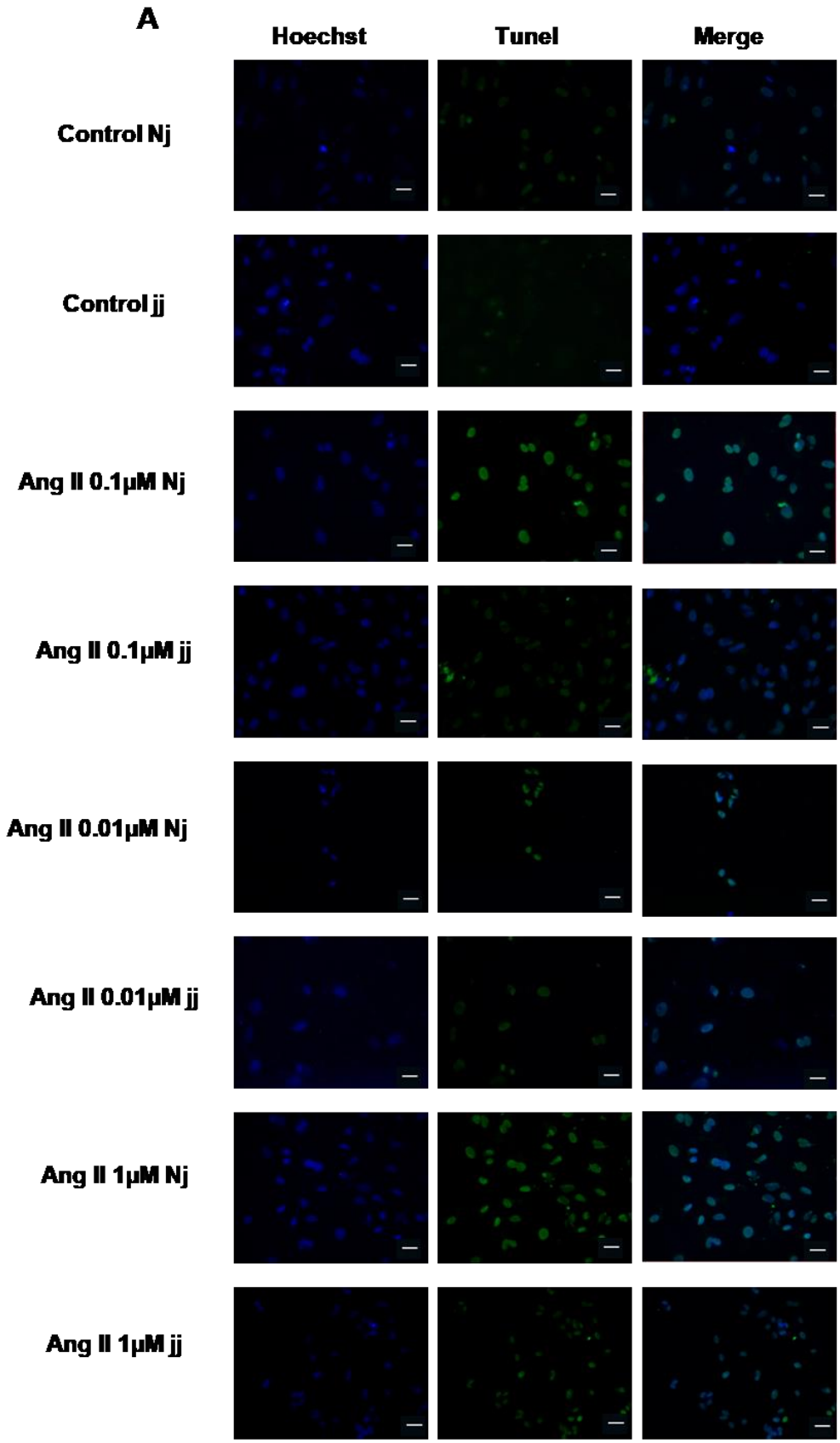
A
Hoechst
Tunel
Merge
Control Nj
Control jj
Ang II 0.1µM Nj
Ang II 0.1µM jj
Ang II 0.01µM Nj
Ang II 0.01µM jj
Ang II 1µM Nj
Ang II 1µM jj

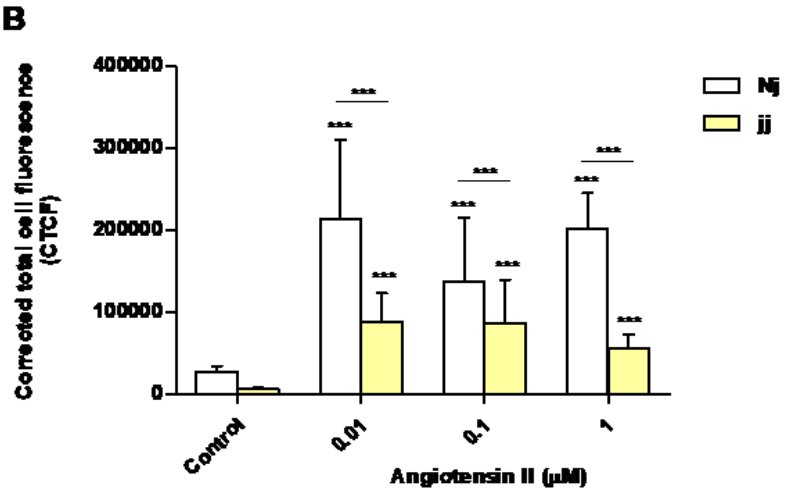

Figure 4.19 TUNEL staining of Nj and jj Gunn rat primary podocytes exposed to Ang II treatments. Primary podocytes were exposed to Ang II 0.01 μM, 0.1 μM, and 1 μM for 24 h. Cells treated with complete growth medium were considered as control. **A)** Apoptotic cells were detected by TUNEL assay. Green fluorescence indicated TUNEL-positive and blue indicated Hoechst nuclear dye. Magnification 40X. Scale bar 50μm. **B)** Quantification of fluorescence intensity. The fluorescence intensity was quantified using ImageJ and displayed as corrected total cell fluorescence (CTCF). Results shown represented the mean ± SD of three independent experiments. Significativity was calculated compared to the control or between samples indicated with bars at each sampling concentration point. *p<0.05, **p<0.01, ***p<0.001.

In normobilirubinemic podocytes, Angiotensin II treatment induced a dose-dependent increase in cleaved caspase-3 expression assessed by immunofluorescence. Conversely, only 1 μM Ang II significantly increased the expression of cleaved caspase-3 in hyperbilirubinemic podocytes. Hence caspase-3 activation significantly differed between the two genotypes upon all Ang II treatments **(Figure 4.20 A and B)**. Due to the limited yield of total protein obtained from primary podocyte cultures, WB analysis was performed only on Ang II 0.01 and 0.1 μM treatments for cleaved PARP and cleaved caspase-3 **(Figure 4.20 C)**. Both treatments induced an almost two-fold increase in the protein level of activated caspase-3 only in cells form Nj rats, while the expression remained similar to control levels in podocytes from jj rats **(Figure 4.20 D).** The cleaved PARP expression was slightly induced in podocytes from Nj rats, while its expression is reduced compared to control cells in podocytes from jj rats **(Figure 4.20 E).**

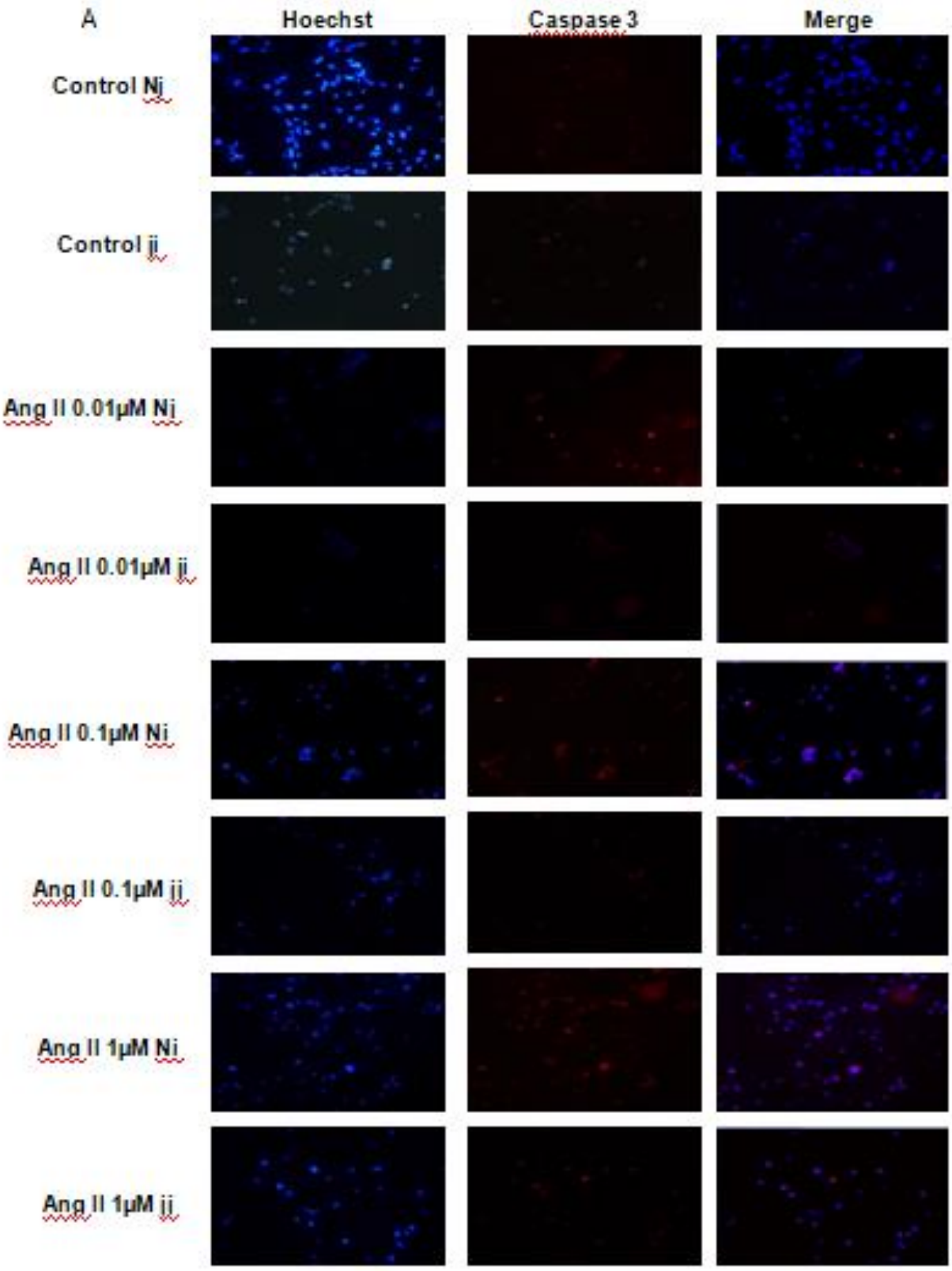
A
Hoechst
Caspase 3
Merge
Control Nj
Control ji
Ang II 0.01μM Nj
Ang II 0.01μM ji
Ang II 0.1μM Nj
Ang II 0.1μM ji
Ang II 1μM Nj
Ang II 1μM ji

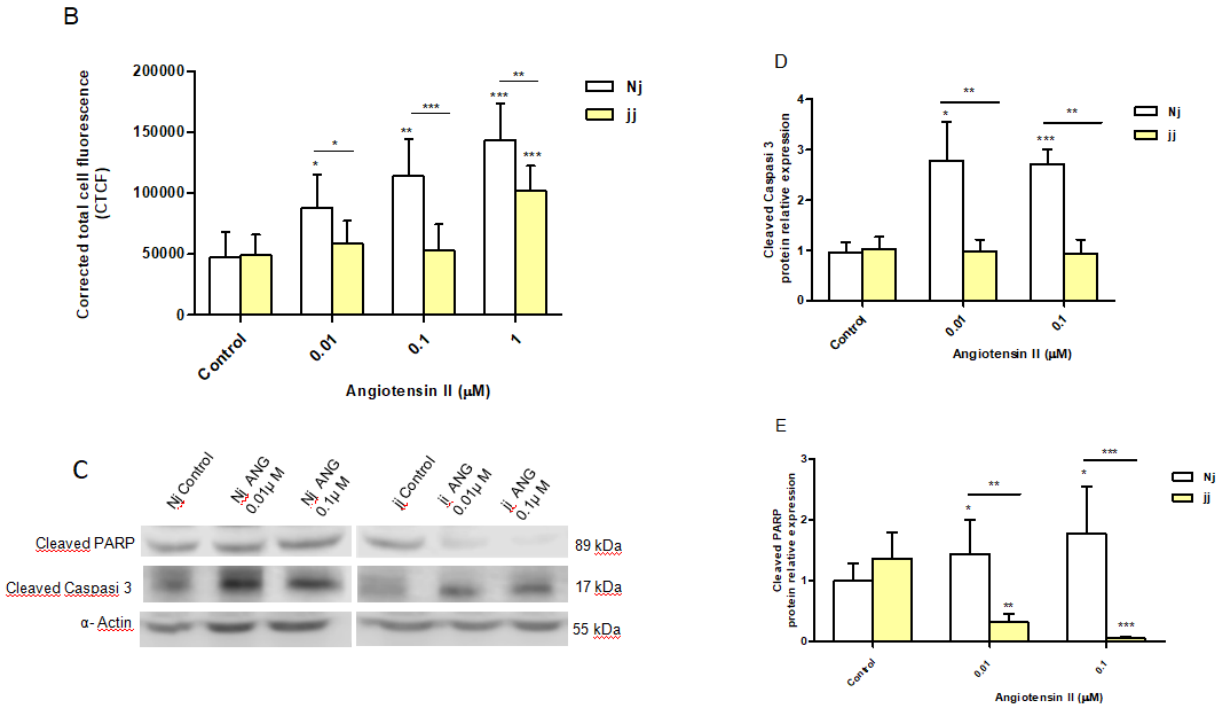

Figure 4.20 Activation of apoptosis signaling by Ang II in Nj and jj podocytes primary cells. Primary podocytes were exposed to Ang II 0.01 µM, 0.1 µM, and 1 µM for 24 h. Cells treated with complete growth medium were considered as control. **A)** Representative immunofluorescence (n = 3) images showing immunostaining for cleaved Caspase-3 (red) and Hoechst (blue) for nuclei. Magnification 20X. Scale bar 50µm. **B)** Quantification of Cleaved Caspase-3 fluorescence intensity. The fluorescence intensity was quantified using ImageJ and displayed in corrected total cell fluorescence (CTCF). **C)** Representative Western blot analysis of cleaved PARP, cleaved caspase-3, and α-Actin expression in total cell lysates. **D)** The optical density of cleaved caspase-3 protein from three independent experiments was normalized to α-Actin and represented as relative to untreated cells. **E)** The optical density of cleaved PARP protein from three independent experiments was normalized to α-Actin and represented as relative to untreated cells. Significativity was calculated compared to the control or between samples indicated with bars at each sampling concentration point. *p<0.05, **p<0.01, ***p<0.001.

4.2.4.2 Basal autophagy (LC3 II expression): comparison between Nj and jj

We monitored autophagy by analyzing the conversion of LC3-I into LC3-II and taking the latter as an autophagic marker by Western blot (Tanida et al., 2008). The basal expression of LC3-II protein was higher in podocytes from jj Gunn rats than in podocytes from Nj Gunn rats (**Figure 4.21**). It is worth to note that the higher basal autophagy level in jj primary podocytes correlates with a lower induction of apoptosis by Angiotensin II (**Figure 4.20**).

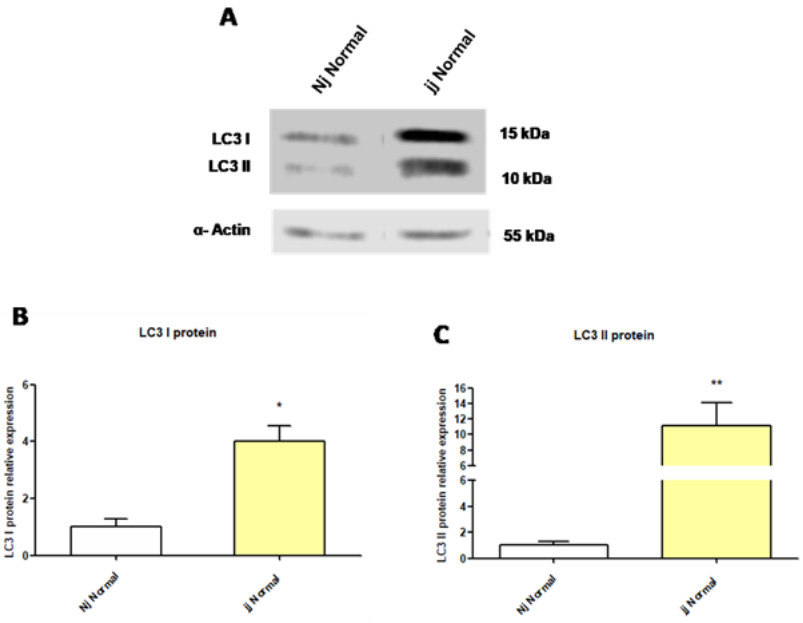

Figure 4.21 LC3 basal expression in Nj and jj primary podocytes. A) Representative Western blot of LC3I and LC3II protein on total proteins extracts from Nj and jj primary podocytes. **B)** LC3 I protein quantification. Expression of LC3I protein was normalized to α-actin and represented as relative to the control (untreated Nj podocytes). **C)** LC3 II protein quantification. Expression of LC3II protein was normalized to α-actin and represented as relative to the control (untreated Nj podocytes). Results are reported as average ±SD of three independent experiments. Student's T - test was performed against Nj podocytes. *p<0.05, **p<0.01, ***p<0.001.

4.2.5 Impact of UCB on proximal tubular epithelial cells fibrosis

4.2.5.1 Effect of Ang II on of HIF-1α and LOXl2 protein expressions

A dose-dependent increase of HIF-1α and LOXl2 protein expression compared to the control (cells untreated) was detected on immortalized human proximal tubular epithelial cells (HK-2) exposed to increasing concentration of Ang II ranging from 0.01 μM to 10 μM for 24 h. Treatment with Ang II concentrations 0.5 μM and 1 μM showed a significantly up-regulation of HIF-1α protein expression while LOXl2 protein expression was significantly up-regulated by Ang II 0.05 μM **(Figure 4.22 A and B)**. Moreover, the effects of Ang II on HIF-1α mRNA expression did not show any variation compared to the controls **(data not shown).**

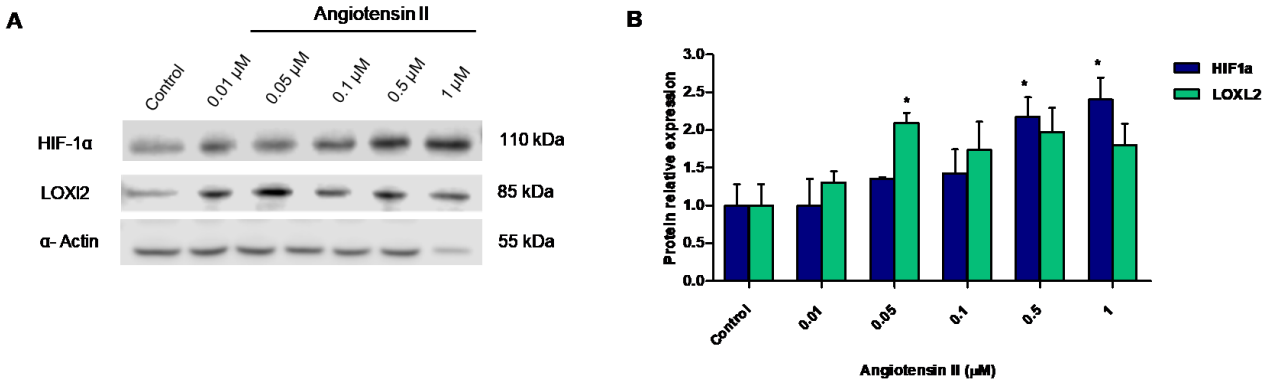

Figure 4.22 The impact of Ang II on proximal tubular epithelial cells. A) Representative Western blot analysis of HIF-1α, LOXl2, and α-Actin expression in HK2 cells treated with increasing doses of UCB for 24 h. **B)** The optical density of each band was normalized to α-Actin and represented as relative to control cells. Data were expressed as mean ± SD of three independent experiments. Significativity was calculated compared to the control at each sampling concentration point. *p<0.05, **p<0.01, ***p<0.001.

4.2.5.2 Effect of increasing doses of UCB on of HIF-1α and LOXl2 protein expressions

The effect of UCB alone on HIF-1α and LOXl2 protein expression was evaluated by exposing HK2 cells to a dose-dependent UCB treatment (from 0.6 µM to 10 µM) for 24 h. HIF-1α and LOXl2 expression was reduced by UCB treatment up to 2.5 µM, while higher concentrations induced their expression **(Figure 4.23 A and B).**

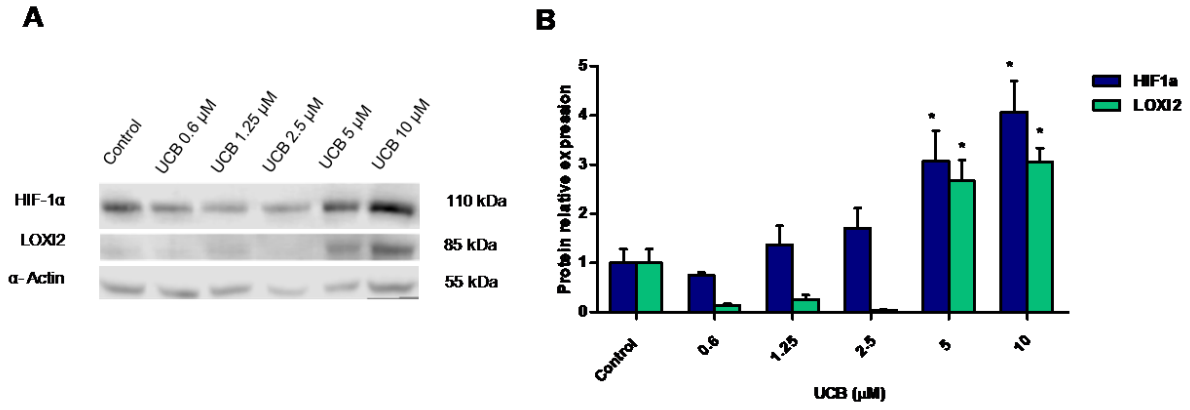

Figure 4.23 The impact of UCB on proximal tubular epithelial cells. **A)** Representative Western blot analysis of HIF-1a, LOXl2, and α-Actin expression in HK2 cells treated with increasing doses of Ang II for 24 h**. B)**The optical density of each band was normalized to α-Actin and represented as relative to control cells. Data were expressed as mean ± SD of three independent experiments. Significativity was calculated compared to the control or between samples indicated with bars at each sampling concentration point. *p<0.05, **p<0.01, ***p<0.001.

4.2.5.3 UCB effect on HIF-1α and LOXl2 induction by angiotensin II

Considering the induction of HIF-1α and LOXl2 protein by Ang II, we investigated whether UCB pretreatment or post-treatment may influence their expression. Pretreatment with 1.25 μM or 2.5 UCB significantly reduced HIF-1α protein induction by Ang II in a dose-dependent manner. UCB pretreatment also reduced significantly LOXl2 protein expression to 0.5 fold of control cells **(Figure 4.24 A and B)**.

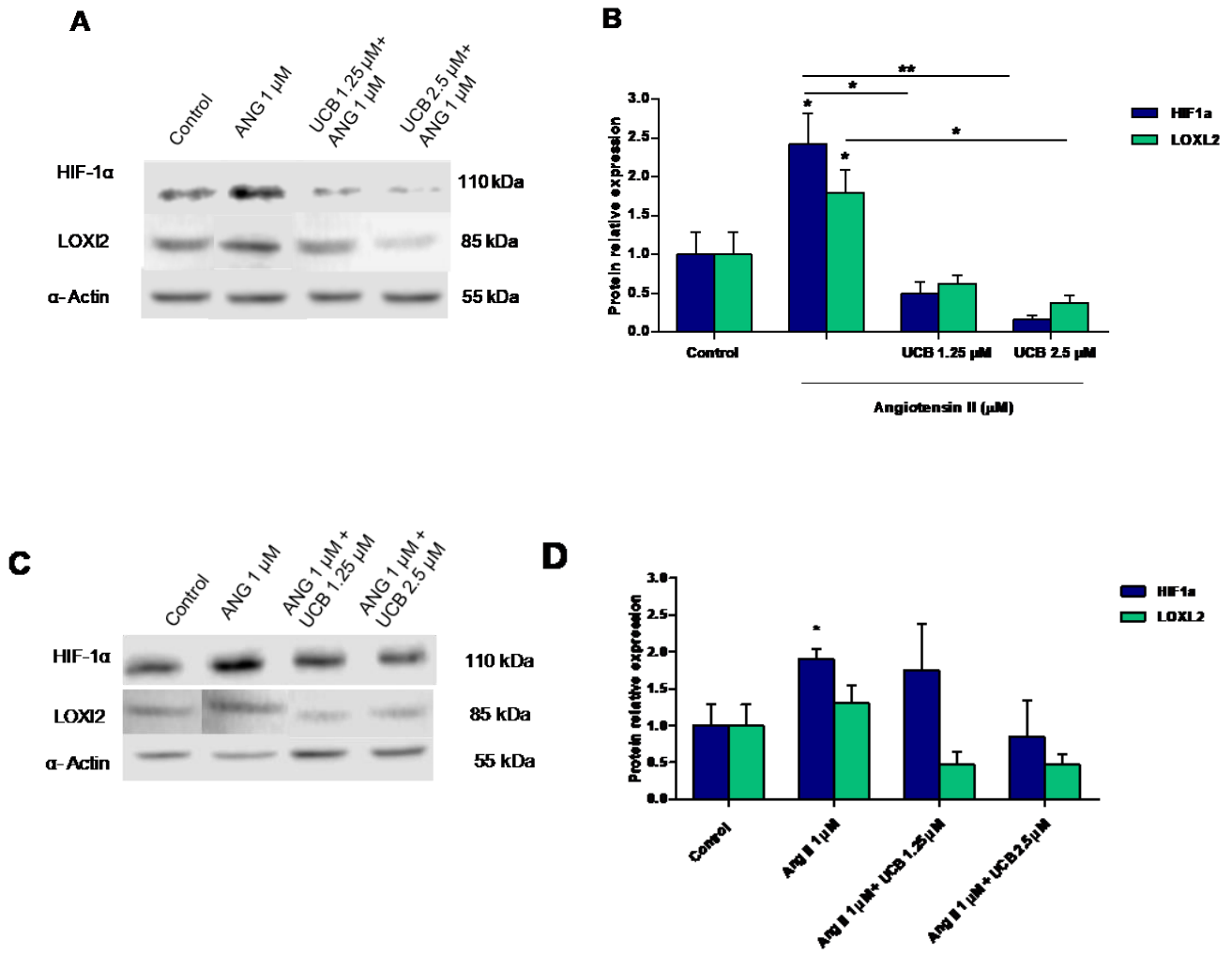

Figure 4.24 The impact of UCB on proximal tubular epithelial cells fibrosis induced by Ang II. A) Representative Western blot analysis of HIF-1α, LOXl2, and α-Actin expression in HK2. Cells were pre-incubated with UCB 1.25 or 2.5 μM or DMSO 0.1% in the presence of BSA 30 μM for 16 h. At the end of incubation, UCB was removed and cells treated with Ang II 1 μM for 24 h. **B)** The optical density of each band was normalized to α-Actin and represented as relative to control cells. **C)** Representative Western blot analysis of HIF-1α, LOXl2, and α-Actin expression in HK2. Cells were incubated with Ang II 1 μM for 24 h. At the end of incubation, Ang II was removed and cells were post-treated with UCB 1.25 or 2.5 μM or DMSO 0.1% in the presence of BSA 30 μM for 16 h. **D)** The optical density of each band was normalized to α-Actin and represented as relative to control cells in a post-treatment. Data were expressed as mean ± SD of three independent experiments. Significativity was calculated compared to the control or between samples indicated with bars at each sampling concentration point. *p<0.05, **p<0.01, ***p<0.001.

In UCB post-treatment, UCB 1.25 μM and UCB 2.5 μM also reduced HIF-1α and LOXl2 protein induction by Ang II reporting their level to those of control , even not significantly (**Figure 4.24 C and D**).
In this context, we also evaluated the effects of UCB on α-SMA mRNA expression in presence of Ang II as damage agent.
Ang II treatment showed a significantly increase in α-SMA mRNA expression (data not shown). Both UCB 1.25 μM and 2.5 μM pre-treatment, but not post-treatment, showed a slight decrease in α-SMA mRNA expression (not significant) (data not shown).

4.2.5.4 UCB effect on HIF-1α induction by AGE

To confirm the ability of UCB to modulate HIF-1α expression during diabetic nephropathy, we exposed HK-2 cells also to Advanced glycation end products (AGEs). Cells treated with AGE 20 μM showed a slight increase of HIF-1α protein expression compared to the control (untreated cells). In pre-treatment, UCB 2.5 μM significantly reduced HIF-1α protein expression to 0.3 fold of control expression, while UCB 1.25 μM led its expression to control level (**Figure 2.25 A and B).** In post-treatment, only UCB 2.5 μM seemed to reduce HIF-1 α expression even not significantly (**Figure 2.25 C and D**). In this context of treatment, we also studied HIF-1α mRNA expression that showed a similar behavior compared to protein expression, indicating a more effective role of UCB in pre-treatment than in post-treatment (data not shown).

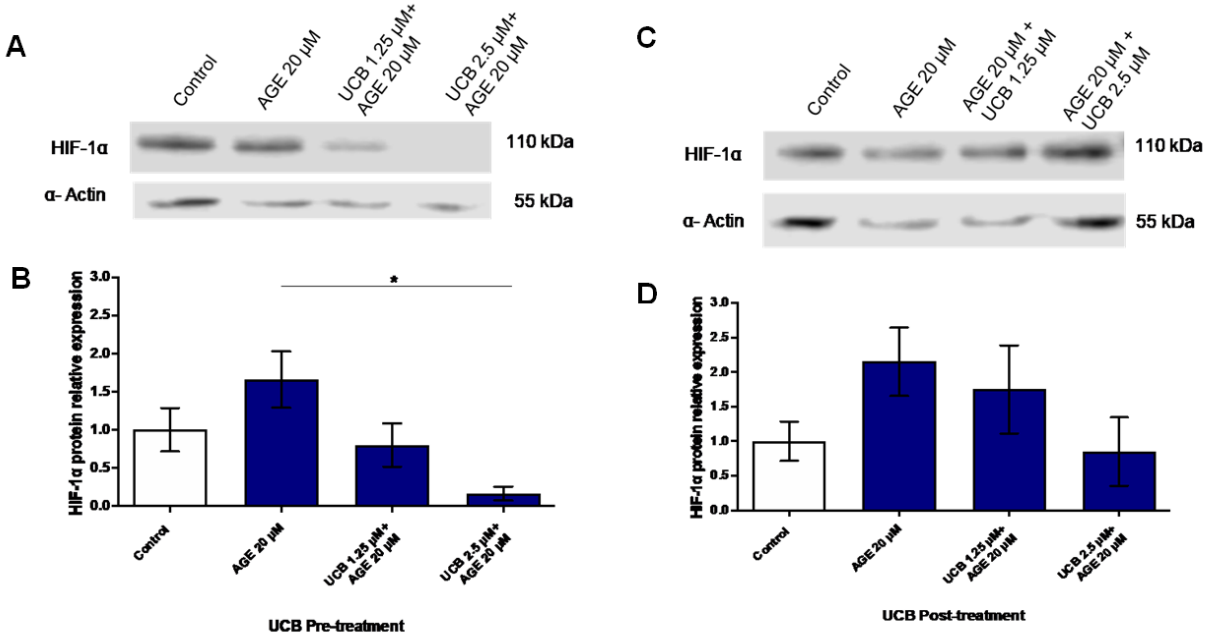

Figure 4.25 Effects of UCB pre and post-treatment in HK-2 expose to AGE. A) Representative Western blot analysis for total proteins extracts from HK-2 cells pre-treated with UCB for 16 hours and then exposed to AGE for 72 hours **B)** HIF-1α protein quantification. Expression of HIF-1α protein was normalized to α-actin and represented as relative to the control (untreated HK-2 cells). **C)** Representative Western blot analysis for total proteins extracts from HK-2 cells treated with AGE for 72 hours and then exposed to UCB for 16 h. **D)** HIF-1α protein quantification. Expression of HIF-1α protein was normalized to α-actin and represented as relative to the control (untreated HK-2 cells) Results were reported as average ±SD of three independent experiments. Student's T - test was performed against control cells for AGEs treated cells. Student's T - test was performed against AGE treated cells for UCB pre and post-treated samples *$p<0.05$

4.3 Task 3 Impact of serum bilirubin levels on Metabolic Syndrome and NAFLD: A cross-sectional study in 1672 extremely obese children

4.3.1 Measurements of the children and adolescents

The children were aged from 5 to 18 years and were mostly post-pubertal. Fatty liver (FL) was present in 38% of them, being light in 15%, moderate in 18%, and severe in 5%.Metabolic Syndrome was present in 23.6%.**Table 4.3** gives the measurements of the 1672 obese children.

Table 4.3 Measurements of obese children and adolescences patients

	Total
	N=1,672
Sex	
F	980 (58.6%)
M	692 (41.4%)
Age (years)	15 (13; 16)
Age (year)	
5	1 (0.1%)
6	5 (0.3%)
7	12 (0.7%)
8	18 (1.1%)
9	38 (2.3%)
10	72 (4.3%)
11	113 (6.8%)
12	148 (8.9%)
13	182 (10.9%)
14	238 (14.2%)
15	288 (17.2%)
16	282 (16.9%)
17	228 (13.6%)
18	47 (2.8%)
Pubertal stage (Tanner)	
1	194 (11.6%)
2	144 (8.6%)
3	213 (12.7%)
4	373 (22.3%)
5	748 (44.7%)
Weight (kg)	96 (83; 112)
Weight (SDS Cacciari 2006)	3.01 (2.47; 3.57)
Height (m)	1.63 (1.56; 1.69)
Height (SDS Cacciari 2006)	0.33 (-0.30; 1.04)

BMI (kg/m2)	36 (32; 40)
BMI (SDS Cacciari 2006)	2.92 (2.50; 3.32)
Waist circumference (cm)	111 (101; 122)
Large waist circumference	
No	26 (1.6%)
Yes	1,646 (98.4%)
Waist : height (dimensionless)	0.68 (0.63; 0.74)
ALT (U/l)	23 (16; 35)
AST (U/l)	21 (17; 26)
GGT (U/l)	16 (12; 22)
Alkaline phosphatase (U/L)	164 (91; 263)
Total bilirubin (mg/dl)	0.64 (0.49; 0.82)
Glucose (mg/dl)	79 (74; 83)
Insulin (mg/dl)	13 (9; 18)
HOMA (dimensionless)	2.4 (1.6; 3.5)
Cholesterol (mg/dl)	162 (142; 182)
HDL-cholesterol (mg/dl)	43 (37; 51)
Low HDL	
No	991 (59.3%)
Yes	681 (40.7%)
LDL-cholesterol (mg/dl)	102 (85; 122)
Triglycerides (mg/dl)	87 (66; 114)
High triglycerides	
No	1,509 (90.3%)
Yes	163 (9.7%)
CRP (mg/l)	0.4 (0.2; 0.7)
Systolic blood pressure (mm hg)	120 (120; 130)
Diastolic blood pressure (mm hg)	80 (70; 80)
High blood pressure	
No	985 (58.9%)
Yes	687 (41.1%)
Fatty liver	
No	1,030 (61.6%)
Yes	642 (38.4%)
Fatty liver degree	
None	1,030 (61.6%)
Light	250 (15.0%)
Moderate	300 (17.9%)
Severe	92 (5.5%)
Metabolic syndrome score	

0	589 (35.2%)
1	686 (41.0%)
2	337 (20.2%)
3	59 (3.5%)
4	1 (0.1%)
Metabolic syndrome	
No	1,277 (76.4%)
Yes	395 (23.6%)

4.3.2 Multivariable association between bilirubin, age, pubertal state and sex

Total bilirubin level correlates positively and significantly, even if weakly, with age in the total population, showing an higher correlation in male compared to female. **Figure 4.26** plots the multivariable association between bilirubin, age (continuous, years) and sex (0 = female; 1 = male). The corresponding regression model is given in **table 4.4** (left column).

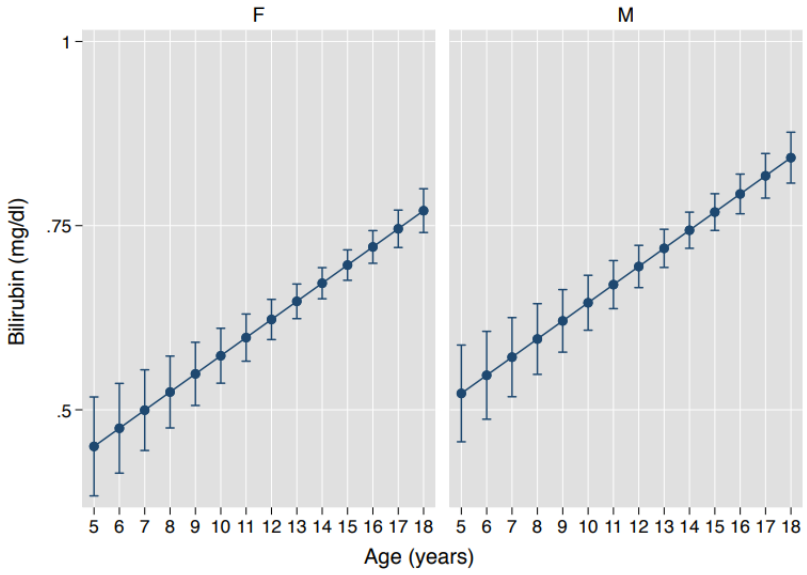

Figure 4.26 Multivariable association between bilirubin, age (continuous, years) and sex.

Table 4.4 Multivariable association between bilirubin, Tunner pubertal status and sex

	Total bilirubin (mg/dl)	Total bilirubin (mg/dl)
Age (years)	0.02***	
	[0.02,0.03]	
F	0.00	0.00
	[0.00,0.00]	[0.00,0.00]
M	0.07***	0.09***
	[0.04,0.10]	[0.06,0.13]
Pubertal stage (Tanner)=1		0.00
		[0.00,0.00]
Pubertal stage (Tanner)=2		0.06
		[-0.01,0.14]
Pubertal stage (Tanner)=3		0.12***
		[0.06,0.19]
Pubertal stage (Tanner)=4		0.16***
		[0.10,0.22]
Pubertal stage (Tanner)=5		0.19***
		[0.13,0.24]
Constant	0.33***	0.54***
	[0.23,0.43]	[0.49,0.59]
Observations	1672	1672
Adjusted R-squared	**0.038**	**0.037**
Values are linear regression coefficients with 95% confidence intervals in brackets		
*** p<0.05, ** p<0.01, *** p<0.001**		

Correlation coefficients between bilirubin and pubertal stage are higher in man compared to female. Correlation coefficients increased according to the increase of pubertal stage, reaching 0.2 at pubertal stage 5, in the total population. **Figure 4.27** plots the multivariable association between bilirubin, pubertal status (discrete, five Tanner stages) and sex (0 = female; 1 = male). The corresponding regression model is given in **Table 4.4** (right column). The variance of bilirubin explained by age and pubertal status was quite low, being less than 4%.

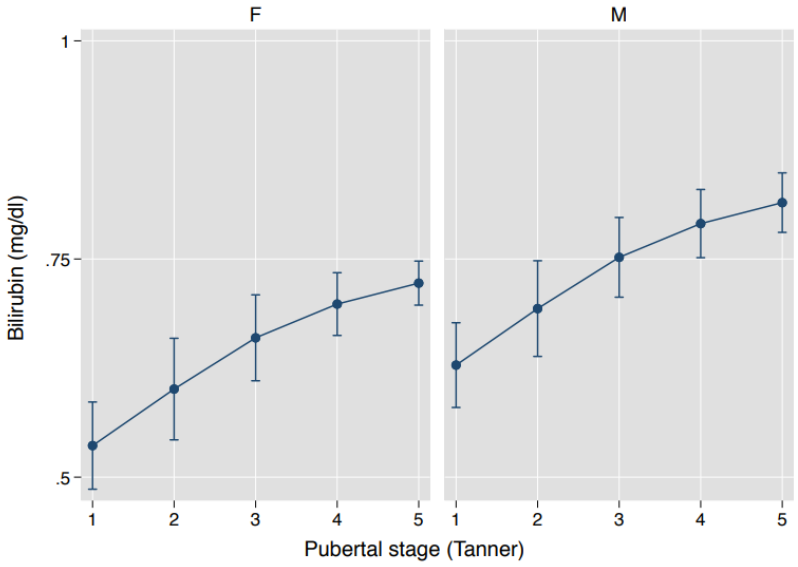

Figure 4.27 Multivariable association between bilirubin and Tanner pubertal stage.

4.3.3 Univariable associations between bilirubin and BMI (SDS), waist / height ratio, insulin, HOMA and C-reactive protein

Waist / height ratio, insulin, HOMA and C-reactive protein negative correlates with bilirubin, while BI showed a correlation coefficient of 0. HOMA showed the highest correlation coefficient, while CRP the highest significance. **Figure 4.28** plots the univariable associations between BMI (SDS), waist / height ratio, insulin, HOMA and C-reactive protein. The corresponding linear regression models are given in **Table 4.5**.

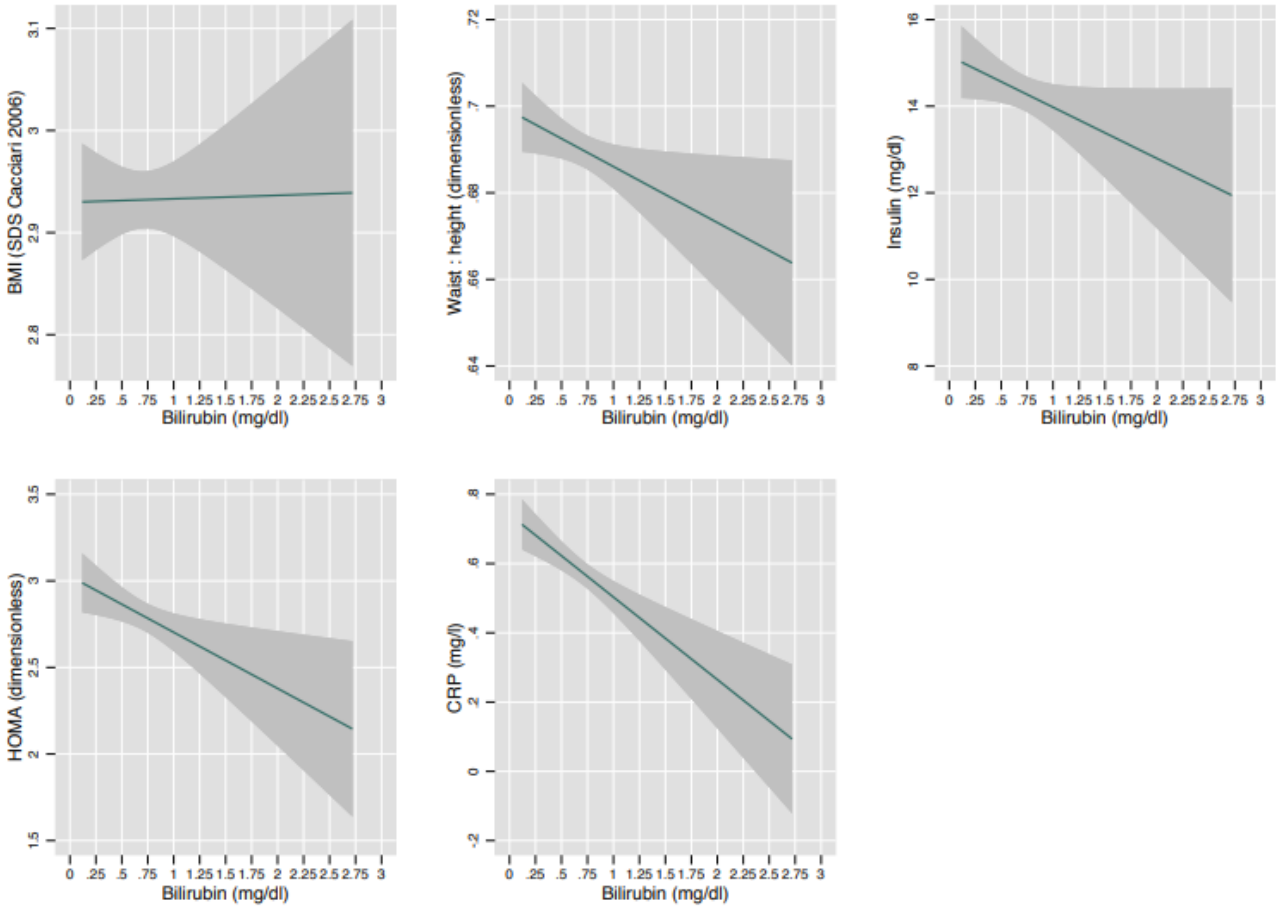

Figure 4.28 Associations between bilirubin and BMI (SDS), waist / height ratio, insulin, HOMA and C-reactive protein. Linear regression models were used to quantify the association of continuous outcomes with bilirubin.

Table 4.5 Correlation between Total bilirubin and BMI (SDS), waist / height ratio, insulin, HOMA and C-reactive protein

	BMI (SDS Cacciari 2006)	Waist : height (dimensionless)	Insulin (mg/dl)	HOMA (dimensionless)	CRP (mg/l)
Total bilirubin (mg/dl)	0.00	-0.01*	-1.18	-0.32*	-0.24***
	[-0.08,0.09]	[-0.02,-0.00]	[-2.40,0.03]	[-0.57,-0.07]	[-0.34,-0.13]
Constant	2.93***	0.70***	15.16***	3.03***	0.74***
	[2.86,3.00]	[0.69,0.71]	[14.20,16.12]	[2.83,3.22]	[0.66,0.83]
Observations	1672	1672	1672	1672	1672
Adjusted R-squared	**0.001**	**0.002**	**0.002**	**0.003**	**0.011**
Values are linear regression coefficients with 95% confidence intervals in brackets					
*** p<0.05, ** p<0.01, *** p<0.001**					

4.3.4 Univariable associations between bilirubin and FL and MetS

Bilirubin weakly, not significantly and positively correlated with MetS. When we considered the single components of MetS, we noticed a positive correlation with high blood pressure and impaired fasting glucose, while a negative one with large waist circumference, high triglycerides, low HDL-cholesterol. **Figure 4.29** plots the univariable associations between FL, MetS and the single components of the MetS, i.e. large waist circumference, high blood pressure, high triglycerides, impaired fasting glucose and low HDL-cholesterol. The corresponding logistic regression models are given in **Table 4.5**.

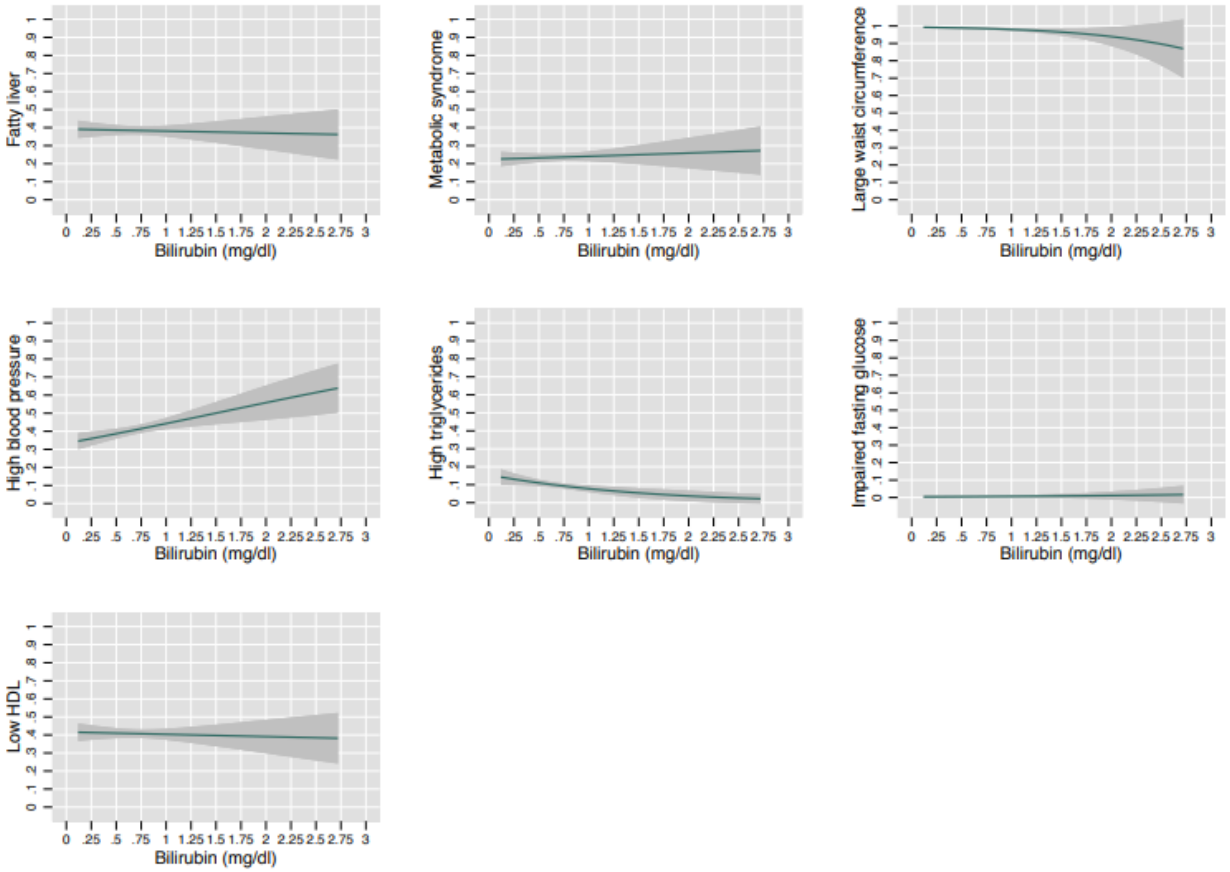

Figure 4.29 Associations between bilirubin between bilirubin and FL and Mets. Logistic regression models were used to quantify the association of binary outcomes with bilirubin.

Table 4.6 Correlation between Total bilirubin and clinical and anthropometric measurements

	Fatty liver	Metabolic syndrome	Large waist circumference	High blood pressure	High triglycerides	Impaired fasting glucose	Low HDL
Total bilirubin (mg/dl)	-0.05	0.10	-1.17**	0.46**	-0.77**	0.53	-0.05
	[-0.34, 0.25]	[-0.24,0.43]	[-1.96,-0.38]	[0.17, 0.76]	[-1.35,-0.18]	[-1.02, 2.09]	[-0.35, 0.24]
Constant	-0.44***	-1.24***	5.08***	-0.69***	-1.70***	-5.51***	-0.34**
	[-0.67,-0.21]	[-1.51,-0.98]	[4.27,5.89]	[-0.93,-0.46]	[-2.12,-1.28]	[-6.88,-4.14]	[-0.57,-0.11]
Observations	1672	1672	1672	1672	1672	1672	1672
Values are logistic regression coefficients with 95% confidence intervals in brackets							
*** p<0.05, ** p<0.01, *** p<0.001**							

Bilirubin weakly, not significantly and negatively correlated with fatty liver. **Figure 4.30** plots the univariable association between FL degree and bilirubin as estimated by OGLM (model not shown). The figure clearly shows that the frequency of all degrees of fatty liver (0 = none; 1 = light; 2 = moderate; 3 = severe) was constant across a range of bilirubin values comprised between the 5th and the 95th internal percentiles.

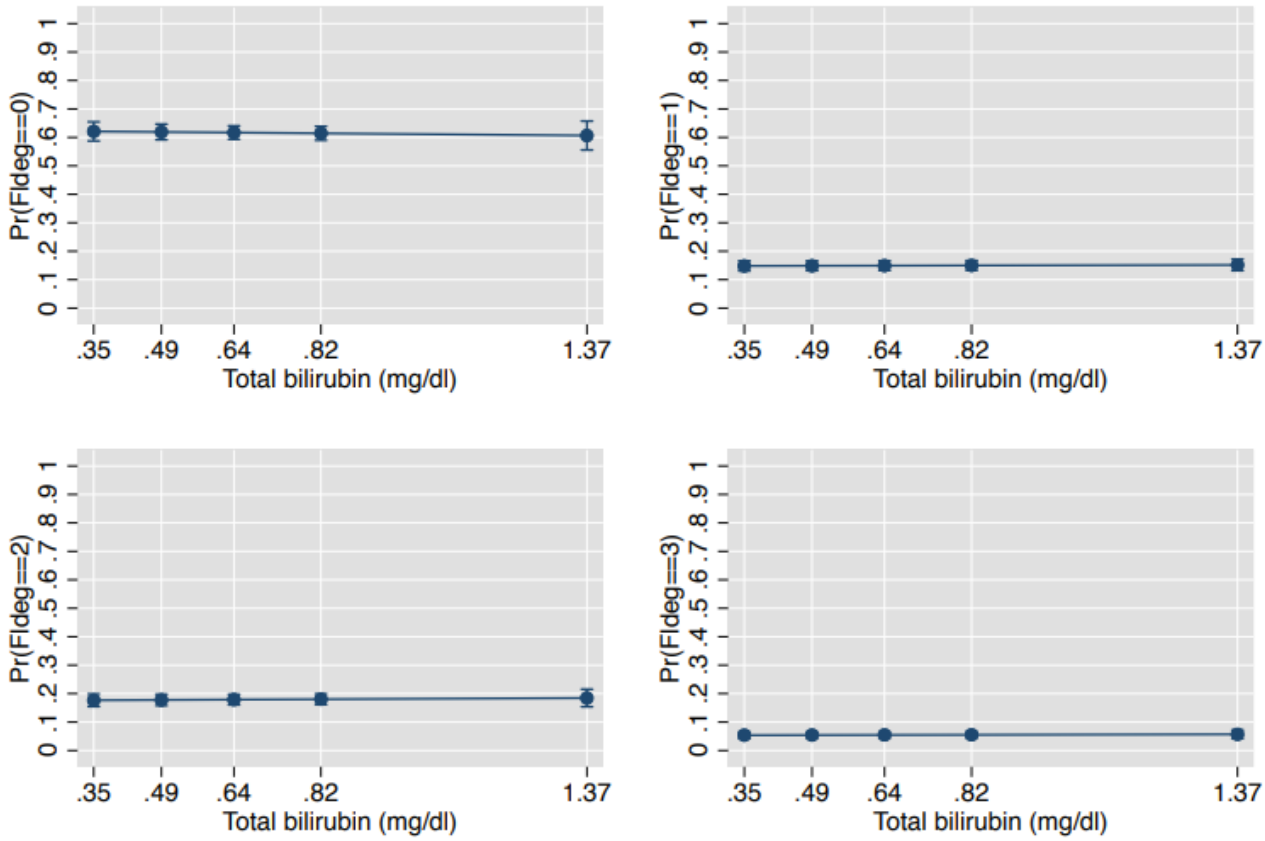

Figure 4.30 Correlation between bilirubin and fatty liver degree. Ordinal generalized linear model (OGLM) was used to quantify the association between fatty liver degree (0 = none; 1 = light; 2 = moderate; 3 = severe) and bilirubin. The value on the X-axis correspond to 5th,25th,50th, 75thand 95th percentiles of bilirubin.

Chapter 5
Discussion and Conclusions

5.DISCUSSION AND CONCLUSIONS

Unconjugated bilirubin (UCB) is more than just a metabolic waste end-product. Bilirubin's behaviour in a human body has two faces similar to Janus Bifrons. Severe hyperbilirubinemia can cause permanent neurological damage in neonates. The cascade of molecular and cellular events and the pathogenesis of bilirubin-induced brain damage was extensively studied (Watchko and Tiribelli, 2014) and it is out of the interest of the present work. Conversely, recent data convincingly suggest that mild elevation of systemic bilirubin concentrations, such as in Gilbert syndrome, protects against some diseases such as CVD and diabetes (Vitek et al., 2018). Since Gilbert syndrome was considered as a selective genetic advantage, some scientists suggested that a mildly increase of bilirubin levels could have a the rapeutical potential to suppress pathway leading to the development of metabolic diseases (Erlinger et al., 2014).The main aim of the present thesis is to contribute to a better understanding of the molecular and cellular mechanism involved in the protective impact of bilirubin. Our study was developed through three interlinked tasks: Task 1was focused to define the intracellular bilirubin thresholds for UCB anti- and pro-oxidant effects; Task 2 was aimed to investigate the pathways involved in mild hyperbilirubimia protective effect in *in vitro* models of atherosclerosis and diabetic nephropathy; Task 3 tried to hit the correlation between serum UCB level, metabolic syndrome (MetS) and non alcoholic fatty liver disease (NAFLD) in a cohort of obese children and adolescents.

The potent antioxidant properties of bilirubin were at first described decades ago and increasing evidence confirms the biological impacts of this activity by bilirubin (Vítek and Schwertner, 2007). However, the exact concentration thresholds between its anti-and pro-oxidant effects remained undefined (Gazzin et al., 2012). We performed a comparative study exposing immortalized cell lines coming from different organs to the same UCB treatment. Measuring the concentration of bilirubin internalized, we noticed that intracellular UCB concentration substantially differed amongHepG2, H5V, HK2 and SH-SY5Y even if exposed to the same UCB treatments (Table 4.1). HepG2 hepatic cells had the lowest concentrations, while the SH-SY5Y neuronal cells was the most sensitive. Intracellular UCB concentration depend on several factors including the extent of uptake, excretion, and metabolic transformation, and each of these factors could be different among the various organs considered. The ability of HepG2 to maintain an intracellular UCB equilibrium in the presence of increasing extracellular UCB treatment is not surprising since the hepatocyte has a flexible and robust system of bilirubin metabolism and detoxification via its conjugation with glucuronic acid by bilirubin UDP-glucuronosyltransferase (UGT1A1) (Abu-Bakar et al., 2012; Iusuf et al., 2012; Keppler, 2014). In contrast, many cells of different origins do not possess UGT1A1 activity (Nakamura et al., 2008) and must either oxidize or export UCB to prevent its intracellular accumulation (Bellarosa et al., 2009; Gazzin et al., 2012). Hence, the vulnerability of the neurons may be due to lower activities of the mitochondrial enzymes that oxidize UCB as well as the decreased expression of MRP1, one of the bilirubin efflux pump limiting the intracellular accumulation of the pigment (Rigato et al., 2004; Calligaris et al., 2006; Corich et al., 2009; Brites, 2011).A different pattern of expression of efflux transporters and UCB metabolizing enzymes occurs also on H5V and HK2 cells (Jenkinson et al., 2012) and it can explain the difference of UCB accumulation between hepatic compared to those of non-hepatic origin cells.
Not only intracellular accumulation, but also UCB cytotoxicity showed three different levels of susceptibility among the cell lines (Figure 4.1). As expected, the hepatic HepG2 cell line was less sensitive to UCB toxicity, even at the highest UCB concentration tested (corresponding to an intracellular UCB concentration of 21 ng/mg of protein). Conversely, the neuronal cells appeared to be the most sensitive since cytotoxicity started at UCB concentration of 3.6 μM corresponding to

an intracellular UCB concentration of 25 ng/mg protein. Both HK2 and H5V showed an intermediate behavior because UCB cytotoxicity arises from concentrations of 15 μM corresponding to an intracellular UCB concentration of around 40 ng/mg protein. Our results are consistent with previous data showing that different cells exhibited different susceptibilities to the cytotoxic effects of bilirubin, being neuroblastoma cells the most susceptible and hepatocytes the least vulnerable (Ngai et al., 2000).Measuring the effect of UCB on metabolic activity (Figure 4.2),we noticed that it presented a substantial different trend compared to cell death (Figure 4.1). The reduction in the metabolic activity occurring in HepG2 cells at UCB above 3.6 μM was not associated with the cell toxicity. In non-hepatic cell lines, the reduction in formazan formation occurred at UCB concentrations lower than those inducing cell mortality (i.e. on SH-SY5Y cells, metabolic activity reduction occurred at 0.4 μM while mortality started from 3.6 μM). Most importantly, the percentage of dead cells detected by PI was dose-dependent while the reduction of formazan reached a plateau (25-30% of reduction) at least from UCB treatment of 7.5 μM in all cell lines.UCB has an anti-proliferative activity preventing the cells to multiply rapidly and maintain the same number of viable cells (Ollinger et al., 2005). MTT test does not discriminate between cell viability and cell proliferation (Chan et al., 2013). The plateau effect seen on MTT test in all cell lines points to the ability of UCB to stop the cell growth. Thanks to this comparative study, we demonstrated that, in case of UCB treatment, MTT test is not a reliable viability test but need to be supported by a test measuring dead cells.

Among the molecular mechanisms contributing to UCB cytotoxicity, oxidative stress has emerged as a potential crucial event (Tell and Gustincich, 2009). In various cellular systems, severe hyperbilirubinemia causes ROS production, protein oxidation, and lipid peroxidation (Brito et al., 2008; Kumar et al., 2008) leading to apoptosis (Oakes and Bend, 2005). Conversely, mild hyperbilirubinemia has been demonstrated to be a powerful antioxidant substance in *in vitro* studies (Farrera et al., 1994; Gopinathan et al., 1994; Marilena, 1997), due to its capacity to suppress oxidation more strongly than many other antioxidants (Stocker et al., 1987b, 1987a; Wu et al., 1991). Bilirubin at low concentrations exerts its potent cytoprotective effects by bilirubin/biliverdin redox cycling (Baranano et al., 2002). Our results showed that even the highest UCB treatment dose do not induce ROS production in the cell line of hepatic origin (HepG2 cells) (Figure 4.3), while intracellular ROS increase starts in neuronal cell line (SH-SY5Y cells) from UCB concentrations of 3.6 μM, and from 15 μM in both aortic endothelial (H5V) and tubular kidney cells (HK2). On the other side, UCB antioxidant activity (Figure 4.4) showed an EC_{50} of 21.8 μM in HepG2 cells, 0.95 μM in SH-SY5Y cells, 2.44 μM in HK2 cells, and 4 μM in H5V cells. Our results expand and better substantiate what has already been published (Doré and Snyder, 1999; Liu et al., 2003) showing that each cell type has a different bilirubin threshold switching between the beneficiary and toxic effects of bilirubin. Total UCB concentration treatment is an uncertain predictor of its biological effects because intracellular levels of UCB are modulated by its oxidation, conjugation, and export from the cells. The ability to measure real UCB concentration in the cells much improve our understanding of UCB-induced cytotoxicity as well as its protective effects (Zelenka et al., 2008).Considering the intracellular UCB concentration regardless of the UCB concentration treatments, the intracellular UCB concentration of around 7 ng/mg protein had antioxidant activities, while its intracellular concentrations >25 ng/mg protein resulted in pro-oxidant and cytotoxic effects (Figure 4.5).

We also wondered if other antioxidant systems are involved in UCB effect on cellular redox state. We showed that total GSH concentrations is not influenced by UCB treatment (Figure 4.6), but instead it maintains the same level shown in control cells. The only exception is represented by SH-SY5Y cell line, where GSH levels increased significantly upon a UCB treatment higher of 7.5

μM (corresponding to an intracellular bilirubin content of 30 ng/mg of total protein). These results confirmed what was previously observed by our group: UCB modulated the GSH concentration in neuroblastoma cells through the induction of the System Xc- increasing cysteine uptake and intracellular GSH content (Giraudi et al., 2011).SOD activity increased in all cell lines in response to UCB pro-oxidant effect (He et al., 2017). Catalase activity (Figure 4.8) showed a similar behavior on HepG2 and SH-SY5Y, but not in the other two cell lines. Its activity increased significantly upon UCB treatment lower of 3.6 μM on HK2 cells and decreased upon UCB treatment higher than 7.5 μM. These behavior might suggest a possible contribution of catalase to UCB antioxidant activity and correlates with clinical observations in which human with low catalase levels are said to be more predisposed to type 2 diabetes mellitus and are sometimes affected by atherosclerosis (Góth et al., 2004).

Moderately elevated serum unconjugated bilirubin level have a number of beneficial effects on oxidative stress-mediated diseases, particularly vascular disease, diabetes, metabolic syndrome, and obesity (Vítek, 2012; Wagner et al., 2015). Thus, Gilbert subjects have a substantially lower risk of a spectrum of diseases characterized by increased oxidation stress, inflammation, or cell proliferation (Gazzin et al., 2016; Vítek, 2019; Vitek et al., 2019). Based on these evidences, in the second task, we investigated if and how life-long hyperbilirubinemia or bilirubin-priming might contribute to the protection against metabolic damage. To achieve this goal, we used primary cells, obtained from hyperbilirubinemic jj and normobilirubinemic Nj Gunn rats, exposed to damaging agents in the absence of UCB or immortalized cell lines pretreated with UCB (bilirubin-priming) and then exposed to damage.
Studies comparing the response to damage between UCB primed and not primed cells are scant. Recently Valaskova et al. showed that the cell viability of primary hepatocytes from jj Gunn rats exposed to TNF-α 100 ng/ml was significantly higher than that of primary hepatocytes from Nj Gunn rats ($p<0.05$) (Valaskova et al., 2019). Our results (Figures4.13 and 4.14) expand this observation given that we assayed the viability of other Gunn rat primary cells (podocytes and primary aortic endothelial cells) exposed to increasing concentration of a damage stimulus (PA and Ang II, respectively). In both cell models and at any toxic agent concentration, we observed that the viability of cells derived from jj Gunn rats was significantly higher than that of Nj cells. In line with this, only UCB pre-treatment in H5V cells exposed to PA reduced the percentage of dead cells and increased cell viability compared to DMSO pretreated cells (Figure 4.15). Bilirubin activates various nuclear and cytoplasmic receptors, resembling the endocrine activities of actual hormonal substances. This is true for the "classical" hepatic nuclear receptors, and for some lesser explored receptors or other signaling molecules (Vítek, 2020). We have previously showed that 24h of bilirubin-priming modulates the glutathione levels in neuroblastoma cells through the induction of the System Xc-, and this renders the cell less prone to oxidative damage (Giraudi et al., 2011).
Bilirubin exerts potent anti-inflammatory and immunomodulatory activities (Jangi et al., 2013) and the interrelation between UCB, ER-Stress, inflammation, and associated cascade of events has been demonstrated (Barateiro et al., 2012). An increasing body of evidence suggests that mildly elevated bilirubin could control inflammation, both *in vitro* and *in vivo*, through the mechanisms involved in NF-κB signaling pathway inhibition as well as through the activation of inflammasomes (Li et al., 2020) and the suppression of pro-inflammatory cytokines production (Liu et al., 2008; Adin et al., 2017). We observed a reduced CHOP expression and IL-6 release in jj aortic endothelial primary cells exposed to PA compared to cells from Nj cells (Figure 4.17). In addition, only pretreatment with UCB significantly reduced CHOP expression and IL-6 release induced by PA treatment in immortalized H5V cell line (Figure 4.18). Similarly, pretreated for 16h with Vaticanol B, a

resveratrol tetramer, regulates endoplasmic reticulum stress and inflammation (Tabata et al., 2007). Co-treatment with UCB resulted in reducing ER-stress and the subsequent inflammatory response also in *in vitro* model of gut inflammation (Gundamaraju et al., 2019). It is very likely that the anti-inflammatory and anti-oxidative effects may contribute to the protective role of bilirubin on vascular damage (Inoguchi et al., 2016).

Bilirubin provided a nephroprotective effect in different *in vivo* models as showed by the finding that jj Gunn rats showed significantly lower creatinine level compared with Wistar rats at day 5 in a cisplatin nephrotoxicity model (Barabas et al., 2008). In streptozotocin-induced diabetic damage, jj Gunn rats exhibited significantly less urinary albumin excretion, did not develop renal mesangial expansion, and expressed lower levels of TGF-α and fibronectin than diabetic Nj Gunn rats (Fujii et al., 2010). We found that, upon Ang II treatment, primary podocytes from jj Gunn rats showed lower DNA fragmentation, cleaved caspase-3 and cleaved PARP induction compared with primary podocytes from Nj Gunn rats (Figures 4.19 and 4.20). Also, on cyclosporine (CsA)-induced nephropathy rat model, a significantly lower number of apoptotic cells was observed in the bilirubin-treated rat kidneys compared to controls, confirming the bilirubin anti-apoptotic effect (Oh et al., 2013). Recent reports have suggested that autophagy is upregulated in glomerular podocytes and plays a protective role in proteinuric kidney diseases(Lin et al., 2019). Our results suggested a relationship between autophagy and apoptosis in Ang II-treated podocytes. We found that the basal expression of LC3-II proteins is higher in jj podocytes than in Nj (Figure 4.21);these data suggest that UCB is able to induce autophagy as a pro-survival cell mechanism. Activation of autophagy defence mechanisms in response to UCB treatment has also been demonstrated in neuronal cells (Qaisiya et al., 2017). Recent studies highlight the renoprotective role of autophagy in podocytes in models of diabetic nephropathy. Xiao et al. demonstrated that rapamycin can ameliorate renal injury in streptozocin (STZ)-induced type I diabetic mice by increasing the autophagy activity and by inhibiting podocytes apoptosis(Xiao et al., 2014). Furthermore, recent study demonstrated that Resveratrol (antioxidant compound) effectively attenuates high glucose-induced apoptosis via activation of autophagy in db/db mice and podocytes (Huang et al., 2017).We also observed that the higher basal autophagy level in jj primary podocytes correlated with a lower induction of apoptosis by Ang II. In this context, as previously showed by Seong et al.(Seong et al., 2019), our results suggested that life-long hyperbilirubinemia contributes to attenuate podocytes apoptosis induced by Ang II via stimulation of autophagy.

Regarding tubular epithelial fibrosis in DN, we found that Ang II acts as pro-fibrotic marker by inducing HIF-1α and LOXl2 protein expression in a dose-dependent manner on HK-2 cells (Figure 4.22). We demonstrated, expanding the previous evidence (Kim et al., 2014), that bilirubin modulated the pro-fibrotic markers expression with double face behavior. This is due to the extent of intracellular UCB concentration which determines the UCB anti-or pro-oxidant effect (Bianco et al., 2020). Both HIF-1α and LOXl2 protein induction by Ang II or AGE was significantly reduced only by UCB pretreatment of 1.25 or 2.5 μM corresponding to an antioxidant intracellular UCB (Bianco et al., 2020).Also UCB post-treatment appears to modulate the expression of HIF-1α and LOXl2 proteins induced by Ang II or AGE treatments, even if not in significant way (Figure 4.24). Histologically, bilirubin has already been shown to have an anti-fibrotic effect on cyclosporine (CsA)-induced nephropathy *in vivo*, given that bilirubin pretreatment significantly improved afferent arteriolopathy, tubulointerstitial fibrosis, and tubular injury compared to the CsA-only treated rats (Oh et al., 2013).

In the third task, the association among total bilirubin levels, age, pubertal stage, anthropometric, clinical, and laboratory data were evaluated in a retrospective cross-sectional study performed on 1672 consecutive obese children and adolescents. Overall, the median age of participants was 15,

body mass index (BMI) 36 and circulating total bilirubin level 0.64 mg/dl. Total bilirubin level correlates positively and significantly, even if weakly, with age and Tanner in the total population, showing an higher correlation in male compared to female (Figure 4.26 and 4.27). These results are in line with what previously observed in the white population aged 5-30 years from the biracial Bogalusa Heart Study (Madhavan et al., 1997). Serum bilirubin levels are significantly higher in men than in women also in United States adults (Zucker et al., 2004). Because the gender disparity in serum bilirubin does not manifest prior to age 10 years (Madhavan et al., 1997), has been postulated that hormonal changes commencing at puberty cause altered bilirubin metabolism (Li et al., 1999). This theory is supported by evidence that testosterone suppresses hepatic UGT activity in orchiectomized rats, while the combination of estradiol and progesterone enhances enzyme activity in gonadectomized female rodents (Muraca and Fevery, 1984).

Total serum bilirubin levels were inversely but weakly (even if significantly) correlated with waist: height ratio ($r=-0.01$; $p<0.05$); homeostatic model assessment (HOMA) ($r=-0.32$; $p<0.05$); C-Reactive Protein(CRP) ($r=-0.24$; $p<0.001$); large waist circumference ($r=-1.17$; $p<0.001$); high triglycerides ($r=-0.77$; $p<0.001$) (Figure 4.28 and Table 4.5).

Although insulin measurement during oral glucose tolerance test (OGTT) is considered the best option to evaluate insulin resistance, it is not simple to perform in epidemiologic studies, where fasting insulin and HOMA are more frequently employed. A strong, independent and inverse association between serum bilirubin levels and HOMA was previously evidenced in adults (Guzek et al., 2012; Zhang et al., 2020) and children ($p<0.001$), similarly to what observed in the present cohort.

Evidence points out that chronic systemic inflammation plays a major role in the pathological process associated with MetS (Ridker Paul M, 2003). The serum levels of an inflammatory marker, CRP, not only correlate with all components of the MetS but also correlate with insulin resistance, endothelial dysfunction, and impaired fibrinolysis (Ridker Paul M, 2003). It is likely that the serum bilirubin might have roles in protecting against the MetS. Within the obese group of Belo study (Belo et al., 2014), total serum bilirubin levels correlated negatively and significantly with CRP ($r=-0.178$, $p= 0.001$). The negative relation that we found between bilirubin and CRP levels (even in their normal ranges) is in line with this data and with the bilirubin's anti-inflammatory activity, as previously reported (Ohnaka et al., 2010; Hwang et al., 2011; Yoshino et al., 2011; Yu et al., 2011).

A mechanistic link between bilirubin and perturbation of lipid status was previously described (Wallner et al., 2013).Reduced circulating total cholesterol (Tapan et al., 2011),Low Density Lipoprotein-Cholesterol(LDL-C)(Očadlík et al., 2011), Triglycerides (TAG)(Vítek et al., 2007) and elevated HDL/LDL ratio(Bulmer et al., 2008) have been documented in mild hyperbilirubinemic adult Gilbert subjects. Inverse association between Ox-LDL (Nascimento et al., 2015), triglycerides (Madhavan et al., 1997)and serum bilirubin was shown in young obese patients. Similarly we detected an inverse correlation between total serum bilirubin levels and high triglycerides ($r=-0.77$; $p<0.001$) (Table 4.6).

Little is known about bilirubin role on MetS among children and adolescents. In a representative sample of the non-institutionalized civilian U.S. population (NAHNES), Lin et al. examined 4723 children and adolescents aged 12–17 years. They identified 190 participants as having MetS, corresponding to 4% of the cohort studied. The serum total bilirubin levels were significantly higher in subjects without MetS than those with MetS. Authors speculated that in these young subjects, when the metabolic dysregulation is in its early stage, bilirubin may exert its anti-oxidative effect within the tissue. (Lin et al., 2009a). Similar results have also been stated in other studies conducted in adults from China (Wu et al., 2011; Hao et al., 2020); Korea (Jo et al., 2011; Choi et al., 2013) and Poland (Guzek et al., 2012).In our study, total serum bilirubin did not

significantly correlate with Mets. The only study performed on a population of young obese was Portuguese(Belo et al., 2014) and showed a causal association for total bilirubin and body fat percentage. It is worth to note that the BMI mean ±SD was 30.7±5.8 for female and 30.5±6.4 for males. We think that the severe obesity of the cohort studied in the present work, doesn't allow to evidence the ability of serum bilirubin to modulate MetS in young ages as when the metabolic dysregulation is in its early stage.

38.4 % of a large sample of obese children studied had NAFLD defined as the presence of liver steatosis at ultrasonography. Even if a prevalence of 38% is within the expected range, it is substantially lower than that observed in a series of Chinese children with a similar degree of obesity (77%, Po0.0001, Fisher's exact test)(Chan et al., 2004). This difference is of interest because it may be explained by genetic and/or environmental factors, similarly to what has been hypothesized for adults (Browning et al., 2004; Weston et al., 2005). In our cohort bilirubin weakly, not significantly and negatively correlated with fatty liver (Figure 4.30).The same association was investigated in a Taiwanese cohort of obese children, with stratification according to UGT1A1 genotype and NAFLD defined by ultrasonography 12% of the obese children studied had NAFLD. Serum total bilirubin levels were lower in the subjects with pediatric NAFLD and they found an independent association between variant UGT1A1*6 genotypes and decreasing prevalence of pediatric NAFLD(Lin et al., 2009b). The main differences between that cohort and our cohort consisted in the number of participants (234 vs 1672) and in the severity of obesity (mean±SD BMI: 24.2±0.88 vs median (interquartile range) BMI:36 (Kunutsor, 2015; Seyed Khoei et al., 2018).

The study presents some limitation. First, its results cannot be extended to the general population. The lack of a control group of normal-weight children, due mainly to ethical constraints, does not allow to establish whether the identified parameters will work equally well in non-obese children. Second, although ultrasonography is a desirable technique for epidemiologic studies owing to being readily available and non-invasive, it cannot detect a fatty infiltration of 30%, thus possibly underestimating the prevalence of fatty liver.

We believe that the present thesis work have contributed to a better understanding of the molecular mechanism involved in the protective impact of bilirubin through 3 statements:

1) The definition of intracellular UCB thresholds that set the switch between anti- and pro-oxidant effects of bilirubin. An intracellular UCB concentration of around 7 ng/mg protein had antioxidant activities, while its intracellular concentrations >25 ng/mg protein resulted in pro-oxidant and cytotoxic effects;

2) the demonstration that life-long hyperbilirubinemia exposure or bilirubin-priming significantly contribute to the activation of protection against metabolic syndrome, by enhancing responses to damage and increasing cell viability in *in vitro* models of atherosclerosis and DN;

3) the observation that serum bilirubin levels, even in their normal ranges, might have graded associations with the prevalence of the MetS and NAFLD in young ages, when the metabolic dysregulation is in its early stage, but not in extremely obese population.

Chapter 6
References

6. REFERENCES

Abu-Bakar, A., Arthur, D. M., Wikman, A. S., Rahnasto, M., Juvonen, R. O., Vepsäläinen, J., et al. (2012). Metabolism of bilirubin by human cytochrome P450 2A6. *Toxicol. Appl. Pharmacol.* 261, 50–58. doi:10.1016/j.taap.2012.03.010.

Aebi, H. (1984). Catalase in vitro. *Methods Enzymol* 105, 121–126. doi:10.1016/s0076-6879(84)05016-3.

Ahlfors, C. E., Wennberg, R. P., Ostrow, J. D., and Tiribelli, C. (2009). Unbound (free) bilirubin: improving the paradigm for evaluating neonatal jaundice. *Clin. Chem.* 55, 1288–1299. doi:10.1373/clinchem.2008.121269.

Alberti, K. G. M. M., Eckel, R. H., Grundy, S. M., Zimmet, P. Z., Cleeman, J. I., Donato, K. A., et al. (2009). Harmonizing the metabolic syndrome: a joint interim statement of the International Diabetes Federation Task Force on Epidemiology and Prevention; National Heart, Lung, and Blood Institute; American Heart Association; World Heart Federation; International Atherosclerosis Society; and International Association for the Study of Obesity. *Circulation* 120, 1640–1645. doi:10.1161/CIRCULATIONAHA.109.192644.

Andersson, C., Weeke, P., Fosbøl, E. L., Brendorp, B., Køber, L., Coutinho, W., et al. (2009). Acute effect of weight loss on levels of total bilirubin in obese, cardiovascular high-risk patients: an analysis from the lead-in period of the Sibutramine Cardiovascular Outcome trial. *Metabolism* 58, 1109–1115. doi:10.1016/j.metabol.2009.04.003.

Baranano, D. E., Rao, M., Ferris, C. D., and Snyder, S. H. (2002). Biliverdin reductase: a major physiologic cytoprotectant. *Proc. Natl. Acad. Sci. U.S.A.* 99, 16093–16098. doi:10.1073/pnas.252626999.

Bellarosa, C., Bortolussi, G., and Tiribelli, C. (2009). The role of ABC transporters in protecting cells from bilirubin toxicity. *Curr. Pharm. Des.* 15, 2884–2892. doi:10.2174/138161209789058246.

Belo, L., Nascimento, H., Kohlova, M., Bronze-da-Rocha, E., Fernandes, J., Costa, E., et al. (2014). Body fat percentage is a major determinant of total bilirubin independently of UGT1A1*28 polymorphism in young obese. *PLoS ONE* 9, e98467. doi:10.1371/journal.pone.0098467.

Bertolotti, A., Zhang, Y., Hendershot, L. M., Harding, H. P., and Ron, D. (2000). Dynamic interaction of BiP and ER stress transducers in the unfolded-protein response. *Nat Cell Biol* 2, 326–332. doi:10.1038/35014014.

Bhogal, R. H., Weston, C. J., Curbishley, S. M., Adams, D. H., and Afford, S. C. (2012). Autophagy: a cyto-protective mechanism which prevents primary human hepatocyte apoptosis during oxidative stress. *Autophagy* 8, 545–558. doi:10.4161/auto.19012.

Bhuiyan, A. R., Srinivasan, S. R., Chen, W., Sultana, A., and Berenson, G. S. (2008). Association of serum bilirubin with pulsatile arterial function in asymptomatic young adults: the Bogalusa Heart Study. *Metabolism* 57, 612–616. doi:10.1016/j.metabol.2007.12.003.

Bonder, M. J., Kasela, S., Kals, M., Tamm, R., Lokk, K., Barragan, I., et al. (2014). Genetic and epigenetic regulation of gene expression in fetal and adult human livers. *BMC Genomics* 15, 860. doi:10.1186/1471-2164-15-860.

Boon, A.-C., Hawkins, C. L., Bisht, K., Coombes, J. S., Bakrania, B., Wagner, K.-H., et al. (2012). Reduced circulating oxidized LDL is associated with hypocholesterolemia and enhanced thiol status in Gilbert syndrome. *Free Radic Biol Med* 52, 2120–2127. doi:10.1016/j.freeradbiomed.2012.03.002.

Bose, M., Almas, S., and Prabhakar, S. (2017). Wnt signaling and podocyte dysfunction in diabetic nephropathy. *J Investig Med* 65, 1093–1101. doi:10.1136/jim-2017-000456.

Brites, D. (2011). Bilirubin injury to neurons and glial cells: new players, novel targets, and newer insights. *Semin. Perinatol.* 35, 114–120. doi:10.1053/j.semperi.2011.02.004.

Brito, M. A., Lima, S., Fernandes, A., Falcão, A. S., Silva, R. F. M., Butterfield, D. A., et al. (2008). Bilirubin injury to neurons: contribution of oxidative stress and rescue by glycoursodeoxycholic acid. *Neurotoxicology* 29, 259–269. doi:10.1016/j.neuro.2007.11.002.

Browning, J. D., Szczepaniak, L. S., Dobbins, R., Nuremberg, P., Horton, J. D., Cohen, J. C., et al. (2004). Prevalence of hepatic steatosis in an urban population in the United States: impact of ethnicity. *Hepatology* 40, 1387–1395. doi:10.1002/hep.20466.

Brufani, C., Fintini, D., Giordano, U., Tozzi, A. E., Barbetti, F., and Cappa, M. (2011). Metabolic syndrome in italian obese children and adolescents: stronger association with central fat depot than with insulin sensitivity and birth weight. *Int J Hypertens* 2011, 257168. doi:10.4061/2011/257168.

Bulmer, A. C., Blanchfield, J. T., Toth, I., Fassett, R. G., and Coombes, J. S. (2008). Improved resistance to serum oxidation in Gilbert's syndrome: a mechanism for cardiovascular protection. *Atherosclerosis* 199, 390–396. doi:10.1016/j.atherosclerosis.2007.11.022.

Cacciari, E., Milani, S., Balsamo, A., Spada, E., Bona, G., Cavallo, L., et al. (2006). Italian cross-sectional growth charts for height, weight and BMI (2 to 20 yr). *J Endocrinol Invest* 29, 581–593. doi:10.1007/BF03344156.

Calcaterra, V., Klersy, C., Muratori, T., Telli, S., Caramagna, C., Scaglia, F., et al. (2008). Prevalence of metabolic syndrome (MS) in children and adolescents with varying degrees of obesity. *Clin Endocrinol (Oxf)* 68, 868–872. doi:10.1111/j.1365-2265.2007.03115.x.

Calligaris, S., Cekic, D., Roca-Burgos, L., Gerin, F., Mazzone, G., Ostrow, J. D., et al. (2006). Multidrug resistance associated protein 1 protects against bilirubin-induced cytotoxicity. *FEBS Lett.* 580, 1355–1359. doi:10.1016/j.febslet.2006.01.056.

Camhi, S. M., Kuo, J., and Young, D. R. (2008). Identifying Adolescent Metabolic Syndrome Using Body Mass Index and Waist Circumference. *Prev Chronic Dis* 5. Available at: https://www.ncbi.nlm.nih.gov/pmc/articles/PMC2578768/ [Accessed January 2, 2021].

Ceriello, A., Morocutti, A., Mercuri, F., Quagliaro, L., Moro, M., Damante, G., et al. (2000). Defective intracellular antioxidant enzyme production in type 1 diabetic patients with nephropathy. *Diabetes* 49, 2170–2177. doi:10.2337/diabetes.49.12.2170.

Chan, D. F. Y., Li, A. M., Chu, W. C. W., Chan, M. H. M., Wong, E. M. C., Liu, E. K. H., et al. (2004a-b). Hepatic steatosis in obese Chinese children. *Int J Obes Relat Metab Disord* 28, 1257–1263. doi:10.1038/sj.ijo.0802734.

Chan, G. K. Y., Kleinheinz, T. L., Peterson, D., and Moffat, J. G. (2013). A Simple High-Content Cell Cycle Assay Reveals Frequent Discrepancies between Cell Number and ATP and MTS Proliferation Assays. *PLoS One* 8. doi:10.1371/journal.pone.0063583.

Chen, L., Chen, D.-Q., Wang, M., Liu, D., Chen, H., Dou, F., et al. (2017). Role of RAS/Wnt/β-catenin axis activation in the pathogenesis of podocyte injury and tubulo-interstitial nephropathy. *Chem Biol Interact* 273, 56–72. doi:10.1016/j.cbi.2017.05.025.

Chen, Y., Azad, M. B., and Gibson, S. B. (2010). Methods for detecting autophagy and determining autophagy-induced cell death. *Can. J. Physiol. Pharmacol.* 88, 285–295. doi:10.1139/Y10-010.

Chen, Y.-H., Chau, L.-Y., Chen, J.-W., and Lin, S.-J. (2008). Serum bilirubin and ferritin levels link heme oxygenase-1 gene promoter polymorphism and susceptibility to coronary artery disease in diabetic patients. *Diabetes Care* 31, 1615–1620. doi:10.2337/dc07-2126.

Cheriyath, P., Gorrepati, V. S., Peters, I., Nookala, V., Murphy, M. E., Srouji, N., et al. (2010). High Total Bilirubin as a Protective Factor for Diabetes Mellitus: An Analysis of NHANES Data From 1999 - 2006. *J Clin Med Res* 2, 201–206. doi:10.4021/jocmr425w.

Chin, H. J., Cho, H. J., Lee, T. W., Na, K. Y., Oh, K. H., Joo, K. W., et al. (2009). The Mildly Elevated Serum Bilirubin Level is Negatively Associated with the Incidence of End Stage Renal Disease in Patients with IgA Nephropathy. *J Korean Med Sci* 24, S22–S29. doi:10.3346/jkms.2009.24.S1.S22.

Choi, S. H., Yun, K. E., and Choi, H. J. (2013a-b). Relationships between serum total bilirubin levels and metabolic syndrome in Korean adults. *Nutr Metab Cardiovasc Dis* 23, 31–37. doi:10.1016/j.numecd.2011.03.001.

Coles, B. F., and Kadlubar, F. F. (2005). "Human Alpha Class Glutathione S-Transferases: Genetic Polymorphism, Expression, and Susceptibility to Disease," in *Methods in Enzymology* Gluthione Transferases and Gamma-Glutamyl Transpeptidases., eds. H. Sies and L. Packer (Academic Press), 9–42. doi:10.1016/S0076-6879(05)01002-5.

Corich, L., Aranda, A., Carrassa, L., Bellarosa, C., Ostrow, J. D., and Tiribelli, C. (2009). The cytotoxic effect of unconjugated bilirubin in human neuroblastoma SH-SY5Y cells is modulated by the expression level of MRP1 but not MDR1. *Biochem. J.* 417, 305–312. doi:10.1042/BJ20080918.

Dai, H., Liu, Q., and Liu, B. (2017). Research Progress on Mechanism of Podocyte Depletion in Diabetic Nephropathy. *J Diabetes Res* 2017, 2615286. doi:10.1155/2017/2615286.

Danoff, T. M., Campbell, D. A., McCarthy, L. C., Lewis, K. F., Repasch, M. H., Saunders, A. M., et al. (2004). A Gilbert's syndrome UGT1A1 variant confers susceptibility to tranilast-induced hyperbilirubinemia. *Pharmacogenomics J* 4, 49–53. doi:10.1038/sj.tpj.6500221.

Daverey, A., and Agrawal, S. K. (2018). Pre and post treatment with curcumin and resveratrol protects astrocytes after oxidative stress. *Brain Res* 1692, 45–55. doi:10.1016/j.brainres.2018.05.001.

De Matteis, F., Lord, G. A., Kee Lim, C., and Pons, N. (2006). Bilirubin degradation by uncoupled cytochrome P450. Comparison with a chemical oxidation system and characterization of the products by high-performance liquid chromatography/electrospray ionization mass spectrometry. *Rapid Commun. Mass Spectrom.* 20, 1209–1217. doi:10.1002/rcm.2431.

Derick, S., Gironde, C., Perio, P., Reybier, K., Nepveu, F., Jauneau, A., et al. (2017). LUCS (Light-Up Cell System), a universal high throughput assay for homeostasis evaluation in live cells. *Sci Rep* 7, 18069. doi:10.1038/s41598-017-18211-2.

DeRubertis, F. R., Craven, P. A., and Melhem, M. F. (2007). Acceleration of diabetic renal injury in the superoxide dismutase knockout mouse: effects of tempol. *Metabolism* 56, 1256–1264. doi:10.1016/j.metabol.2007.04.024.

Dong, Y., Fernandes, C., Liu, Y., Wu, Y., Wu, H., Brophy, M. L., et al. (2017). Role of endoplasmic reticulum stress signalling in diabetic endothelial dysfunction and atherosclerosis. *Diab Vasc Dis Res* 14, 14–23. doi:10.1177/1479164116666762.

Doré, S., and Snyder, S. H. (1999). Neuroprotective action of bilirubin against oxidative stress in primary hippocampal cultures. *Ann. N. Y. Acad. Sci.* 890, 167–172. doi:10.1111/j.1749-6632.1999.tb07991.x.

Elmore, S. (2007). Apoptosis: A Review of Programmed Cell Death. *Toxicol Pathol* 35, 495–516. doi:10.1080/01926230701320337.

Emi, Y., Omura, S., Ikushiro, S., and Iyanagi, T. (2002). Accelerated degradation of mislocalized UDP-glucuronosyltransferase family 1 (UGT1) proteins in Gunn rat hepatocytes. *Arch Biochem Biophys* 405, 163–169. doi:10.1016/s0003-9861(02)00351-x.

Erlinger, S., Arias, I. M., and Dhumeaux, D. (2014). Inherited disorders of bilirubin transport and conjugation: new insights into molecular mechanisms and consequences. *Gastroenterology* 146, 1625–1638. doi:10.1053/j.gastro.2014.03.047.

Ewing, J. F., and Janero, D. R. (1995). Microplate superoxide dismutase assay employing a nonenzymatic superoxide generator. *Anal. Biochem.* 232, 243–248. doi:10.1006/abio.1995.0014.

Falcão, A. S., Bellarosa, C., Fernandes, A., Brito, M. A., Silva, R. F. M., Tiribelli, C., et al. (2007). Role of multidrug resistance-associated protein 1 expression in the in vitro susceptibility of rat nerve cell to unconjugated bilirubin. *Neuroscience* 144, 878–888. doi:10.1016/j.neuroscience.2006.10.026.

Fang, L., Li, X., Luo, Y., He, W., Dai, C., and Yang, J. (2014). Autophagy inhibition induces podocyte apoptosis by activating the pro-apoptotic pathway of endoplasmic reticulum stress. *Experimental Cell Research* 322, 290–301. doi:10.1016/j.yexcr.2014.01.001.

Farrera, J. A., Jaumà, A., Ribó, J. M., Peiré, M. A., Parellada, P. P., Roques-Choua, S., et al. (1994). The antioxidant role of bile pigments evaluated by chemical tests. *Bioorg. Med. Chem.* 2, 181–185. doi:10.1016/s0968-0896(00)82013-1.

Fazio, S., Babaev, V. R., Murray, A. B., Hasty, A. H., Carter, K. J., Gleaves, L. A., et al. (1997). Increased atherosclerosis in mice reconstituted with apolipoprotein E null macrophages. *Proc Natl Acad Sci U S A* 94, 4647–4652. doi:10.1073/pnas.94.9.4647.

Fevery, J. (2008). Bilirubin in clinical practice: a review. *Liver Int* 28, 592–605. doi:10.1111/j.1478-3231.2008.01716.x.

Finelli, C., Sommella, L., Gioia, S., La Sala, N., and Tarantino, G. (2013). Should visceral fat be reduced to increase longevity? *Ageing Res. Rev.* 12, 996–1004. doi:10.1016/j.arr.2013.05.007.

Forbes, J. M., Coughlan, M. T., and Cooper, M. E. (2008). Oxidative stress as a major culprit in kidney disease in diabetes. *Diabetes* 57, 1446–1454. doi:10.2337/db08-0057.

Ford, E. S. (2005). Risks for all-cause mortality, cardiovascular disease, and diabetes associated with the metabolic syndrome: a summary of the evidence. *Diabetes Care* 28, 1769–1778. doi:10.2337/diacare.28.7.1769.

Ford, E. S., Giles, W. H., and Mokdad, A. H. (2004). Increasing prevalence of the metabolic syndrome among u.s. Adults. *Diabetes Care* 27, 2444–2449. doi:10.2337/diacare.27.10.2444.

Fujii, M., Inoguchi, T., Sasaki, S., Maeda, Y., Zheng, J., Kobayashi, K., et al. (2010). Bilirubin and biliverdin protect rodents against diabetic nephropathy by downregulating NAD(P)H oxidase. *Kidney Int* 78, 905–919. doi:10.1038/ki.2010.265.

Fukui, M., Tanaka, M., Shiraishi, E., Harusato, I., Hosoda, H., Asano, M., et al. (2008). Relationship between serum bilirubin and albuminuria in patients with type 2 diabetes. *Kidney Int* 74, 1197–1201. doi:10.1038/ki.2008.398.

Gallo, D., Cocchietto, M., Masat, E., Agostinis, C., Harei, E., Veronesi, P., et al. (2014). Human recombinant lysozyme downregulates advanced glycation endproduct-induced interleukin-6 production and release in an in-vitro model of human proximal tubular epithelial cells. *Exp. Biol. Med. (Maywood)* 239, 337–346. doi:10.1177/1535370213518281.

Gazzin, S., Zelenka, J., Zdrahalova, L., Konickova, R., Zabetta, C. C., Giraudi, P. J., et al. (2012). Bilirubin accumulation and Cyp mRNA expression in selected brain regions of jaundiced Gunn rat pups. *Pediatr. Res.* 71, 653–660. doi:10.1038/pr.2012.23.

Gazzin, S., Strazielle, N., Tiribelli, C., and Ghersi-Egea, J.-F. (2012). Transport and Metabolism at Blood–Brain Interfaces and in Neural Cells: Relevance to Bilirubin-Induced Encephalopathy. *Front. Pharmacol.* 3. doi:10.3389/fphar.2012.00089.

Gazzin, S., Vitek, L., Watchko, J., Shapiro, S. M., and Tiribelli, C. (2016). A Novel Perspective on the Biology of Bilirubin in Health and Disease. *Trends Mol Med* 22, 758–768. doi:10.1016/j.molmed.2016.07.004.

Gilbert, R. E., and Cooper, M. E. (1999). The tubulointerstitium in progressive diabetic kidney disease: more than an aftermath of glomerular injury? *Kidney Int.* 56, 1627–1637. doi:10.1046/j.1523-1755.1999.00721.x.

Giraudi, P. J., Bellarosa, C., Coda-Zabetta, C. D., Peruzzo, P., and Tiribelli, C. (2011). Functional induction of the cystine-glutamate exchanger system Xc(-) activity in SH-SY5Y cells by unconjugated bilirubin. *PLoS ONE* 6, e29078. doi:10.1371/journal.pone.0029078.

Gironde, C., Rigal, M., Dufour, C., and Furger, C. (2020). AOP1, a New Live Cell Assay for the Direct and Quantitative Measure of Intracellular Antioxidant Effects. *Antioxidants (Basel)* 9. doi:10.3390/antiox9060471.

Gopinathan, V., Miller, N. J., Milner, A. D., and Rice-Evans, C. A. (1994). Bilirubin and ascorbate antioxidant activity in neonatal plasma. *FEBS Lett.* 349, 197–200. doi:10.1016/0014-5793(94)00666-0.

Gorin, Y., Block, K., Hernandez, J., Bhandari, B., Wagner, B., Barnes, J. L., et al. (2005). Nox4 NAD(P)H oxidase mediates hypertrophy and fibronectin expression in the diabetic kidney. *J Biol Chem* 280, 39616–39626. doi:10.1074/jbc.M502412200.

Góth, L., Rass, P., and Páy, A. (2004). Catalase enzyme mutations and their association with diseases. *Mol Diagn* 8, 141–149. doi:10.1007/BF03260057.

Grasl-Kraupp, B., Ruttkay-Nedecky, B., Koudelka, H., Bukowska, K., Bursch, W., and Schulte-Hermann, R. (1995). In situ detection of fragmented DNA (TUNEL assay) fails to discriminate among apoptosis, necrosis, and autolytic cell death: a cautionary note. *Hepatol. Baltim*. Md 21, 1465–1468. doi:10.1002/hep.1840210534.

Grundy, S. M., Brewer, H. B., Cleeman, J. I., Smith, S. C., Lenfant, C., National Heart, Lung, and Blood Institute, et al. (2004). Definition of metabolic syndrome: report of the National Heart, Lung, and Blood Institute/American Heart Association conference on scientific issues related to definition. *Arterioscler Thromb Vasc Biol* 24, e13-18. doi:10.1161/01.ATV.0000111245.75752.C6.

Guzek, M., Jakubowski, Z., Bandosz, P., Wyrzykowski, B., Smoczyński, M., Jabloiska, A., et al. (2012). Inverse association of serum bilirubin with metabolic syndrome and insulin resistance in Polish population. *Przegl Epidemiol* 66, 495–501.

Haase, V. H. (2006). Hypoxia-inducible factors in the kidney. *Am J Physiol Renal Physiol* 291, F271-281. doi:10.1152/ajprenal.00071.2006.

Haase, V. H. (2012). Hypoxia-inducible factor signaling in the development of kidney fibrosis. *Fibrogenesis Tissue Repair* 5, S16. doi:10.1186/1755-1536-5-S1-S16.

Halberg, N., Khan, T., Trujillo, M. E., Wernstedt-Asterholm, I., Attie, A. D., Sherwani, S., et al. (2009). Hypoxia-inducible factor 1alpha induces fibrosis and insulin resistance in white adipose tissue. *Mol Cell Biol* 29, 4467–4483. doi:10.1128/MCB.00192-09.

Haley, K. E., Kronenberg, N. M., Liehm, P., Elshani, M., Bell, C., Harrison, D. J., et al. (2018). Podocyte injury elicits loss and recovery of cellular forces. *Sci Adv* 4, eaap8030. doi:10.1126/sciadv.aap8030.

Han, S. S., Na, K. Y., Chae, D.-W., Kim, Y. S., Kim, S., and Chin, H. J. (2010). High serum bilirubin is associated with the reduced risk of diabetes mellitus and diabetic nephropathy. *Tohoku J. Exp. Med.* 221, 133–140.

Hao, H., Guo, H., Ma, R.-L., Yan, Y.-Z., Hu, Y.-H., Ma, J.-L., et al. (2020). Association of total bilirubin and indirect bilirubin content with metabolic syndrome among Kazakhs in Xinjiang. *BMC Endocr Disord* 20, 110. doi:10.1186/s12902-020-00563-y.

Harrison, S. A., and Neuschwander-Tetri, B. A. (2004). Nonalcoholic fatty liver disease and nonalcoholic steatohepatitis. *Clin Liver Dis* 8, 861–879, ix. doi:10.1016/j.cld.2004.06.008.

Hartleben, B., Gödel, M., Meyer-Schwesinger, C., Liu, S., Ulrich, T., Köbler, S., et al. (2010). Autophagy influences glomerular disease susceptibility and maintains podocyte homeostasis in aging mice. *J. Clin. Invest.* 120, 1084–1096. doi:10.1172/JCI39492.

He, C., Zhu, H., Li, H., Zou, M.-H., and Xie, Z. (2013). Dissociation of Bcl-2-Beclin1 complex by activated AMPK enhances cardiac autophagy and protects against cardiomyocyte apoptosis in diabetes. *Diabetes* 62, 1270–1281. doi:10.2337/db12-0533.

He, L., He, T., Farrar, S., Ji, L., Liu, T., and Ma, X. (2017). Antioxidants Maintain Cellular Redox Homeostasis by Elimination of Reactive Oxygen Species. *CPB* 44, 532–553. doi:10.1159/000485089.

Higgins, D. F., Kimura, K., Bernhardt, W. M., Shrimanker, N., Akai, Y., Hohenstein, B., et al. (2007). Hypoxia promotes fibrogenesis in vivo via HIF-1 stimulation of epithelial-to-mesenchymal transition. *J Clin Invest* 117, 3810–3820. doi:10.1172/JCI30487.

Hinds, T. D., and Stec, D. E. (2019). Bilirubin Safeguards Cardiorenal and Metabolic Diseases: a Protective Role in Health. Curr. Hypertens. Rep. 21, 87. doi:10.1007/s11906-019-0994-z.

Huang, S.-S., Ding, D.-F., Chen, S., Dong, C.-L., Ye, X.-L., Yuan, Y.-G., et al. (2017). Resveratrol protects podocytes against apoptosis via stimulation of autophagy in a mouse model of diabetic nephropathy. *Scientific Reports* 7, 45692. doi:10.1038/srep45692.

Huang, T. T.-K., Ball, G. D. C., and Franks, P. W. (2007). Metabolic syndrome in youth: current issues and challenges. *Appl Physiol Nutr Metab* 32, 13–22. doi:10.1139/h06-094.

Hwang, H.-J., Lee, S.-W., and Kim, S.-H. (2011). Relationship between bilirubin and C-reactive protein. *Clin Chem Lab Med* 49, 1823–1828. doi:10.1515/CCLM.2011.662.

Iusuf, D., van de Steeg, E., and Schinkel, A. H. (2012). Hepatocyte hopping of OATP1B substrates contributes to efficient hepatic detoxification. *Clin. Pharmacol. Ther.* 92, 559–562. doi:10.1038/clpt.2012.143.

Iyanagi, T. (1991). Molecular basis of multiple UDP-glucuronosyltransferase isoenzyme deficiencies in the hyperbilirubinemic rat (Gunn rat). *J Biol Chem* 266, 24048–24052.

Jašprová, J., Dvořák, A., Vecka, M., Leníček, M., Lacina, O., Valášková, P., et al. (2020). A novel accurate LC-MS/MS method for quantitative determination of Z-lumirubin. *Sci Rep* 10, 4411. doi:10.1038/s41598-020-61280-z.

Jenkinson, S. E., Chung, G. W., van Loon, E., Bakar, N. S., Dalzell, A. M., and Brown, C. D. A. (2012). The limitations of renal epithelial cell line HK-2 as a model of drug transporter expression and function in the proximal tubule. *Pflugers Arch.* 464, 601–611. doi:10.1007/s00424-012-1163-2.

Jo, J., Yun, J. E., Lee, H., Kimm, H., and Jee, S. H. (2011). Total, direct, and indirect serum bilirubin concentrations and metabolic syndrome among the Korean population. *Endocrine* 39, 182–189. doi:10.1007/s12020-010-9417-2.

Kaneko, M., Niinuma, Y., and Nomura, Y. (2003). Activation signal of nuclear factor-kappa B in response to endoplasmic reticulum stress is transduced via IRE1 and tumor necrosis factor receptor-associated factor 2. *Biol Pharm Bull* 26, 931–935. doi:10.1248/bpb.26.931.

Kang, S. J., Lee, C., and Kruzliak, P. (2014). Effects of serum bilirubin on atherosclerotic processes. *Ann. Med.* 46, 138–147. doi:10.3109/07853890.2014.895588.

Kapitulnik, J., and Gonzalez, F. J. (1993). Marked endogenous activation of the CYP1A1 and CYP1A2 genes in the congenitally jaundiced Gunn rat. *Mol. Pharmacol.* 43, 722–725.

Kawasaki, T., Hashimoto, N., Kikuchi, T., Takahashi, H., and Uchiyama, M. (1997). The relationship between fatty liver and hyperinsulinemia in obese Japanese children. *J Pediatr Gastroenterol Nutr* 24, 317–321. doi:10.1097/00005176-199703000-00015.

Keppler, D. (2014). The roles of MRP2, MRP3, OATP1B1, and OATP1B3 in conjugated hyperbilirubinemia. *Drug Metab. Dispos.* 42, 561–565. doi:10.1124/dmd.113.055772.

Kheirouri, S., Alizadeh, M., and Maleki, V. (2018). Zinc against advanced glycation end products. *Clin Exp Pharmacol Physiol* 45, 491–498. doi:10.1111/1440-1681.12904.

Kimura, K., Iwano, M., Higgins, D. F., Yamaguchi, Y., Nakatani, K., Harada, K., et al. (2008). Stable expression of HIF-1alpha in tubular epithelial cells promotes interstitial fibrosis. *Am J Physiol Renal Physiol* 295, F1023-1029. doi:10.1152/ajprenal.90209.2008.

Kumar, S., Guha, M., Choubey, V., Maity, P., Srivastava, K., Puri, S. K., et al. (2008). Bilirubin inhibits Plasmodium falciparum growth through the generation of reactive oxygen species. *Free Radic. Biol. Med.* 44, 602–613. doi:10.1016/j.freeradbiomed.2007.10.057.

Kunutsor, S. K. (2015). Serum total bilirubin levels and coronary heart disease--Causal association or epiphenomenon? *Exp Gerontol* 72, 63–66. doi:10.1016/j.exger.2015.09.014.

Kunutsor, S. K., Bakker, S. J. L., Gansevoort, R. T., Chowdhury, R., and Dullaart, R. P. F. (2015). Circulating total bilirubin and risk of incident cardiovascular disease in the general population. *Arterioscler. Thromb. Vasc. Biol.* 35, 716–724. doi:10.1161/ATVBAHA.114.304929.

Kunutsor, S. K., Frysz, M., Verweij, N., Kieneker, L. M., Bakker, S. J. L., and Dullaart, R. P. F. (2020). Circulating total bilirubin and risk of non-alcoholic fatty liver disease in the

PREVEND study: observational findings and a Mendelian randomization study. *Eur J Epidemiol* 35, 123–137. doi:10.1007/s10654-019-00589-0.

Kunutsor, S. K., Kieneker, L. M., Burgess, S., Bakker, S. J. L., and Dullaart, R. P. F. (2017a-b). Circulating Total Bilirubin and Future Risk of Hypertension in the General Population: The Prevention of Renal and Vascular End-Stage Disease (PREVEND) Prospective Study and a Mendelian Randomization Approach. *J Am Heart Assoc* 6. doi:10.1161/JAHA.117.006503.

Kwak, M.-S., Kim, D., Chung, G. E., Kang, S. J., Park, M. J., Kim, Y. J., et al. (2012a-b). Serum bilirubin levels are inversely associated with nonalcoholic fatty liver disease. *Clin Mol Hepatol* 18, 383–390. doi:10.3350/cmh.2012.18.4.383.

Kwon, Y.-J., Lee, Y.-J., Park, B.-J., Hong, K.-W., and Jung, D.-H. (2017). Total serum bilirubin and 8-year incident type 2 diabetes mellitus: The Korean Genome and Epidemiology Study. *Diabetes Metab.* doi:10.1016/j.diabet.2017.07.004.

Lafortuna, C. L., Adorni, F., Agosti, F., De Col, A., Sievert, K., Siegfried, W., et al. (2010). Prevalence of the metabolic syndrome among extremely obese adolescents in Italy and Germany. *Diabetes Res Clin Pract* 88, 14–21. doi:10.1016/j.diabres.2010.01.008.

Lanone, S., Bloc, S., Foresti, R., Almolki, A., Taillé, C., Callebert, J., et al. (2005). Bilirubin decreases nos2 expression via inhibition of NAD(P)H oxidase: implications for protection against endotoxic shock in rats. *FASEB J. Off. Publ. Fed. Am. Soc. Exp. Biol.* 19, 1890–1892. doi:10.1096/fj.04-2368fje.

Lazebnik, Y. A., Kaufmann, S. H., Desnoyers, S., Poirier, G. G., and Earnshaw, W. C. (1994). Cleavage of poly(ADP-ribose) polymerase by a proteinase with properties like ICE. *Nature* 371, 346–347. doi:10.1038/371346a0.

Lenna, S., Han, R., and Trojanowska, M. (2014). Endoplasmic reticulum stress and endothelial dysfunction. *IUBMB Life* 66, 530–537. doi:10.1002/iub.1292.

Li, Y. Q., Prentice, D. A., Howard, M. L., Mashford, M. L., and Desmond, P. V. (1999). The effect of hormones on the expression of five isoforms of UDP-glucuronosyltransferase in primary cultures of rat hepatocytes. *Pharm. Res.* 16, 191–197.

Li, X., Gonzalez, O., Shen, X., Barnhart, S., Kramer, F., Kanter, J. E., et al. (2013). Endothelial Acyl-CoA Synthetase 1 is not Required for Inflammatory and Apoptotic Effects of a Saturated Fatty Acid-Rich Environment. Arterioscler. *Thromb. Vasc. Biol.* 33, 232–240. doi:10.1161/ATVBAHA.112.252239.

Lin, L.-Y., Kuo, H.-K., Hwang, J.-J., Lai, L.-P., Chiang, F.-T., Tseng, C.-D., et al. (2009a). Serum bilirubin is inversely associated with insulin resistance and metabolic syndrome among children and adolescents. *Atherosclerosis* 203, 563–568. doi:10.1016/j.atherosclerosis.2008.07.021.

Lin, T.-A., Wu, V. C.-C., and Wang, C.-Y. (2019). Autophagy in Chronic Kidney Diseases. *Cells* 8. doi:10.3390/cells8010061.

Lin, Y.-C., Chang, P.-F., Hu, F.-C., Chang, M.-H., and Ni, Y.-H. (2009b-c). Variants in the UGT1A1 gene and the risk of pediatric nonalcoholic fatty liver disease. *Pediatrics* 124, e1221-1227. doi:10.1542/peds.2008-3087.

Lind, M., Hayes, A., Caprnda, M., Petrovic, D., Rodrigo, L., Kruzliak, P., et al. (2017). Inducible nitric oxide synthase: Good or bad? *Biomed Pharmacother* 93, 370–375. doi:10.1016/j.biopha.2017.06.036.

Liu, L., and Shi, G.-P. (2012). CD31: beyond a marker for endothelial cells. *Cardiovasc Res* 94, 3–5. doi:10.1093/cvr/cvs108.

Liu, W. J., Gan, Y., Huang, W. F., Wu, H., Zhang, X., Zheng, H. J., et al. (2019). Lysosome restoration to activate podocyte autophagy: a new therapeutic strategy for diabetic kidney disease. *Cell Death Dis* 10. doi:10.1038/s41419-019-2002-6.

Liu, Y., Zhu, B., Wang, X., Luo, L., Li, P., Paty, D. W., et al. (2003). Bilirubin as a potent antioxidant suppresses experimental autoimmune encephalomyelitis: implications for the role of oxidative stress in the development of multiple sclerosis. *J. Neuroimmunol.* 139, 27–35. doi:10.1016/s0165-5728(03)00132-2.

Lohman, T. G., 1940-, Roche, A. F., 1921-, Martorell, R., and 1947- (1988). *Anthropometric standardization reference manual*. Human Kinetics Books Available at: https://agris.fao.org/agris-search/search.do?recordID=US201300646503 [Accessed January 5, 2021].

Lohmann, F., Sachs, M., Meyer, T. N., Sievert, H., Lindenmeyer, M. T., Wiech, T., et al. (2014). UCH-L1 induces podocyte hypertrophy in membranous nephropathy by protein accumulation. *Biochim Biophys Acta* 1842, 945–958. doi:10.1016/j.bbadis.2014.02.011.

Madhavan, M., Wattigney, W. A., Srinivasan, S. R., and Berenson, G. S. (1997). Serum bilirubin distribution and its relation to cardiovascular risk in children and young adults. *Atherosclerosis* 131, 107–113. doi:10.1016/s0021-9150(97)06088-7.

Maezawa, Y., Takemoto, M., and Yokote, K. (2015). Cell biology of diabetic nephropathy: Roles of endothelial cells, tubulointerstitial cells and podocytes. *J Diabetes Investig* 6, 3–15. doi:10.1111/jdi.12255.

Maiuri, M. C., Zalckvar, E., Kimchi, A., and Kroemer, G. (2007). Self-eating and self-killing: crosstalk between autophagy and apoptosis. *Nat. Rev. Mol. Cell Biol.* 8, 741–752. doi:10.1038/nrm2239.

Marchesini, G., Bugianesi, E., Forlani, G., Cerrelli, F., Lenzi, M., Manini, R., et al. (2003). Nonalcoholic fatty liver, steatohepatitis, and the metabolic syndrome. *Hepatology* 37, 917–923. doi:10.1053/jhep.2003.50161.

Marilena, G. (1997). New physiological importance of two classic residual products: carbon monoxide and bilirubin. *Biochem. Mol. Med.* 61, 136–142. doi:10.1006/bmme.1997.2610.

Maritim, A. C., Sanders, R. A., and Watkins, J. B. (2003). Diabetes, oxidative stress, and antioxidants: a review. *J Biochem Mol Toxicol* 17, 24–38. doi:10.1002/jbt.10058.

McCullough, K. D., Martindale, J. L., Klotz, L. O., Aw, T. Y., and Holbrook, N. J. (2001). Gadd153 sensitizes cells to endoplasmic reticulum stress by down-regulating Bcl2 and perturbing the cellular redox state. *Mol Cell Biol* 21, 1249–1259. doi:10.1128/MCB.21.4.1249-1259.2001.

McDonagh, A. F., and Assisi, F. (1972). The ready isomerization of bilirubin IX- in aqueous solution. *Biochem J* 129, 797–800. doi:10.1042/bj1290797.

Méndez-Sánchez, N., Qi, X., Vitek, L., and Arrese, M. (2019). Evaluating an Outpatient With an Elevated Bilirubin. *Am J Gastroenterol* 114, 1185–1188. doi:10.14309/ajg.0000000000000336.

Mizushima, N., Yoshimori, T., and Levine, B. (2010). Methods in Mammalian Autophagy Research. *Cell* 140, 313–326. doi:10.1016/j.cell.2010.01.028.

Mortada, I. (2017). Hyperbilirubinemia, Hypertension, and CKD: the Links. *Curr Hypertens Rep* 19, 58. doi:10.1007/s11906-017-0756-8.

Mozzini, C., Cominacini, L., Garbin, U., and Fratta Pasini, A. M. (2017). Endoplasmic Reticulum Stress, NRF2 Signalling and Cardiovascular Diseases in a Nutshell. *Curr Atheroscler Rep* 19, 33. doi:10.1007/s11883-017-0669-7.

Mullins, L. J., Conway, B. R., Menzies, R. I., Denby, L., and Mullins, J. J. (2016). Renal disease pathophysiology and treatment: contributions from the rat. *Dis Model Mech* 9, 1419–1433. doi:10.1242/dmm.027276.

Muraca, M., and Fevery, J. (1984). Influence of sex and sex steroids on bilirubin uridine diphosphate-glucuronosyltransferase activity of rat liver. *Gastroenterology* 87, 308–313.

Nakamura, A., Nakajima, M., Yamanaka, H., Fujiwara, R., and Yokoi, T. (2008). Expression of UGT1A and UGT2B mRNA in human normal tissues and various cell lines. *Drug Metab. Dispos.* 36, 1461–1464. doi:10.1124/dmd.108.021428.

Nano, J., Muka, T., Cepeda, M., Voortman, T., Dhana, K., Brahimaj, A., et al. (2016a-b). Association of circulating total bilirubin with the metabolic syndrome and type 2 diabetes: A systematic review and meta-analysis of observational evidence. *Diabetes Metab.* 42, 389–397. doi:10.1016/j.diabet.2016.06.002.

Nascimento, H., Alves, A. I., Coimbra, S., Catarino, C., Gomes, D., Bronze-da-Rocha, E., et al. (2015). Bilirubin is independently associated with oxidized LDL levels in young obese patients. *Diabetol Metab Syndr* 7, 4. doi:10.1186/1758-5996-7-4.

Nathan, B. M., and Moran, A. (2008a-b). Metabolic complications of obesity in childhood and adolescence: more than just diabetes. *Curr Opin Endocrinol Diabetes Obes* 15, 21–29. doi:10.1097/MED.0b013e3282f43d19.

National Institute of Diabetes and Digestive and Kidney Diseases (NIDDK) | National Institutes of Health (NIH) Available at: https://www.nih.gov/about-nih/what-we-do/nih-almanac/national-institute-diabetes-digestive-kidney-diseases-niddk [Accessed December 28, 2020].

Neuschwander-Tetri, B. A., and Caldwell, S. H. (2003). Nonalcoholic steatohepatitis: summary of an AASLD Single Topic Conference. *Hepatology* 37, 1202–1219. doi:10.1053/jhep.2003.50193.

Ng, M., Fleming, T., Robinson, M., Thomson, B., Graetz, N., Margono, C., et al. (2014). Global, regional, and national prevalence of overweight and obesity in children and adults during 1980-2013: a systematic analysis for the Global Burden of Disease Study 2013. *Lancet* 384, 766–781. doi:10.1016/S0140-6736(14)60460-8.

Ngai, K.-C., Yeung, C.-Y., and Leung, C.-S. (2000). Difference in susceptibilities of different cell lines to bilirubin damage. *Journal of Paediatrics and Child Health* 36, 51–55. doi:10.1046/j.1440-1754.2000.00436.x.

Nicholson, D. W., Ali, A., Thornberry, N. A., Vaillancourt, J. P., Ding, C. K., Gallant, M., et al. (1995). Identification and inhibition of the ICE/CED-3 protease necessary for mammalian apoptosis. *Nature* 376, 37–43. doi:10.1038/376037a0.

Oakes, G. H., and Bend, J. R. (2005). Early steps in bilirubin-mediated apoptosis in murine hepatoma (Hepa 1c1c7) cells are characterized by aryl hydrocarbon receptor-independent oxidative stress and activation of the mitochondrial pathway. *J. Biochem. Mol. Toxicol.* 19, 244–255. doi:10.1002/jbt.20086.

Očadlík, I., Hlinštáková, S., and Oravec, S. (2011). Relationship between unconjugated hyperbilirubinemia and lipoprotein spectrum. *Neuro Endocrinol Lett* 32, 360–364.

Oda, S., Fukami, T., Yokoi, T., and Nakajima, M. (2013). Epigenetic regulation is a crucial factor in the repression of UGT1A1 expression in the human kidney. *Drug Metab Dispos* 41, 1738–1743. doi:10.1124/dmd.113.051201.

Oh, S. W., Lee, E. S., Kim, S., Na, K. Y., Chae, D. W., Kim, S., et al. (2013). Bilirubin attenuates the renal tubular injury by inhibition of oxidative stress and apoptosis. *BMC Nephrology* 14, 105. doi:10.1186/1471-2369-14-105.

Ohnaka, K., Kono, S., Inoguchi, T., Yin, G., Morita, M., Adachi, M., et al. (2010). Inverse associations of serum bilirubin with high sensitivity C-reactive protein, glycated hemoglobin, and prevalence of type 2 diabetes in middle-aged and elderly Japanese men and women. *Diabetes Res. Clin. Pract.* 88, 103–110. doi:10.1016/j.diabres.2009.12.022.

Okada, H., Fukui, M., Tanaka, M., Matsumoto, S., Kobayashi, K., Iwase, H., et al. (2014). Low serum bilirubin concentration is a novel risk factor for the development of albuminuria in patients with type 2 diabetes. *Metabolism* 63, 409–414. doi:10.1016/j.metabol.2013.11.011.

Oliver, F. J., de la Rubia, G., Rolli, V., Ruiz-Ruiz, M. C., de Murcia, G., and Murcia, J. M. (1998). Importance of poly(ADP-ribose) polymerase and its cleavage in apoptosis. Lesson from an uncleavable mutant. *J Biol Chem* 273, 33533–33539. doi:10.1074/jbc.273.50.33533.

Ollinger, R., Bilban, M., Erat, A., Froio, A., McDaid, J., Tyagi, S., et al. (2005). Bilirubin: a natural inhibitor of vascular smooth muscle cell proliferation. *Circulation* 112, 1030–1039. doi:10.1161/CIRCULATIONAHA.104.528802.

O'Neill, S., and O'Driscoll, L. (2015). Metabolic syndrome: a closer look at the growing epidemic and its associated pathologies. *Obes Rev* 16, 1–12. doi:10.1111/obr.12229.

Organization, W. H. (2011). *Waist circumference and waist-hip ratio : report of a WHO expert consultation, Geneva, 8-11 December 2008*. World Health Organization Available at: https://apps.who.int/iris/handle/10665/44583 [Accessed January 17, 2021].

Ostrow, J. D., and Mukerjee, P. (2007). Solvent partition of 14C-unconjugated bilirubin to remove labeled polar contaminants. *Transl Res* 149, 37–45. doi:10.1016/j.trsl.2006.07.006.

Ostrow, J. D., Mukerjee, P., and Tiribelli, C. (1994). Structure and binding of unconjugated bilirubin: relevance for physiological and pathophysiological function. *J. Lipid Res.* 35, 1715–1737.

Otero Regino, W., Velasco, H., and Sandoval, H. (2009). The protective role of bilirubin in human beings. *Revista Colombiana de Gastroenterologia* 24, 293–301.

Ottevaere, C., Huybrechts, I., Benser, J., De Bourdeaudhuij, I., Cuenca-Garcia, M., Dallongeville, J., et al. (2011). Clustering patterns of physical activity, sedentary and dietary behavior among European adolescents: The HELENA study. *BMC Public Health* 11, 328. doi:10.1186/1471-2458-11-328.

Ouyang, C., You, J., and Xie, Z. (2014). The interplay between autophagy and apoptosis in the diabetic heart. *J. Mol. Cell. Cardiol.* 71, 71–80. doi:10.1016/j.yjmcc.2013.10.014.

Park, J., Hilmers, D. C., Mendoza, J. A., Stuff, J. E., Liu, Y., and Nicklas, T. A. (2010). Prevalence of Metabolic Syndrome and Obesity in Adolescents Aged 12 to 19 Years: Comparison between the United States and Korea. *J Korean Med Sci* 25, 75–82. doi:10.3346/jkms.2010.25.1.75.

Pflueger, A., Croatt, A. J., Peterson, T. E., Smith, L. A., d'Uscio, L. V., Katusic, Z. S., et al. (2005). The hyperbilirubinemic Gunn rat is resistant to the pressor effects of angiotensin II. *Am. J. Physiol. Renal Physiol.* 288, F552-558. doi:10.1152/ajprenal.00278.2004.

Puri, K., Nobili, V., Melville, K., Corte, C. D., Sartorelli, M. R., Lopez, R., et al. (2013a-b). Serum bilirubin level is inversely associated with nonalcoholic steatohepatitis in children. *J. Pediatr. Gastroenterol. Nutr.* 57, 114–118. doi:10.1097/MPG.0b013e318291fefe.

Qaisiya, M., Mardešić, P., Pastore, B., Tiribelli, C., and Bellarosa, C. (2017). The activation of autophagy protects neurons and astrocytes against bilirubin-induced cytotoxicity. *Neuroscience Letters* 661, 96–103. doi:10.1016/j.neulet.2017.09.056.

Qi, C., Mao, X., Zhang, Z., and Wu, H. (2017). Classification and Differential Diagnosis of Diabetic Nephropathy. *J Diabetes Res* 2017. doi:10.1155/2017/8637138.

Rao, X., Huang, X., Zhou, Z., and Lin, X. (2013). An improvement of the 2ˆ(–delta delta CT) method for quantitative real-time polymerase chain reaction data analysis. Biostat. Bioinforma. Biomath. 3, 71–85.

Rauti, R., Qaisiya, M., Tiribelli, C., Ballerini, L., and Bellarosa, C. (2020). Bilirubin disrupts calcium homeostasis in neonatal hippocampal neurons: a new pathway of neurotoxicity. *Arch Toxicol* 94, 845–855. doi:10.1007/s00204-020-02659-9.

Ridker Paul M (2003). Clinical Application of C-Reactive Protein for Cardiovascular Disease Detection and Prevention. *Circulation* 107, 363–369. doi:10.1161/01.CIR.0000053730.47739.3C.

Rigato, I., Ostrow, J. D., and Tiribelli, C. (2005). Bilirubin and the risk of common non-hepatic diseases. *Trends in Molecular Medicine* 11, 277–283. doi:10.1016/j.molmed.2005.04.008.

Rigato, I., Pascolo, L., Fernetti, C., Ostrow, J. D., and Tiribelli, C. (2004). The human multidrug-resistance-associated protein MRP1 mediates ATP-dependent transport of unconjugated bilirubin. *Biochem. J.* 383, 335–341. doi:10.1042/BJ20040599.

Riphagen, I. J., Deetman, P. E., Bakker, S. J. L., Navis, G., Cooper, M. E., Lewis, J. B., et al. (2014). Bilirubin and progression of nephropathy in type 2 diabetes: a post hoc analysis of RENAAL with independent replication in IDNT. *Diabetes* 63, 2845–2853. doi:10.2337/db13-1652.

Roberts, C. K., and Sindhu, K. K. (2009). Oxidative stress and metabolic syndrome. *Life Sci* 84, 705–712. doi:10.1016/j.lfs.2009.02.026.

Roca, L., Calligaris, S., Wennberg, R. P., Ahlfors, C. E., Malik, S. G., Ostrow, J. D., et al. (2006). Factors affecting the binding of bilirubin to serum albumins: validation and application of the peroxidase method. *Pediatr Res* 60, 724–728. doi:10.1203/01.pdr.0000245992.89965.94.

Ryan, M. J., Johnson, G., Kirk, J., Fuerstenberg, S. M., Zager, R. A., and Torok-Storb, B. (1994). HK-2: an immortalized proximal tubule epithelial cell line from normal adult human kidney. *Kidney Int* 45, 48–57. doi:10.1038/ki.1994.6.

Rutkowski, D. T., and Kaufman, R. J. (2004). A trip to the ER: coping with stress. *Trends Cell Biol* 14, 20–28. doi:10.1016/j.tcb.2003.11.001.

Salomone, F., Li Volti, G., Rosso, C., Grosso, G., and Bugianesi, E. (2013). Unconjugated bilirubin, a potent endogenous antioxidant, is decreased in patients with non-alcoholic steatohepatitis and advanced fibrosis. *J Gastroenterol Hepatol* 28, 1202–1208. doi:10.1111/jgh.12155.

Santoro, N., Amato, A., Grandone, A., Brienza, C., Savarese, P., Tartaglione, N., et al. (2013). Predicting metabolic syndrome in obese children and adolescents: look, measure and ask. *Obes Facts* 6, 48–56. doi:10.1159/000348625.

Sartorio, A., Del Col, A., Agosti, F., Mazzilli, G., Bellentani, S., Tiribelli, C., et al. (2007). Predictors of non-alcoholic fatty liver disease in obese children. *Eur J Clin Nutr* 61, 877–883. doi:10.1038/sj.ejcn.1602588.

Saverymuttu, S. H., Joseph, A. E., and Maxwell, J. D. (1986). Ultrasound scanning in the detection of hepatic fibrosis and steatosis. *Br Med J (Clin Res Ed)* 292, 13–15. doi:10.1136/bmj.292.6512.13.

Scheffer, G. L., Kool, M., de Haas, M., de Vree, J. M. L., Pijnenborg, A. C. L. M., Bosman, D. K., et al. (2002). Tissue distribution and induction of human multidrug resistant protein 3. *Lab. Invest.* 82, 193–201. doi:10.1038/labinvest.3780411.

Schietke, R., Warnecke, C., Wacker, I., Schödel, J., Mole, D. R., Campean, V., et al. (2010). The lysyl oxidases LOX and LOXL2 are necessary and sufficient to repress E-cadherin in hypoxia: insights into cellular transformation processes mediated by HIF-1. *J Biol Chem* 285, 6658–6669. doi:10.1074/jbc.M109.042424.

Schinkel, A. H. (1997). The physiological function of drug-transporting P-glycoproteins. *Semin. Cancer Biol.* 8, 161–170. doi:10.1006/scbi.1997.0068.

Schwimmer, J. B., Behling, C., Newbury, R., Deutsch, R., Nievergelt, C., Schork, N. J., et al. (2005). Histopathology of pediatric nonalcoholic fatty liver disease. *Hepatology* 42, 641–649. doi:10.1002/hep.20842.

Schwimmer, J. B., Deutsch, R., Rauch, J. B., Behling, C., Newbury, R., and Lavine, J. E. (2003). Obesity, insulin resistance, and other clinicopathological correlates of pediatric nonalcoholic fatty liver disease. *J Pediatr* 143, 500–505. doi:10.1067/S0022-3476(03)00325-1.

Seong, S.-B., Ha, D.-S., Min, S.-Y., and Ha, T.-S. (2019). Autophagy Precedes Apoptosis in Angiotensin II-Induced Podocyte Injury. *Cell Physiol Biochem* 53, 747–759. doi:10.33594/000000170.

Seyed Khoei, N., Grindel, A., Wallner, M., Mölzer, C., Doberer, D., Marculescu, R., et al. (2018). Mild hyperbilirubinaemia as an endogenous mitigator of overweight and obesity: Implications for improved metabolic health. *Atherosclerosis* 269, 306–311. doi:10.1016/j.atherosclerosis.2017.12.021.

Sherif, Z. A. (2019). The Rise in the Prevalence of Nonalcoholic Fatty Liver Disease and Hepatocellular Carcinoma. *Nonalcoholic Fatty Liver Disease - An Update*. doi:10.5772/intechopen.85780.

Siddiqui RA, Kabir N, Ateeq M, Simjee SU, Shah MR. Characterizing kidney structures in health and diseases using eosin fluorescence from hematoxylin and eosin stained sections. *Journal of Histotechnology*. 1 ottobre 2016;39(4):107–15.

Sigit, F. S., Tahapary, D. L., Trompet, S., Sartono, E., Willems van Dijk, K., Rosendaal, F. R., et al. (2020). The prevalence of metabolic syndrome and its association with body fat distribution in middle-aged individuals from Indonesia and the Netherlands: a cross-sectional analysis of two population-based studies. *Diabetology & Metabolic Syndrome* 12, 2. doi:10.1186/s13098-019-0503-1.

Slyne, J., Slattery, C., McMorrow, T., and Ryan, M. P. (2015). New developments concerning the proximal tubule in diabetic nephropathy: *in vitro* models and mechanisms. *Nephrol. Dial. Transplant.* 30, iv60–iv67. doi:10.1093/ndt/gfv264.

Song, W., Patel, A., Qureshi, H. Y., Han, D., Schipper, H. M., and Paudel, H. K. (2009). The Parkinson disease-associated A30P mutation stabilizes alpha-synuclein against

proteasomal degradation triggered by heme oxygenase-1 over-expression in human neuroblastoma cells. *J Neurochem* 110, 719–733. doi:10.1111/j.1471-4159.2009.06165.x.

Sticova, E., and Jirsa, M. (2013). New insights in bilirubin metabolism and their clinical implications. *World J Gastroenterol* 19, 6398–6407. doi:10.3748/wjg.v19.i38.6398.

Stocker, R., Glazer, A. N., and Ames, B. N. (1987a). Antioxidant activity of albumin-bound bilirubin. *Proc. Natl. Acad. Sci. U.S.A.* 84, 5918–5922. doi:10.1073/pnas.84.16.5918.

Stocker, R., and Keaney, J. F. (2004). Role of oxidative modifications in atherosclerosis. *Physiol. Rev.* 84, 1381–1478. doi:10.1152/physrev.00047.2003.

Stocker, R., Yamamoto, Y., McDonagh, A. F., Glazer, A. N., and Ames, B. N. (1987b-c). Bilirubin is an antioxidant of possible physiological importance. *Science* 235, 1043–1046. doi:10.1126/science.3029864.

Sundaram, S. S., Zeitler, P., and Nadeau, K. (2009). The Metabolic Syndrome and Non-Alcoholic Fatty Liver Disease in Children. *Curr Opin Pediatr* 21, 529–535. doi:10.1097/MOP.0b013e32832cb16f.

Szegezdi, E., Logue, S. E., Gorman, A. M., and Samali, A. (2006). Mediators of endoplasmic reticulum stress-induced apoptosis. *EMBO Rep* 7, 880–885. doi:10.1038/sj.embor.7400779.

Tabata, Y., Takano, K., Ito, T., Iinuma, M., Yoshimoto, T., Miura, H., et al. (2007). Vaticanol B, a resveratrol tetramer, regulates endoplasmic reticulum stress and inflammation. 293, 8.

Tanida, I., Ueno, T., and Kominami, E. (2008). LC3 and Autophagy. *Methods Mol Biol* 445, 77–88. doi:10.1007/978-1-59745-157-4_4.

Tanner, J. M., and Whitehouse, R. H. (1976). Clinical longitudinal standards for height, weight, height velocity, weight velocity, and stages of puberty. *Arch Dis Child* 51, 170–179. doi:10.1136/adc.51.3.170.

Tapan, S., Karadurmus, N., Dogru, T., Ercin, C. N., Tasci, I., Bilgi, C., et al. (2011). Decreased small dense LDL levels in Gilbert's syndrome. *Clin Biochem* 44, 300–303. doi:10.1016/j.clinbiochem.2010.12.003.

Tell, G., and Gustincich, S. (2009). Redox state, oxidative stress, and molecular mechanisms of protective and toxic effects of bilirubin on cells. *Curr. Pharm. Des.* 15, 2908–2914. doi:10.2174/138161209789058174.

Tewari, M., Quan, L. T., O'Rourke, K., Desnoyers, S., Zeng, Z., Beidler, D. R., et al. (1995). Yama/CPP32 beta, a mammalian homolog of CED-3, is a CrmA-inhibitable protease that cleaves the death substrate poly(ADP-ribose) polymerase. *Cell* 81, 801–809. doi:10.1016/0092-8674(95)90541-3.

Urra, H., Dufey, E., Lisbona, F., Rojas-Rivera, D., and Hetz, C. (2013). When ER stress reaches a dead end. *Biochim Biophys Acta* 1833, 3507–3517. doi:10.1016/j.bbamcr.2013.07.024.

Vianello, E., Zampieri, S., Marcuzzo, T., Tordini, F., Bottin, C., Dardis, A., et al. (2018). Histone acetylation as a new mechanism for bilirubin-induced encephalopathy in the Gunn rat. *Sci Rep* 8, 13690. doi:10.1038/s41598-018-32106-w.

Viggiano, D., De Filippo, G., Rendina, D., Fasolino, A., D'Alessio, N., Avellino, N., et al. (2009). Screening of metabolic syndrome in obese children: a primary care concern. *J Pediatr Gastroenterol Nutr* 49, 329–334. doi:10.1097/MPG.0b013e31819b54b7.

Vistoli, G., De Maddis, D., Cipak, A., Zarkovic, N., Carini, M., and Aldini, G. (2013). Advanced glycoxidation and lipoxidation end products (AGEs and ALEs): an overview of their mechanisms of formation. *Free Radic Res* 47 Suppl 1, 3–27. doi:10.3109/10715762.2013.815348.

Vítek, L., Jirsa, M., Brodanová, M., Kalab, M., Marecek, Z., Danzig, V., et al. (2002). Gilbert syndrome and ischemic heart disease: a protective effect of elevated bilirubin levels. *Atherosclerosis* 160, 449–456. doi:10.1016/s0021-9150(01)00601-3.

Vitek, L. (2012). The Role of Bilirubin in Diabetes, Metabolic Syndrome, and Cardiovascular Diseases. *Front. Pharmacol.* 3. doi:10.3389/fphar.2012.00055.

Vítek, L. (2019). Bilirubin as a predictor of diseases of civilization. Is it time to establish decision limits for serum bilirubin concentrations? *Arch Biochem Biophys* 672, 108062. doi:10.1016/j.abb.2019.108062.

Vítek, L. (2020). Bilirubin as a signaling molecule. *Med Res Rev* 40, 1335–1351. doi:10.1002/med.21660.

Vitek, L., Bellarosa, C., and Tiribelli, C. (2018). Induction of Mild Hyperbilirubinemia: Hype or Real Therapeutic Opportunity? *Clin. Pharmacol. Ther.* doi:10.1002/cpt.1341.

Vitek, L., Bellarosa, C., and Tiribelli, C. (2019a). Induction of Mild Hyperbilirubinemia: Hype or Real Therapeutic Opportunity? *Clinical Pharmacology & Therapeutics* 106, 568–575. doi:https://doi.org/10.1002/cpt.1341.

Vitek, L., Hubacek, J. A., Pajak, A., Doryńska, A., Kozela, M., Eremiasova, L., et al. (2019b). Association between plasma bilirubin and mortality. *Ann Hepatol* 18, 379–385. doi:10.1016/j.aohep.2019.02.001.

Vítek, L., Kráslová, I., Muchová, L., Novotný, L., and Yamaguchi, T. (2007). Urinary excretion of oxidative metabolites of bilirubin in subjects with Gilbert syndrome. *J Gastroenterol Hepatol* 22, 841–845. doi:10.1111/j.1440-1746.2006.04564.x.

Vítek, L., and Schwertner, H. A. (2007). The heme catabolic pathway and its protective effects on oxidative stress-mediated diseases. *Adv Clin Chem* 43, 1–57. doi:10.1016/s0065-2423(06)43001-8.

Wagner, K.-H., Shiels, R. G., Lang, C. A., Seyed Khoei, N., and Bulmer, A. C. (2018). Diagnostic criteria and contributors to Gilbert's syndrome. *Crit Rev Clin Lab Sci* 55, 129–139. doi:10.1080/10408363.2018.1428526.

Wagner, K.-H., Wallner, M., Mölzer, C., Gazzin, S., Bulmer, A. C., Tiribelli, C., et al. (2015). Looking to the horizon: the role of bilirubin in the development and prevention of age-related chronic diseases. *Clin Sci (Lond)* 129, 1–25. doi:10.1042/CS20140566.

Wallner, M., Marculescu, R., Doberer, D., Wolzt, M., Wagner, O., Vitek, L., et al. (2013). Protection from age-related increase in lipid biomarkers and inflammation contributes to cardiovascular protection in Gilbert's syndrome. *Clin. Sci.* 125, 257–264. doi:10.1042/CS20120661.

Wang, Z., Tang, L., Zhu, Q., Yi, F., Zhang, F., Li, P.-L., et al. (2011). Hypoxia-inducible factor-1α contributes to the profibrotic action of angiotensin II in renal medullary interstitial cells. *Kidney Int* 79, 300–310. doi:10.1038/ki.2010.326.

Watchko, J. F., and Tiribelli, C. (2014). Bilirubin-induced neurologic damage. *N. Engl. J. Med.* 370, 979. doi:10.1056/NEJMc1315973.

Weiss, R., Dziura, J., Burgert, T. S., Tamborlane, W. V., Taksali, S. E., Yeckel, C. W., et al. (2004). Obesity and the metabolic syndrome in children and adolescents. *N Engl J Med* 350, 2362–2374. doi:10.1056/NEJMoa031049.

Weston, S. R., Leyden, W., Murphy, R., Bass, N. M., Bell, B. P., Manos, M. M., et al. (2005). Racial and ethnic distribution of nonalcoholic fatty liver in persons with newly diagnosed chronic liver disease. *Hepatology* 41, 372–379. doi:10.1002/hep.20554.

Wu, T.-W., Carey, D., Wu, J., and Sugiyama, H. (1991). The cytoprotective effects of bilirubin and biliverdin on rat hepatocytes and human erythrocytes and the impact of albumin. *Biochem. Cell Biol.* 69, 828–834. doi:10.1139/o91-123.

Wu, Y., Li, M., Xu, M., Bi, Y., Li, X., Chen, Y., et al. (2011a-b). Low serum total bilirubin concentrations are associated with increased prevalence of metabolic syndrome in Chinese. *J Diabetes* 3, 217–224. doi:10.1111/j.1753-0407.2011.00138.x.

Wu, D., Liu, J., Pang, X., Wang, S., Zhao, J., Zhang, X., et al. (2014). Palmitic acid exerts pro-inflammatory effects on vascular smooth muscle cells by inducing the expression of C-reactive protein, inducible nitric oxide synthase and tumor necrosis factor-α. Int. J. Mol. Med. 34, 1706–1712. doi:10.3892/ijmm.2014.1942.

Xiao, T., Guan, X., Nie, L., Wang, S., Sun, L., He, T., et al. (2014). Rapamycin promotes podocyte autophagy and ameliorates renal injury in diabetic mice. *Mol Cell Biochem* 394, 145–154. doi:10.1007/s11010-014-2090-7.

Xiong, A., and Liu, Y. (2017). Targeting Hypoxia Inducible Factors-1α As a Novel Therapy in Fibrosis. *Front Pharmacol* 8. doi:10.3389/fphar.2017.00326.

Yoshino, S., Hamasaki, S., Ishida, S., Kataoka, T., Yoshikawa, A., Oketani, N., et al. (2011). Relationship between bilirubin concentration, coronary endothelial function, and inflammatory stress in overweight patients. *J Atheroscler Thromb* 18, 403–412. doi:10.5551/jat.6346.

Yu, K., Kim, C., Sung, E., Shin, H., and Lee, H. (2011). Association of Serum Total Bilirubin with Serum High Sensitivity C-reactive Protein in Middle-aged Men. *Korean J Fam Med* 32, 327–333. doi:10.4082/kjfm.2011.32.6.327.

Zelenka, J., Muchova, L., Zelenkova, M., Vanova, K., Vreman, H. J., Wong, R. J., et al. (2012). Intracellular accumulation of bilirubin as a defense mechanism against increased oxidative stress. *Biochimie* 94, 1821–1827. doi:10.1016/j.biochi.2012.04.026.

Zelenka, J., Dvořák, A., Alán, L., Zadinová, M., Haluzík, M., and Vítek, L. (2016). Hyperbilirubinemia Protects against Aging-Associated Inflammation and Metabolic Deterioration. *Oxid Med Cell Longev* 2016, 6190609. doi:10.1155/2016/6190609.

Zelenka, J., Lenícek, M., Muchová, L., Jirsa, M., Kudla, M., Balaz, P., et al. (2008a-b). Highly sensitive method for quantitative determination of bilirubin in biological fluids and tissues. *J. Chromatogr. B Analyt. Technol. Biomed. Life Sci.* 867, 37–42. doi:10.1016/j.jchromb.2008.03.005.

Zennaro, C., Mariotti, M., Carraro, M., Pasqualetti, S., Corbelli, A., Armelloni, S., et al. (2014). Podocyte developmental defects caused by adriamycin in zebrafish embryos and larvae: a novel model of glomerular damage. *PLoS One* 9, e98131. doi:10.1371/journal.pone.0098131.

Zhang, F., Guan, W., Fu, Z., Zhou, L., Guo, W., Ma, Y., et al. (2020). Relationship between Serum Indirect Bilirubin Level and Insulin Sensitivity: Results from Two Independent Cohorts of Obese Patients with Impaired Glucose Regulation and Type 2 Diabetes Mellitus in China. *Int J Endocrinol* 2020, 5681296. doi:10.1155/2020/5681296.

Zhang, L., Livingston, M. J., Chen, J.-K., and Dong, Z. (2014). Autophagy in Podocytes. *Podocytopathy* 183, 83–100. doi:10.1159/000360015.

Zimmet, P., Alberti, G., Kaufman, F., Tajima, N., Silink, M., Arslanian, S., et al. (2007). The metabolic syndrome in children and adolescents. *Lancet* 369, 2059–2061. doi:10.1016/S0140-6736(07)60958-1.

Zinszner, H., Kuroda, M., Wang, X., Batchvarova, N., Lightfoot, R. T., Remotti, H., et al. (1998). CHOP is implicated in programmed cell death in response to impaired function of the endoplasmic reticulum. *Genes Dev* 12, 982–995. doi:10.1101/gad.12.7.982.

Zucker, S. D., Goessling, W., and Hoppin, A. G. (1999). Unconjugated bilirubin exhibits spontaneous diffusion through model lipid bilayers and native hepatocyte membranes. *J. Biol. Chem.* 274, 10852–10862. doi:10.1074/jbc.274.16.10852.

Zucker, S. D., Horn, P. S., and Sherman, K. E. (2004). Serum bilirubin levels in the U.S. population: gender effect and inverse correlation with colorectal cancer. *Hepatology* 40, 827–835. doi:10.1002/hep.20407.

Chapter 7
List of Publications

7. LIST OF PUBLICATIONS

Bianco A., Dvořák A., Capková N., Gironde C., Tiribelli C., Furger C., et al. *"The Extent of Intracellular Accumulation of Bilirubin Determines Its Anti- or Pro-Oxidant Effect"*. Int. J. Mol. Sci. 2020, 21, 8101;doi:10.3390/ijms21218101.

Bianco A., Pinci S., Tiribelli C. and Bellarosa C. "*Life-long hyperbilirubinemia exposure and bilirubin priming prevent cellular metabolic damage"*. Submitted to Frontiers in Pharmacologyon28 Dec 2020. Review is ongoing.

Bellarosa C., Bedogni G., **Bianco A**., Tiribelli C. and Sartorio A. *"Impact of serum bilirubin levels on Metabolic Syndrome and NAFLD: A cross-sectional study in 1672 extremely obese children"*. Manuscript in preparation.

Oral presentations

Bianco A. *"Effects of Bilirubin on Metabolic Syndrome*". Liver Gymnasium 5, September 24, 2018, Padova.

Bianco A.*"Effects of Bilirubin on Metabolic Syndrome in two in vitro models"*26th International Conference of Clinical Diabetes. December 14-15, 2017, Rome.

Poster presentations

Bianco A., Pinci S., Tiribelli C. and Bellarosa C. *"Bilirubin biological effects on different in in vitro systems"*; Don Ostrow Trieste Yellow Retreat. September 4-5, 2019, Trieste.

Pinci S., **Bianco A.,** Tiribelli C. and Bellarosa C. *"Effects of Bilirubin on Metabolic Syndrome in two in vitro models of MetS"*. Don Ostrow Trieste Yellow Retreat. September 4-5, 2019, Trieste.

Bianco A., Tiribelli C. and Bellarosa C. *"Effects of Bilirubin on Metabolic Syndrome*". Liver Gymnasium 5, September 24, 2018, Padova.

Bianco A., Tiribelli C. and Bellarosa C. *"Effects of Bilirubin on Metabolic Syndrome in two in vitro models"*.20th ISANH international conference on oxidative stress, redox homeostasis and antioxidants. June 25-26, 2018, Paris.

Scientific collaboration abroad

Anti Oxidant Power Company, Toulouse, France |Oct 2018 - Nov 2018

Chapter 8
Acknowledgements

8. ACKNOWLEDGEMENTS

Fondazione Italiana Fegato (FIF)

Supervisor: *Prof. Claudio Tiribelli*
Tutor: *Dr. Cristina Bellarosa*

Natalia Rosso, Silvia Gazzin ,Giorgio Bedogni, Devis Pascut, Caecilia Sukowati, Matteo del Ben, Pablo Giraudi, Beatrice Anfuso, Mohammed Qaisiya, Veronica Marin, Ana Ruth Araujo, Rusdina Bte Ladju, Yogi Pratama, Sri Jayanti, Kay Loraine Cabra, Luca Grisetti, Noel Salvoza, Simone Tuniz, Emanuela Fioriti, Serena Pinci, Chiara Andolfi, Clodia Gerotto, Sandra Leal, Sabrina Corsucci, Lucia Napoli.

UNIVERSITÀ DEGLI STUDI DI TRIESTE
DIPARTIMENTO DI SCIENZE DELLA VITA

Università degli studi di Trieste

Prof. Germana Meroni
Dr. Chiara Agostinis
Dr. Fleur Bossi

CHARLES UNIVERSITY IN PRAGUE

Charles University in Prague, 1st Faculty of Medicine and General University Hospital, Institute of Medical Biochemistry and Laboratory Diagnostics
Dr. Ales Dvořák, Dr. Nikola Capková and Prof. Libor Vitek

ANTI OXIDANT POWER

The AOP start-up company
Dr. Christophe Furger
Dr. Camille Gironde

ISTITUTO AUXOLOGICO ITALIANO
Istituto di ricovero e cura a carattere scientifico

Istituto Auxologico Italiano - IRCCS
Dr. Alessandro Sartorio

Dipartimento Universitario Clinico di Scienze mediche, chirurgiche e della Salute. Università degli studi di Trieste
Dr. Cristina Zennaro, Dr. Deborah Bonazza, Dr. Cristina Bottin and Prof. Fabrizio Zanconati

My family